NAVAL POSTGRADUATE SCHOOL
Monterey, California

DTIC
S ELECTE
FEB 14 1994
A

THESIS

ELECTRON BEAMS
AT GEOSYNCHRONOUS ORBIT

by

Raymond C. Gaw

September, 1993

Thesis Advisor: R. C. Olsen

94-04512

94 2 09 047

REPORT DOCUMENTATION PAGE

1a Report Security Classification: Unclassified		1b Restrictive Markings			
2a Security Classification Authority		3 Distribution/Availability of Report			
2b Declassification/Downgrading Schedule		Approved for public release; distribution is unlimited.			
4 Performing Organization Report Number(s)		5 Monitoring Organization Report Number(s)			
6a Name of Performing Organization Naval Postgraduate School	6b Office Symbol *(if applicable)* 3A	7a Name of Monitoring Organization Naval Postgraduate School			
6c Address *(city, state, and ZIP code)* Monterey CA 93943-5000		7b Address *(city, state, and ZIP code)* Monterey CA 93943-5000			
8a Name of Funding/Sponsoring Organization	6b Office Symbol *(if applicable)*	9 Procurement Instrument Identification Number			
Address *(city, state, and ZIP code)*		10 Source of Funding Numbers			
		Program Element No	Project No	Task No	Work Unit Accession No

11 Title *(include security classification)* ELECTRON BEAMS AT GEOSYNCHRONOUS ORBIT

12 Personal Author(s) Gaw, Raymond C.

13a. Type of Report Master's Thesis	13b Time Covered From To	14 Date of Report *(year, month, day)* September, 1993	15 Page Count 102

16 Supplementary Notation The views expressed in this thesis are those of the author and do not reflect the official policy or position of the Department of Defense or the U.S. Government.

17 Cosati Codes			18 Subject Terms *(continue on reverse if necessary and identify by block number)*
Field	Group	Subgroup	Plasmasphere, Plasmapause, Plasmasheet, Ion distribbution, electron distribution, Geosynchronous orbit, Maxwellian distribution, Magnetospheric Plasma Analyzer

19 Abstract *(continue on reverse if necessary and identify by block number)*
This thesis surveys electron and ion measurements collected by the geosynchronous satellite 1989-046. In particular, this survey focuses on a phenomenom known as "electron beams", which are attributed to the sudden acceleration of electrons along the earth's magnetic field lines. Observations over a twelve day period reveal electron beam occurrences during the first few minutes of hot plasma injection associated with a magnetospheric substorm. Analysis of distribution functions show these beams have a characteristic peak. These distributions can be approximately fitted as Maxwellians, providing a means of characterizing the temperature, density, and potential drop associated with the beam. Plots of the differential flux also show a general diffusion of the beam into neighboring pitch angles. Theories on the source of the acceleration and diffusion are presented.

20 Distribution/Availability of Abstract _X_ unclassified/unlimited ___ same as report ___ DTIC users	21 Abstract Security Classification Unclassified	
22a Name of Responsible Individual R. C. Olsen	22b Telephone *(include Area Code)* 408-656-2019	22c Office Symbol Ph/Os

DD FORM 1473, 84 MAR

83 APR edition may be used until exhausted
All other editions are obsolete

Electron Beams
at Geosynchronous Orbit

by

Raymond C. Gaw
Lieutenant, United States Navy
B.S.E., Central Missouri State University

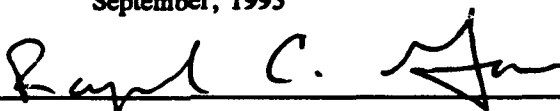Submitted in partial fulfillment
of the requirements for the degree of

MASTER OF SCIENCE IN SYSTEMS TECHNOLOGY

from the

NAVAL POSTGRADUATE SCHOOL
September, 1993

Author: _____
Raymond C. Gaw

Approved by: _____
R. C. Olsen, Thesis Advisor

_____
S. Gnanalingam, Second Reader

_____
Rudolph Panholzer, Chairman
Space Systems Academic Group

ii

ABSTRACT

This thesis surveys electron and ion measurements collected by the geosynchronous satellite 1989-046. In particular, this survey focuses on a phenomenom known as "electron beams", which are attributed to the sudden acceleration of electrons along the earth's magnetic field lines. Observations over a twelve day period reveal electron beam occurrences during the first few minutes of hot plasma injection associated with a magnetospheric substorm. Analysis of distribution functions show these beams have a characteristic peak. The distributions can be approximately fitted as Maxwellians, providing a means of characterizing the temperature, density, and potential drop associated with the beam. Plots of the differential flux also show a general diffusion of the beam into neighboring pitch angles. Theories on the source of the acceleration and diffusion are presented.

iii

TABLE OF CONTENTS

ACKNOWLEDGEMENT

The author wishes to express his gratitude to Professor R.C. Olsen, whose physics knowledge and graphical expertise made this research possible.

I. INTRODUCTION

It is said that 99% of the universe is in the plasma state. A spacecraft in orbit about the earth will likely encounter several distinct plasma environments, each distinguished by energy and density. Depending on the nature of a spacecraft and its mission, it may be important to monitor the plasma environment in which the vehicle and its payload are immersed. These plasma environments have been the subject of intense study by space physicists over the past 40 years, and much is now known about their origin and interaction with earth's magnetic field. This study, though, is by no means complete, and many important questions remain unanswered.

Previous plasma environment studies have reported an intense beam of electrons being accelerated along the local magnetic field line. These electron beams are often associated with plasma injection events (frequently called magnetospheric substorms). The origin of these particles, the acceleration method, and the diffusion process are still questions under debate.

An intense flux of electrons along the magnetic field line was first reported by Hones et al (1971) using data collected by the Vela satellites. He termed these field aligned fluxes 'beams', but stated these fluxes did not contain a secondary

1

peak in their distribution function. Electron beams, with local peaks in their distribution function, were subsequently detected by McIlwain (1975) using the University of California, San Diego auroral particles experiment on the satellite ATS-6. McIlwain showed these narrow field-aligned pitch angle distributions found at geosynchronous orbit were of recent ionospheric origin. Parks et al (1977) and Lin et al (1979) extended these studies of ATS-6 data. The instrument onboard ATS-6 did not have the capability of measuring beams in both directions, and thus could not distinguish whether the beams were bi-directional or uni-directional. Further studies have reported the existence of counterstreaming beams, which are beams propagating in both directions along the field lines (Hada et al, 1981, Moore and Arnoldy, 1982, Klumpar et al, 1988). These latter studies, however, were conducted with instruments which could not resolve the energy distribution well enough to determine if the distributions were beam-like in energy. There remained a need for measurements which provided full pitch angle and energy distributions.

Whatever the method of creating and diffusing these beams, it is undoubtedly true they are directly involved in the optical auroral processes observed in the north and south polar regions. Eather el al (1976) has reported that the auroral precipitation patterns in the polar regions share the same characteristic shape and orientation of the plasma

injection boundary. Mende and Shelley (1976) determined that the presence of hot plasma (plasmasheet electrons) was a necessary but not sufficient condition for the occurrence of conjugate auroras.

The data studied in this research paper was collected by the Magnetospheric Plasma Analyzer (MPA), a Los Alamos National Laboratory instrument. This instrument was mounted on spacecraft 1989-046, which was subsequently launched into geosynchronous orbit (6.6 earth radii). Particle count data from the MPA has an energy spectrum of 1 to 40000 eV in three dimensions for both electrons and ions. The sections that follow further describe the MPA as well as the nominal geosynchronous environment.

II. BACKGROUND

A. HISTORY

Intense fluxes of electrons along the local magnetic field line were first reported by Hones et al (1971) using data collected by the Vela satellites in the plasmasheet. He suggested these electrons were associated with the auroral phenomenon in the polar regions. He showed these fluxes had a narrow angular distribution centered along the field line, and termed them 'beams', but he did not assert that they were beam-like in energy, which a secondary peak in the distribution function would reflect.

McIlwain (1975) also reported intense fluxes of electrons peaked at small pitch angles from data collected by ATS-6 (Figure 1). He plotted the distribution function versus energy, and reported a secondary peak (Figure 2). He named this phenomenon an electron beam, and reported this beam was travelling along the local magnetic field line toward the northern auroral zone. McIlwain concluded these beams originated in either the ionosphere or the magnetosheath, and were produced by either a potential drop or by heating of the ionospheric ambient plasma.

Lin et al (1979) continued to analyze data from ATS-6, and suggested the topside ionosphere as the likely source for the

electron beams. This report also suggested beam particles are scattered to large pitch angles by wave-particle interaction. Further analysis of the ATS-6 data was conducted by Parks et al (1979) who also reported a beam along the local magnetic field line with a secondary distribution peak at approximately 1.5 keV. This report concluded that both the ionosphere and the plasmasheet populations are most likely involved as the source region, and that variations in the distribution function only occurred during the first few minutes of a plasma injection event. Unfortunately, the detector aboard ATS-6 was limited to looking in a single hemisphere, and thus could not detect if the beams were propagating in both directions along the field line.

Hada et al (1981) studied data from Imp 6, and reported field-aligned electron distributions which were bi-directional, and possibly corresponded to beams reported by McIlwain (1975), Parks et al (1977), and Lin et al (1979). These beams occurred in the plasmasheet and had an energy range of several hundred eV to several keV. To explain this phenomenon, he suggested a Fermi-type acceleration where an electric field is induced parallel to the magnetic field.

Klumpar et al (1988) and Klumpar (1989) also reported counterstreaming electrons from data collected by the AMPTE/CCE satellite. These electrons were highly collimated along the local magnetic field line, and were interpreted as having recently emerged from the auroral ionosphere as

5

secondary and backscattered primary electrons (Figure 3). He suggested that hot plasmasheet electrons are accelerated downward into the source region by a parallel electric field. This process creates a population of low energy secondary and backscattered electrons which, if the potential barrier is reduced in magnitude or moves to an adjoining flux tube, would travel along the field line toward the conjugate atmosphere. This intense flux would mirror in the opposite hemisphere, and would be seen at the equatorial plane as highly field aligned counterstreaming electrons. Klumpar, however, did not report that these counterstreaming beams had a secondary peak in their distribution function associated with a beam. Further study was needed to bring these ideas together.

B. THE NOMINAL GEOSYNCHRONOUS ENVIRONMENT

A spacecraft in geosynchronous orbit will likely encounter several distinct plasma environments, therefore it is important to briefly describe these characteristic regions of the terrestrial magnetosphere. The earth's magnetic field creates a semipermeable barrier to the solar wind produced by the sun. This barrier is called the magnetopause and creates a cavity around the earth in which various particle populations exist. The magnetosphere, depicted in Figure 4, is the region of space in which the geomagnetic field plays a dominant role. The position of the boundary, as well as the position of the particle populations within the magnetosphere,

6

are highly variable, depending upon the level of activity of the sun. As the activity increases, the boundary and particle populations move closer to the earth.

In this survey, the spacecraft encounters three different plasma regions: the plasmasphere, plasmapause, and the plasmasheet. The plasmasphere is a region of low energy, dense plasma extending from the top of the ionosphere. Particles measured in this region have typical energies < 20 eV and densities of approximately 10-100 cm^{-3}. The region separating the plasmasphere from the plasmasheet is called the plasmapause, and densities within this region will typically drop to 1 cm^{-3} or less. The distance of the plasmapause from the center of the earth varies according to the level of magnetic activity. McComas (1992) found that the plasmapause moves across geosynchronous orbit in short periods of time, as will be readily seen in this survey.

The plasmasheet is a region of high energy, less dense plasma. Particle energy is on the order of 0.1 keV to 10 keV, and densities are typically 1 cm^{-3}. The primary focus of this research is on the inner boundary of the plasmasheet where electron beams are frequently observed.

C. THE DISTRIBUTION FUNCTION

The distribution function, or phase space density, is the probability of measuring a particle at a position r, with a velocity v, at time t. It is expressed as

$$f = f(\textbf{r}, \textbf{v}, t)$$

One common type of distribution function is called a Maxwellian, or Maxwell-Boltzmann distribution, where

$$f = n(\textbf{r}, t) \left(\frac{m}{2\pi kT}\right)^{\frac{3}{2}} e^{-\frac{E}{kT}}$$

The symbol n(r,t) is the number density, and is given by integrating over all possible velocities:

$$n(\textbf{r}, t) = \iiint f(\textbf{r}, \textbf{v}, t) \, d^3v$$

The symbol m is the mass of the particle (in this case electrons), k is the conversion factor appropriate for the units of T, in this case Joules/eV, T is the temperature in eV, and E is the energy.

When a Maxwellian distribution function is plotted versus energy on a semi-log scale, it forms a straight line in which the slope is inversely proportional to the temperature, and the y-intercept is the particle density. Figure 5 shows a plot of the distribution function versus energy of particles in the plasmasphere just prior to an injection in the dusk region on a semi-log scale. The distribution function is Maxwellian over short energy ranges. This figure shows particles that are characterized by a temperature of 80 eV and a density of 4 cm^{-3}. Lin et al (1979) has shown that plasma at geosynchronous altitude can be characterized by a single

8

Maxwellian or a combination of two Maxwellians. When electron beams are present, the distribution function will contain a secondary peak, or local maximum, as seen in Figure 6. The secondary peak seen in the Figure is nominally due to acceleration of the electrons along the magnetic field line by a parallel electric field. The center of this peak indicates the potential difference between the source region and the detector. Maxwellian approximations, seen as the solid line in both Figures, will be least-squares fitted to the plotted distribution function in chapter IV to analyze electron beam observations.

D. THE MAGNETOSPHERIC PLASMA ANALYZER

Presently, three spacecraft with the international designators 1989-046, 1990-095, and 1991-080 utilize the magnetospheric plasma analyzer (MPA). These spacecraft are currently in geosynchronous orbit sending particle data to Los Alamos National Laboratory (Los Alamos). A detailed description of the MPA is presented by Bame et al (1993). The MPA was designed to measure three dimensional electron and ion distributions in an energy range of 1 eV/q to 40 keV/q. As seen in Figure 7, the MPA is composed of a single electrostatic analyzer (ESA) coupled to an array of six channel electron multipliers (CEM). The ESA is composed of a set of curved plates bent at a constant 60 degree angle, and is independent of the polar angle of entry. The particles are

9

then directed and post accelerated into the CEM array. The six CEMs provide simultaneous measurements over different polar angle field of view (FOV) look directions centered at ±11.5°, ±34.5°, and ±57.5° with respect to the spacecraft spin equator. The top plot of Figure 8 illustrates the calibrated relative response between CEM's. The number three and four channels, at ±11.5° have the highest relative transmission through the ESA section. The bottom plot of Figure 8 illustrates the expected FOV coverage for each CEM on a unit sphere. The spacecraft spin allows the MPA instrument to view over 92% of the unit sphere, allowing for excellent coverage of the surrounding plasma environment. For this report, only data collected by sensors three and four were surveyed as they had the highest probability of being aligned along the magnetic field line due to the alignment of the spacecraft's spin axis.

The MPA produces five different types of data sets. The two data sets utilized in this report are the three dimensional observations of electrons and ions. Each of these data sets consist of 24 uniformly spaced exponential sweeps from the top energy level to the bottom. Each of these sweeps collects counts in 40 nine-millisecond counting bins. Thus, the data set for the three dimensional observation of electrons would contain six 24 by 40 matrices of particle

counts, one for each CEM. Each data set takes 10.15 seconds for a complete sweep of 365.5°.

Pitch angle information in previous plasma studies was obtained by onboard magnetometers. Satellite 1989-046 does not have an onboard magnetometer. The satellite is spin stabilized with its spin axis pointed toward the center of the earth. Its orbit is always within 10° latitude of the equatorial plane. The roll angle of this spacecraft is defined as the angle of rotation completed since the MPA aperture had passed a northward facing orientation. The earth's magnetic field lines are approximately perpendicular to the equatorial plane at geosynchronous altitudes, and thus parallel to the local horizontal. At a roll angle of 0°, the MPA aperture is approximately viewing along the magnetic field line in the northward direction. In this survey, the roll angle of the spacecraft will be used as pitch angle. A pitch angle of approximately 0°, 180°, and 360° will be measuring electrons along the magnetic field line. Equatorial trapped electrons will be measured at approximately 90° and 270°.

III. OBSERVATIONS

Eleven days of data collected by the MPA were observed as electron spectrograms for the purpose of viewing electron beams. Each day contained approximately 470 observations. April 12 through April 21, 1990 were chosen due to a moderate magnetic substorm observed during this period. December 10, 1990 was chosen because the spacecraft did not encounter the plasmasheet during the 24 hour period, indicating a magnetically quiet day. April 5, 1993 was chosen to observe more recent data collected by satellite 1990-095 during a day of moderate magnetic activity. Specific days and hours were then chosen for a case study that will be presented in the next chapter.

A. FORMAT OF DATA PRESENTATION

Figures 9 and 10 show representative spectrograms of both electron and ion fluxes on April 14, 1990. These data were collected by sensors 3 and 4 of the MPA as discussed in Chapter II. These spectrograms were created by integrating counts collected by sensors 3 and 4 in the field aligned and perpendicular directions respectively. Particle flux levels are denoted by a $\log_{10}$ grey scale shown at the bottom of each Figure. The vertical scale represents the 40 energy channels,

measured in eV, through which the instrument swept during each time interval.

The time scale is labeled in universal time (UT). To convert to local time, add 13:00 hours to the universal time for the April days and 13:20 hours for December 10. Each three dimensional measurement, or snapshot takes approximately 10 seconds. Unfortunately, these measurement are not the primary mission of this satellite, and the time resolution suffers considerably. The mean time between collections was 3 minutes for the full 3-D electron mode, with larger time intervals when the satellite's primary mission preempted the telemetry channel. This time resolution had a detrimental effect on this survey of electron beams, which will be explained in a subsequent chapter.

The low energy ions seen between 0100 and 0400 UT indicate the spacecraft is within the plasmasphere. A plasma injection event is seen in the electron spectrogram at approximately 0440 UT. This indicates the spacecraft is being enveloped by the plasmasheet. A second plasma injection event of higher energy electrons is seen at approximately 0630 UT. Data from this event were shown in Figures 5 and 6. The faded vertical strip at 1100 UT indicates the spacecraft is entering eclipse. The low energy electrons seen between 0730 and 1600 UT are those emitted by the spacecraft, and then returned to the spacecraft by the potential barrier. The high energy electrons seen in Figures 9 and 10 after about 0630 UT

indicate both field aligned and equatorially trapped electrons throughout the rest of the day. This research will focus on electrons with an energy greater than about 50 eV. Figure 11 is a plot of the full energy-angle matrix at the injection at 0640 UT. The detector number, the date, and time are listed at the top of the plot. A differential energy flux versus energy and pitch angle plot is in the lower left corner of the Figure. This plot also shows the differential energy flux measured on a grey scale. The $\log_{10}$ grey scale is shown just to the right of the plot, and can be adjusted to highlight the presence of electron beams. As stated earlier, field aligned electrons will be seen at angles of $0°$, $180°$, and $360°$. Equatorially trapped electrons will be seen at $90°$ and $270°$. An electron beam is visible at a pitch angle of $180°$ and an energy of 1 keV. A characteristic sun pulse can be seen in the lower right hand corner of the plot.

The top left hand corner of the Figure is a plot of differential energy flux versus parallel velocity and perpendicular velocity. The parallel velocity will be along the magnetic field line. The grey scale representation of flux is the same as that of the energy versus pitch angle plot in the lower left hand corner. A plot of the distribution function versus energy and pitch angle is seen at the bottom right hand corner of the Figure. The $\log_{10}$ grey scale is shown to the right of the plot. This scale can also be adjusted to

highlight features within the plot. The top right hand corner shows the same distribution function plotted versus parallel and perpendicular velocity. The grey scale representation of the distribution function is the same as that in the lower right hand plot. Data collected at specific pitch angles will be shown in a subsequent chapter.

B. MAGNETIC ACTIVITY

Figure 12 illustrates the level of magnetic activity during the period of April 12,1990 to April 21,1990. A storm began on April 10, and slowly subsided over the next twelve days. April 12 showed the highest level of magnetic activity for the data observed in this survey, and as expected displayed the highest frequency of electron beam occurrence. December 10, 1990 was a magnetically quiet day, resulting in the spacecraft remaining in the plasmasphere the entire day. The magnetic activity for April 5, 1993 was comparable to April 12, 1990, and displayed a similarly high level of electron beam occurrence.

C. QUIET PERIODS

Electron beams were seen on most days, with the exceptions in this study on April 16, April 21 and December 10. April 16 and April 21 are days of low magnetic activity, resulting in relatively mild injection events. The field aligned data for these days are shown as spectrograms in Figures 13 and 14

respectively. The conclusion that no beams occurred during hot plasma injections on these days requires some strong caveats. The minimum three minute time resolution between detector sweeps may have played a substantial role in beam detection. There are many cases in this survey of electron beam distributions fading in less than six minutes. It is quite possible that electron beams were formed at the plasma injection events on 16 and 21 April, but were diffused before the next sweep by the MPA. An increased time resolution between sweeps is required to solve this question.

As stated previously, December 10 was a quiet day, and the plasmasheet remained outside the orbit of the spacecraft. The spectrogram for December 10 is shown in Figure 15. Electron beams were not observed on this day, reinforcing the idea that plasma injection from the plasmasheet is required for electron beam development. Previous articles (Lin et al, 1979, Parks et al, 1977) have shown similar observations.

D. ELECTRON BEAM DETECTION

Data collected by sensors 3 and 4 of the MPA revealed at least one electron beam event for each of the remaining days in this survey. A beam, again, is defined by a local maximum in the distribution function, as illustrated in Figure 6. Every beam detected here occurred within minutes after a plasma injection, signifying a strong coupling between the two events. The intermittent samples prevented determining if

16

these two processes occur simultaneously. A single beam was detected on April 13, April 19, and April 20. Each of these beams diffused prior to the next detector sweep, indicating a maximum lifetime of 6 minutes. Two beams were detected on April 14, each associated with a different plasma injection (see Figure 9). The first was at 0640 UT and the second was at 1000 UT. The 0640 injection (Figure 11) produced the most energetic beam in this survey. Figure 6 shows the distribution versus energy plot of the data, with a large secondary peak at 1900 eV. The accelerating potential was estimated to be 1850 V, and was more than twice as large as any other beam seen in this survey. A Maxwellian fit of this distribution gave a temperature of 576 eV and a density of .27 cm^{-3}. Each beam faded before the next detector sweep, indicating a maximum lifetime of 6 minutes.

The following day, April 15, 1990, was similar in observations. The first beam detection was made at approximately 0550, in conjunction with the first plasma injection event of the day as illustrated in Figure 16. This beam diffused after approximately 9 minutes. A second beam was detected at 0857, and diffused within 6 minutes. Three distinct beams were observed on April 17, 1990. Two of these beams diffused within 6 minutes, while the third beam diffused within 9 minutes.

April 5, 1993 was a magnetically active day, similar to April 12, 1990. Figure 17 shows the field aligned data in energy versus time format for April 5, 1993. The spacecraft was within the plasmasheet until approximately 1000 UT (local noon), and experienced numerous plasma injections from the plasmasheet. The spacecraft then reentered the plasmasheet at about 1600 UT (local dusk). At least 7 electron beams were recorded with energies ranging from about 100 eV to 1 keV and a maximum lifetime of about 20 minutes. The beam with the highest energy is shown in Figure 18. The accelerating potential was estimated to be 800 V. A Maxwellian fit of this distribution gave a temperature of 593 eV and a density of 1.54 cm^{-3} at the source.

April 12 and 18 were magnetically active days, and observations of electron beams were numerous. April 12, April 18, and April 19 will be used for case studies in the next chapter.

A total of approximately 30 electron beams were observed in this survey, with an average lifetime of about 10 minutes. The longest lifetime of a beam occurred on April 12 in which the beam diffused after about 30 minutes. These lifetimes are only rough approximations due to the three minute time lag between detector sweeps, but are considered to be conservatively high. Mauk and McIlwain (1975) reported electron beam lifetimes of hours, which may be explained by

18

the difference in magnetic activity between 1975 and 1990. Work by Mauk and McIlwain (1975) was conducted during a relatively high magnetic activity period compared to the interval presented in this survey.

A second interesting difference between these surveys is in beam energy. McIlwain (1975) and Parks et al (1979) reported electron beam energies of a few keV. By contrast, of the approximately 30 electron beams observed in this research, only a few displayed an energy above 1 keV. Energies of the remaining beams ranged from about 40 eV to 1 keV. These observations are closer to those of Moore and Arnoldy (1982) who reported counterstreaming electron beams of a few hundred eV. The next chapter will present case studies of specific beams found in this survey.

IV. CASE STUDIES

Three days have been selected from the survey for a more detailed analysis. These three days were chosen for a range of quiet to active magnetospheric conditions. A computer program was developed to analyze electron distribution functions in order to determine the temperature and density of observed beams.

A. APRIL 19, 1990

Figure 19 is a spectrogram for the field aligned particle distributions observed on April 19. A single plasma injection event is seen at approximately 1040 UT. The evolution of a beam is illustrated by the sequence of Figures which follows. Figure 20 and 21 show the energy versus pitch angle plots collected by detectors 3 and 4 respectively at the injection boundary when the beam is most distinct. A high flux of electrons is seen in Figure 20 at a pitch angle of 180° and an energy of approximately 600 eV. Figure 21 also shows a high flux of electrons at a pitch angle of 0° and an energy of approximately 600 eV. These two 'beams' are counterstreaming in nature; their appearance in adjacent detectors is a result of the offset between magnetic field direction and the north-south axis. The velocity plots in both Figures also show a

high flux of electrons peaked along the $v_\parallel$ axis. These are the first indications that an electron beam may be present.

The distribution function plots in Figures 20 and 21 also show an increased flux at 180° and 0° respectively. These distribution functions were plotted versus energy at the respective pitch angles, and least-squares fitted with Maxwellian approximations. This is depicted in Figures 22 and 23. As these Figures show, the distribution functions are nearly identical for detectors 3 and 4. This was the case throughout the entire survey, indicating these beams are nominally bi-directional. Therefore, data collected by detector 3 will primarily be used in the remaining case studies. It should be noted that data collected by both detectors were surveyed for this project.

Figures 22 and 23 reveal the characteristic peak in the distribution function indicating an acceleration of electrons along the field line. The temperatures in both Figures were determined from the slope of the fit from 500-3000 eV. This fit assumes the distribution to be Maxwellian.

The density calculation has become inaccurate due to the energy shift in the distribution function. An accelerating potential term must be added to determine the correct particle density of the beam. This correction is seen as:

$$n = n_o e^{\frac{-q\phi}{kT}}$$

where n_o is the original density calculation as obtained from a least squares fit to the distribution function. The term $q\phi$ is the accelerating potential of the electron beam. This correction will be included in a subset of the Figures which follow to determine the density. Figure 24 shows a log-linear plot of the detector 3 data shown previously in Figure 22. The density estimate has been corrected using the assumption that the distribution is Maxwellian at its source.

The following four Figures show the distribution before and after the beam measurement. Figure 25 is the distribution versus energy plot on a log-log scale just prior to beam occurrence. These data has been fitted with a Maxwellian approximation to determine the temperature. Figure 26 shows the data on a semi-log scale. Both plots are fitted from 100-1000 eV, and show similar densities and temperatures prior to beam development.

Six minutes after the beam is observed, it has diffused in energy and pitch angle. Figures 27 and 28 show the distribution function in the same formats as above. Figure 27 shows the distribution function and differential energy flux versus energy about 6 minutes after the beam was detected. A Maxwellian fit is again used. The characteristic peak in the distribution function has practically disappeared, while the

temperature over the same 500-3000 eV energy range has increased to 860 eV. Figure 28 shows the same data on a semi-log scale, and the density of 0.37 cm^{-3} is nearly one quarter that observed in the beam. This indicated the beam had diffused into the surrounding hot plasma. This was the only beam seen on April 19.

B. APRIL 18, 1990

The second case study is from a more active day in the observation period. The energy versus time spectrogram for April 18 is shown in Figure 29. There are three distinct plasma injection events at approximately 0400, 0840, and 1240 UT. This case study will concentrate on events occurring during the second plasma injection, when an approximately 100 eV beam is found. Data are shown for 0843 to 0855 UT, which is approximately 2200 local time.

Figure 30 is the energy versus pitch angle plots at 0843 UT from data collected by detector 3. A high flux of electrons is clearly seen at a pitch angle of 180° and an energy of about 300 eV. The velocity plot also shows an increased flux of electrons being accelerated in the $v_{\parallel}$ direction. This is believed to be the beginning of an electron beam formation. Figure 31 is the distribution versus energy plot at a pitch angle of 180°. The characteristic peak in the distribution function is not yet seen.

Figure 32 shows the data in energy versus pitch angle format three minutes later at 0846 UT. The flux of electrons at 180° pitch angle appears to have increased in amplitude with enhanced fluxes around 100 eV. Figure 33 shows the distribution versus energy on a log-log scale at 180°. The least-squares fit of a Maxwellian shows a small peak in the distribution function at approximately 120 eV. There is also a substantial depression in the distribution function at less than 120 eV below what would be expected for a Maxwellian. Figure 34 shows the same data on a semi-log scale. The fit from 300-900 eV show the temperature to be about 126 eV. The accelerating potential was estimated to be 100 V, giving a source density of 9.34 cm^{-3}.

Figure 35 presents the energy-angle distributions for the next sweep at 0849 UT. The flux at 180° appears to have the same characteristics as that seen at 0846 UT. Figure 36 shows the field aligned data for this snapshot. The data are least-squares fitted with a Maxwellian giving a temperature of 127 eV. Figure 37 shows that once the accelerating potential of approximately 100 V is included, a density of 7.47 cm^{-3} describes the beam. This temperature and density nearly match the temperature and density seen at 0846.

Figure 38 shows the third consecutive beam measurement at 0852 UT. The beam flux at 180° pitch angle has decreased substantially from that seen in the previous two sweeps,

indicating a diffusion of the beam. Figure 39 shows the distribution function and differential energy flux versus energy along with Maxwellian fits. The temperature has dropped to 81 eV, a decrease of about 50 eV from the previous observations. Figure 40 shows the estimated accelerating potential of 80 V, giving a density of 2.02 cm^{-3}.

Figure 41 shows data collected during the next sweep at 0855 UT as the distribution has relaxed. The beam has diffused in energy and pitch angle. The temperature from the least-squares fit is 129 eV. Figure 42 shows the same data on a semi-log scale, and displays the corrected density of 1.29 eV. It appears from this series of Figures that the electron beams observed at approximately 100 eV are from a distribution function which is largely constant in temperature and simply accelerated through varying potential drops.

C. APRIL 12, 1990

April 12 was the most magnetically active day in this survey, and the spacecraft encountered a number of plasma injection events. Figure 43 is the energy versus time spectrogram for April 12, 1990. The first plasma injection was at approximately 0330 UT, and plasma injections continued until about 1215 UT. This case study will focus on a plasma injection at approximately 0520 UT, near local dusk (about 1800 local time).

Data are shown in detail for an 8 minute interval in four snapshots. Figure 44 shows the first segment, collected by detector 3 at 0521 UT. The plot shows a concentration of flux at pitch angles of 0° and 180° and at energies of about 50 eV. The velocity plot shows a high flux along $v_|$ at both positive and negative values. This clearly shows an acceleration in both directions along the magnetic field line. This counterstreaming is seen throughout the injection events on April 12.

Figures 45 and 46 show the field aligned data. The distribution has been least-squares fitted with a Maxwellian distribution, giving a temperature of 54 eV. A small hump appears to be forming at an energy of about 20 eV. Figure 46 shows the data on a semi-log scale. The accelerating potential was estimated to be 40 V giving a density of 13.5 cm^{-3}. It is believed this is the start of a beam development for this injection event.

Figure 47 shows the next sweep at 0524 UT. A concentration of flux is again seen at pitch angles of 0° and 180°. Counterstreaming continues to be observed. The dimensions of the flux appear to be the same as that seen at 0521 UT. Figures 48 and 49 show the field aligned data in line plot form. The data have been least-squares fitted with a Maxwellian, giving a temperature of 34 eV. A peak has formed in the distribution at an energy of about 50 eV.

Figure 49 shows the data in semi-log form. An accelerating potential of 50 V was estimated, giving a source density of 29 cm^{-3}. The distribution function again shows a substantial depression in energies less than the local peak. This depression suggests the possibility that electron beams are due to the dropout of low energy electrons vice the development of a secondary peak in the distribution function.

Figures 50 through 52 show data from the next sweep by the MPA at 0526 UT. The shape of the pitch angle distribution appears to be the same as that seen in the previous sweep. The velocity plot still shows counterstreaming electrons along the magnetic field line. The line plot gives a temperature of 50 eV. The corrected source density is shown to be 17.65 cm^{-3}.

The conclusion of the sequence is shown in Figures 53-55 at 0529 UT. The data are not substantially different from those taken in the previous three sweeps by the MPA. Figure 54 is the distribution versus energy plot on a log-log scale, and again shows the peak characterizing an electron beam. The Maxwellian fit gives a temperature of 52 eV. Figure 55 shows the same data on a semi-log scale. The accelerating potential was estimated to be 80 V, giving a density of 28 cm^{-3}. The next sweep of the MPA was made at 0532 UT, and showed the beam had diffused in pitch angle and energy. This diffusion translates to a beam lifetime of approximately 11 minutes.

V. DISCUSSION

There are three primary questions that remain unanswered with respect to electron beams. These questions are:

1. What is the origin of the particles in the beam?

2. What is the acceleration method?

3. How and where is the electron beam diffused?

This chapter will compare theories presented in previous research to the observations made in this thesis.

A. ORIGIN OF BEAM PARTICLES

Many previous research papers attempted to explain the origin of particles in electron beams. Parks et al (1977) deduced the increased electron flux seen along the magnetic field line originated in the upper atmosphere (ionosphere). Lin et al (1979) reported that the beams were confined to pitch angles of approximately 10-30° at the equatorial plane, and suggested that the ionosphere was the likely source of the particles. Parks et al (1979) reported that electron beams are characteristic of ionospheric potentials, but that the particles are probably of two sources; the ionosphere and the plasmasheet. McIlwain (1975) also argued that the distribution functions of these beams indicate that at least some of the particles in the beam originate in the ionosphere. A recent article by Klumpar (1989) concluded that the enhanced

28

electron fluxes (beams) encountered along the magnetic field line are secondary and backscattered electrons from the auroral ionosphere.

Observations in this thesis also support the topside ionosphere as the likely source for electron beams. The enhanced fluxes are counterstreaming as in Klumpar (1989) and exhibit temperature, flux, and density consistent with particles in the topside ionosphere. The beams appear to be relatively stable through their lifetime, suggesting the particles that constitute the beam originate in a stable environment, such as the ionosphere. The beams are highly field aligned, intimating that the origin of the particles is not local, but at some distance along the magnetic field line.

B. METHOD OF ACCELERATION

Electron beams are the result of particles being accelerated along the magnetic field line. The observations in this thesis suggest these particles originate in the ionosphere. It is also clear from this observation that electron beams are formed at or just after a plasma injection event upon passage of the plasmasheet in the equatorial plane. This suggests that the acceleration method must form a connection between these two events.

A common idea in all acceleration theories is that a potential structure is formed just above the acceleration region. Tetreault (1991) suggested that double layers formed

by hole/clump instability along the magnetic field line can cause a sufficiently large potential drop to form electron beams. The existence of these double layers has been shown, but it is still uncertain whether these interspersed double layers can accumulate the potential necessary to form electron beams.

A second acceleration theory involves parallel electric fields. Lin et al (1982) suggested the acceleration method is oppositely directed electric fields pointing to the spacecraft along the magnetic field. Mizera (1977) showed that substantial electric fields along the magnetic field line are operating over both hemispheres at an altitude of less than two earth radii. These electric fields produce accelerating potentials along the magnetic field line at low altitude.

Klumpar (1989) has suggested that plasmasheet electrons are accelerated downward by a parallel electric field. These energetic electrons produce secondary and backscattered electrons in the ionosphere. A diminishing or movement of the potential structure above the ionosphere would allow these electrons to escape along the magnetic field line, forming the beams seen at the equatorial plane. Figure 56 is an illustration of this theory, and is considered by the author to be the most viable theory in the formation of electron beams.

30

C. DIFFUSION PROCESS

Observations in this research indicate the lifetimes of electron beams are on the order of minutes. This dictates that a strong diffusion process must take place along the field line to dissipate the beam, although part of the evolution may be due to the relative motion of the spacecraft to the injection front. Figure 57 is the energy versus pitch angle plot from data collected by detector three on April 17, 1990. An electron beam is seen at a pitch angle of about 180° and at an energy of 200 eV. Just above the beam are two concentrations of flux bending toward equatorially trapped pitch angles. Figure 58 also shows a concentration of flux bending away from the beam and towards pitch angles of 90° and 270°.

Two contrasting conclusions can be drawn from these Figures. The first possibility is that electrons at equatorially trapped pitch angles are losing energy and forming an electron beam along the field line. Observations shown here indicate that the beam densities require that the beam originate in the ionosphere, not the equatorially trapped particle population. The second possibility is that particles within the beam are gaining energy and diffusing into neighboring pitch angles. A widely cited diffusion process by whistler mode waves, as discussed in Johnstone (1993), provide the mechanism necessary to support this possibility.

31

VI. CONCLUSION

Electron beams are a common occurrence in the Magnetosphere. Observations of spectrograms from 11 days disclosed the presence of over 30 distinct electron beams. These beams appear at or just after a plasma injection from the plasmasheet. The beams are travelling in both directions along the magnetic field line, indicating counterstreaming. An interesting observation is that beam temperature is not dependent on substorm intensity. April 12, 1990 displayed the highest magnetic activity, but the beam temperature was no higher than in other days. Beam lifetime, though, did appear to depend on substorm intensity as beams detected on April 12 lasted up to five times as long as beams detected on other days.

Beam temperature and density were determined using Maxwellian approximations. The estimated temperature and density remained nearly constant through the beam's lifetime, and are consistent with particles found in the topside ionosphere. The topside ionosphere is the suggested choice for the origin of the particles in the beam.

Klumpar's (1989) electric field model is consistent with the observations in this research, and is marked as a viable solution to the acceleration question. Hada et al's (1981) conclusions are also supported by observations in this

research. Lack of a wave sensor on the spacecraft prevented determining if a wave-particle interaction caused dispersion of the beam. Observations in this report suggest particles within the beam gain energy and are diffused into neighboring pitch angles. Whistler mode waves are suggested as the cause of this diffusion.

The three minute time lag between sweeps was detrimental in the analysis of this data. The number of beams and their respective lifetimes can only be estimated, as their development and diffusion could have occurred between sweeps. Improvements in the time resolution would prove helpful in answering some of these questions. While it is essential in plasma physics to collect data at all pitch angles, it would also prove useful to train a plasma detector along the magnetic field line to continuously collect data. Beam development and diffusion would be accurately recorded by such a detector.

The observations made in this report cover a relatively short period, and conclusions drawn are subject to change by a more extensive survey. It is recommended that data collected by the MPA on satellites 1989-046, 1990-095, and 1991-080 be furthered studied to accurately analyze electron beams.
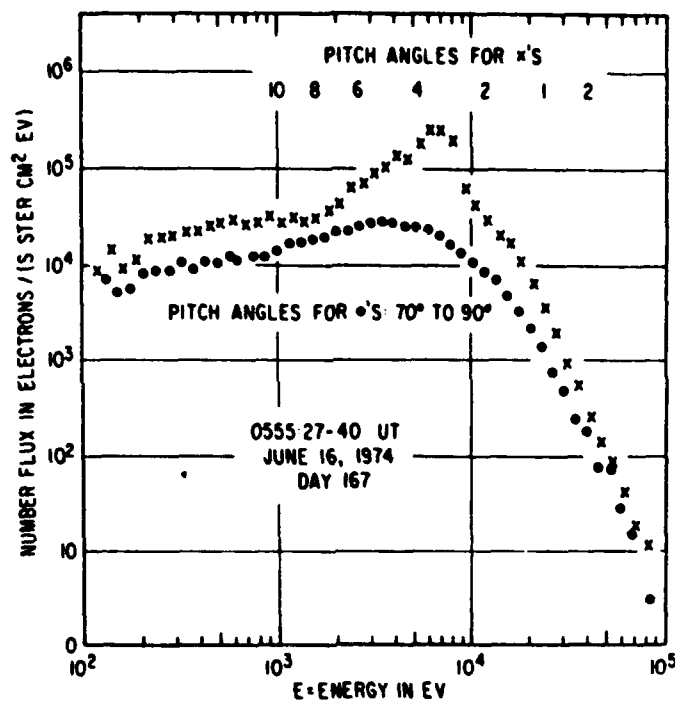
Figure 1 The differential number flux of electrons travelling
close to the magnetic field direction measured during the first
minutes of a magnetospheric substorm plasma injection.

Figure 1 Electron Flux versus Energy, McIlwain (1975)
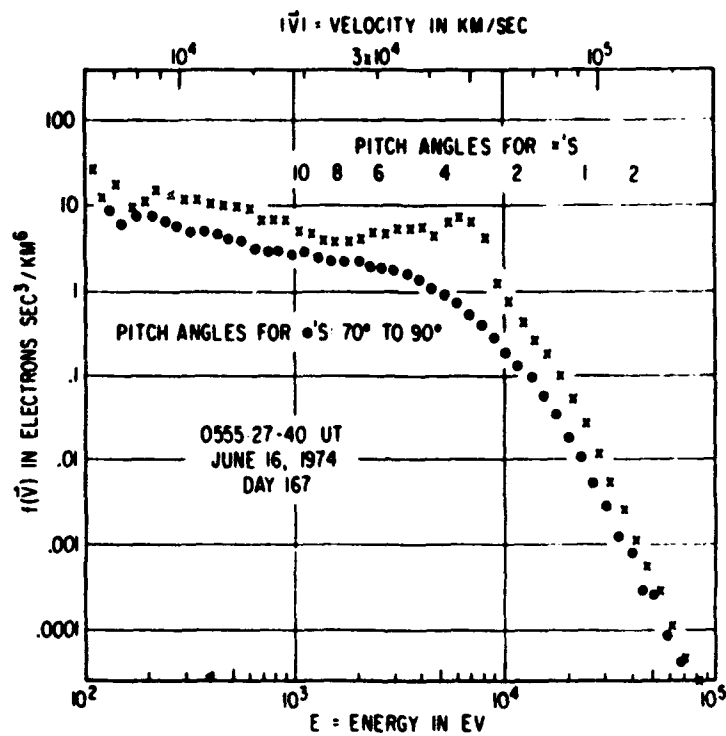
Figure 4 The distribution function replotted using logarithmic scales.

Figure 2   Distribution versus Energy, McIlwain (1975)

35
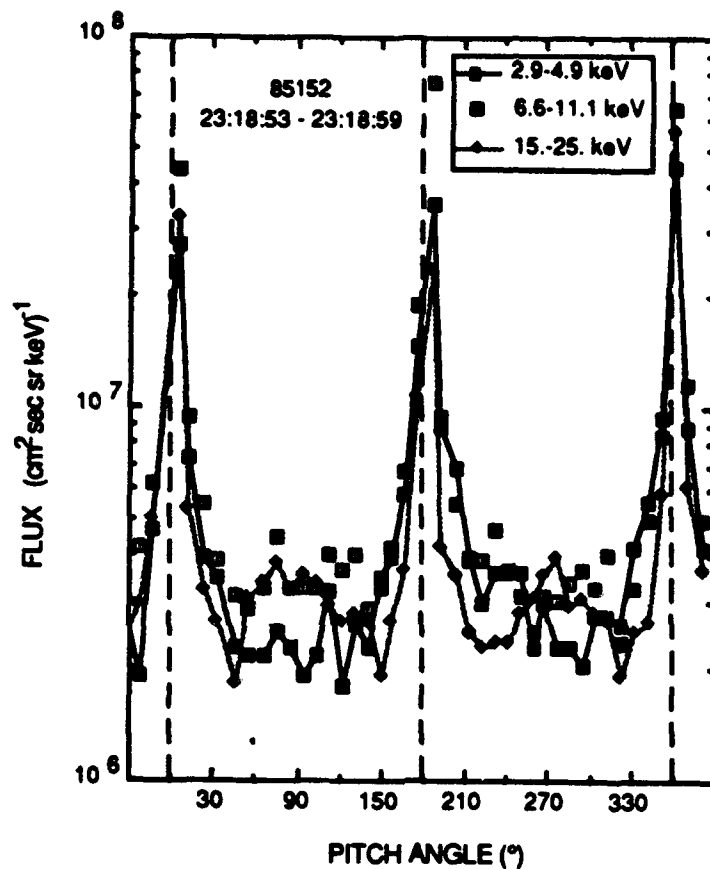
Figure 3. Pitch angle distribution showing the three components of the distribution: loss cone component, halo component, and locally trapped component.

Figure 3   Electron Flux versus Pitch Angle, Klumpar (1989)

36

APPENDIX B   FIGURES

Magnetosphere
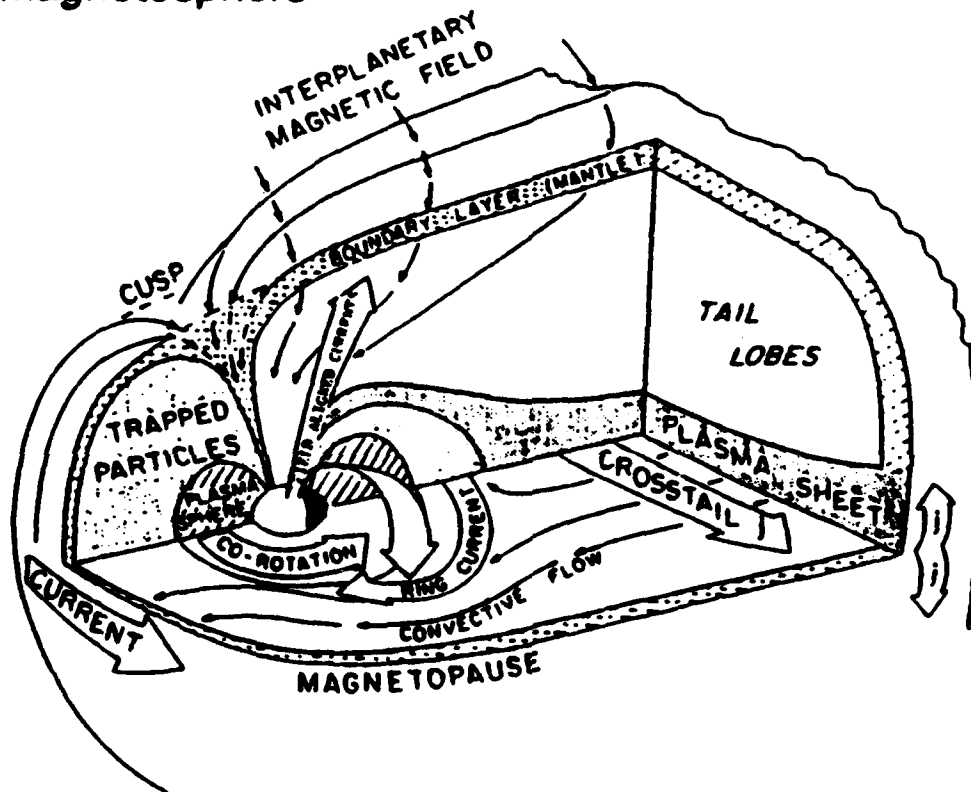
Figure 5.4   Cross section of the magnetosphere showing the principal current systems: magnetopause current, cross-tail (or neutral) current sheet, ring current, and field aligned currents. Also shown are the regions of convective and co-rotation plasma flow directions

Figure 4   Cross Section of the Earth's Magnetosphere
Tascione (1988)
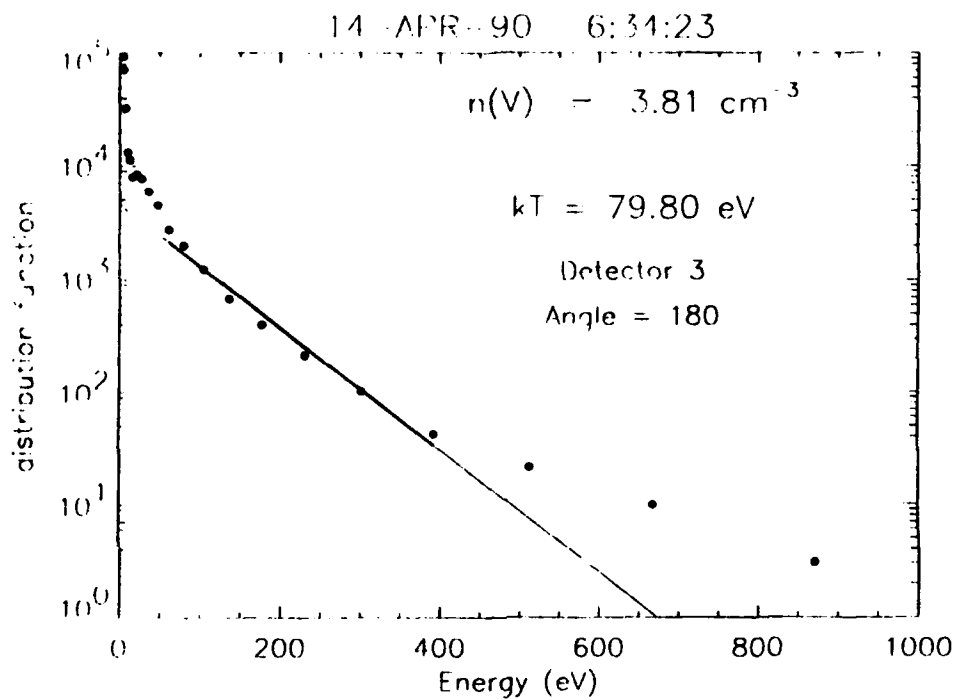
Figure 5   Representation of Distribution Function
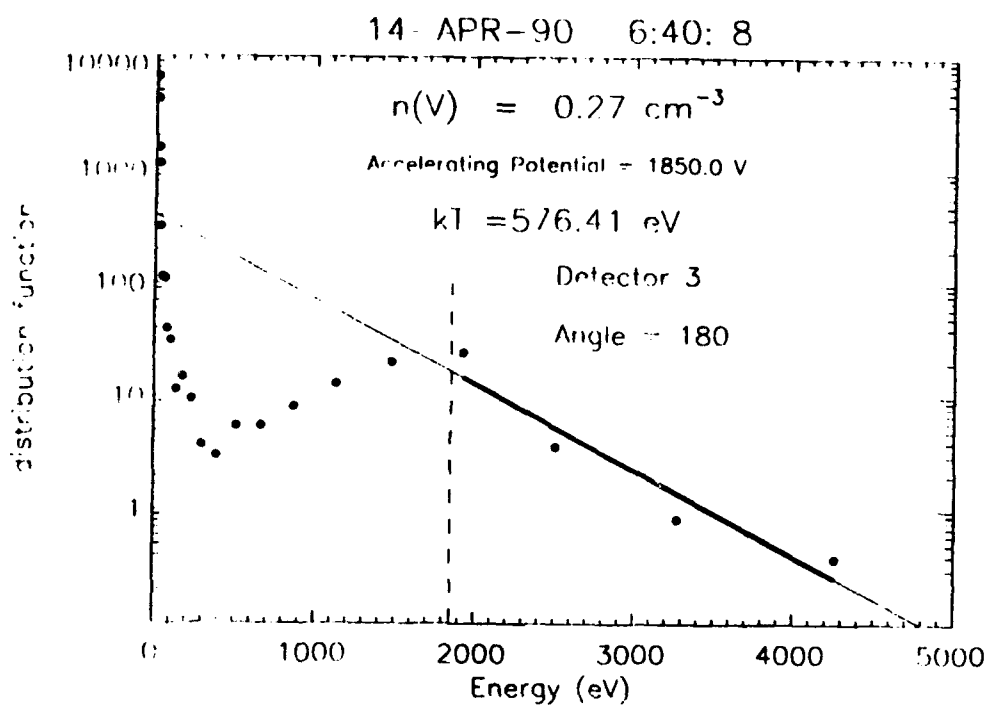
Figure 6   Representation of Distribution Function with
Electron Beam
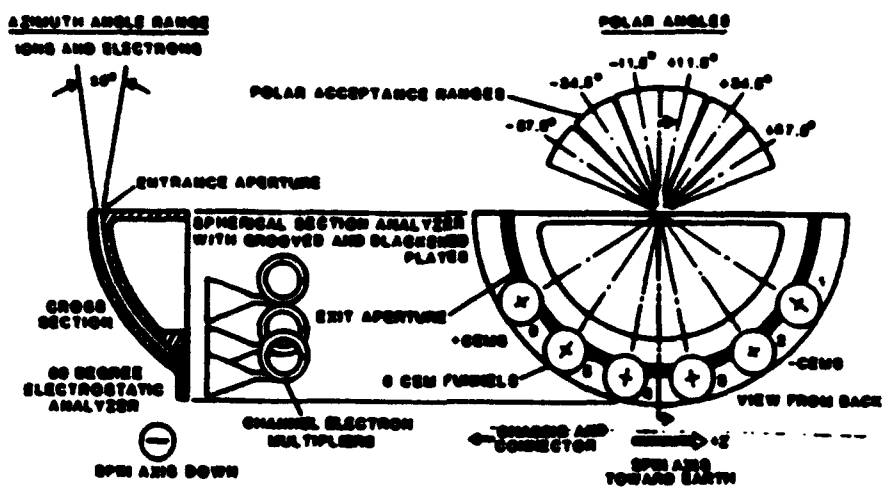
FIG. 1. Cross-sectional view of the MPA charged particle optics system, on the left. A view of the system on the right, taken from behind the analyzer, shows the locations of the six CEM funnels and their nominal polar angle fields-of-view.
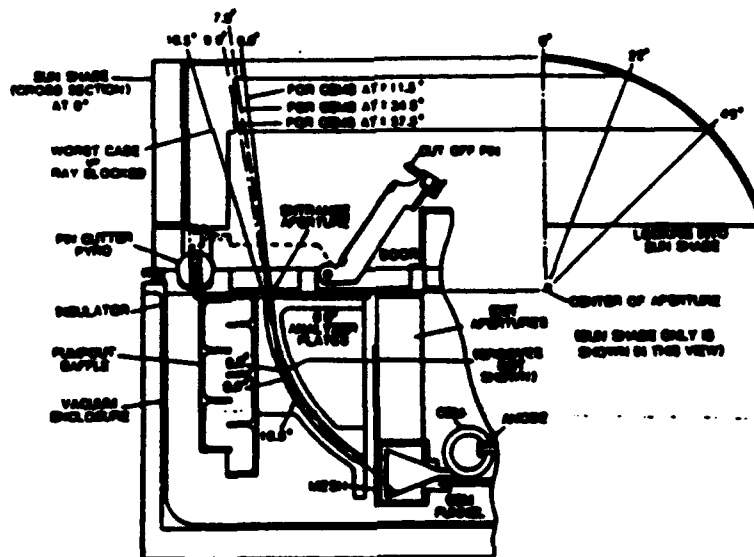
FIG. 2. Cross-sectional view of the entrance aperture end of MPA showing the cylindrically shaped sun shade which limits how deep into the gap solar UV can fall before scattering or producing photoelectrons, as well as other features of the sensor package. Grooving of the plates, not shown in the drawing, reduces the area from which UV can scatter into the CEMs or produce photoelectrons that might reach the CEMs.

Figure 7   Cross Sectional Views of the MPA

Bame (1993)

40
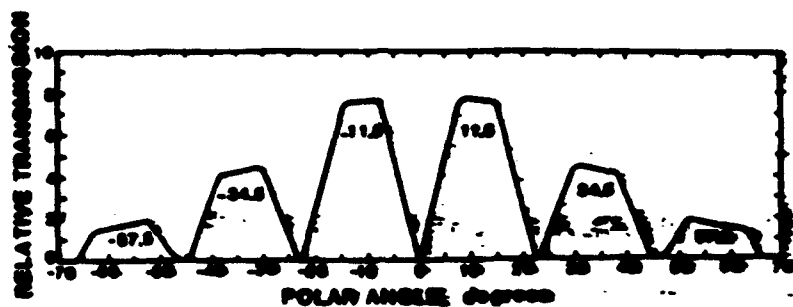
FIG. 6. Calculated MPA response profiles in polar angle, integrated over azimuth. The CEMs at nominal polar angles of ±11.5°, ±34.5°, and ±57.5°.
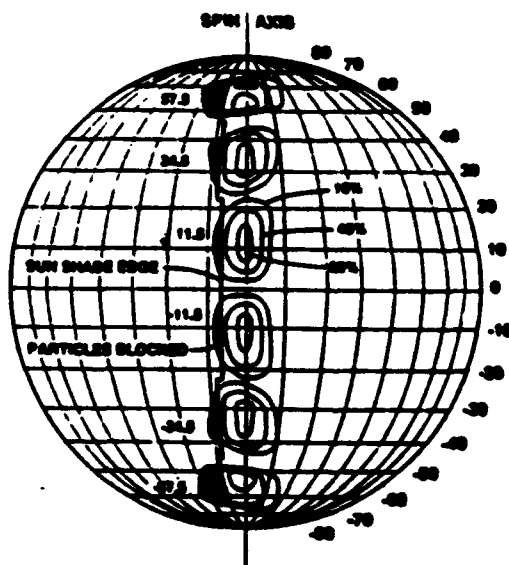
FIG. 8. Contours of MPA transmission response shown on the unit sphere at the 10%, 40%, and 80% transmission levels.

Figure 8 MPA Transmission Response Curves and Unit Sphere,

Bame (1993)

41

1989-046   14-APR-1990

Field-Aligned
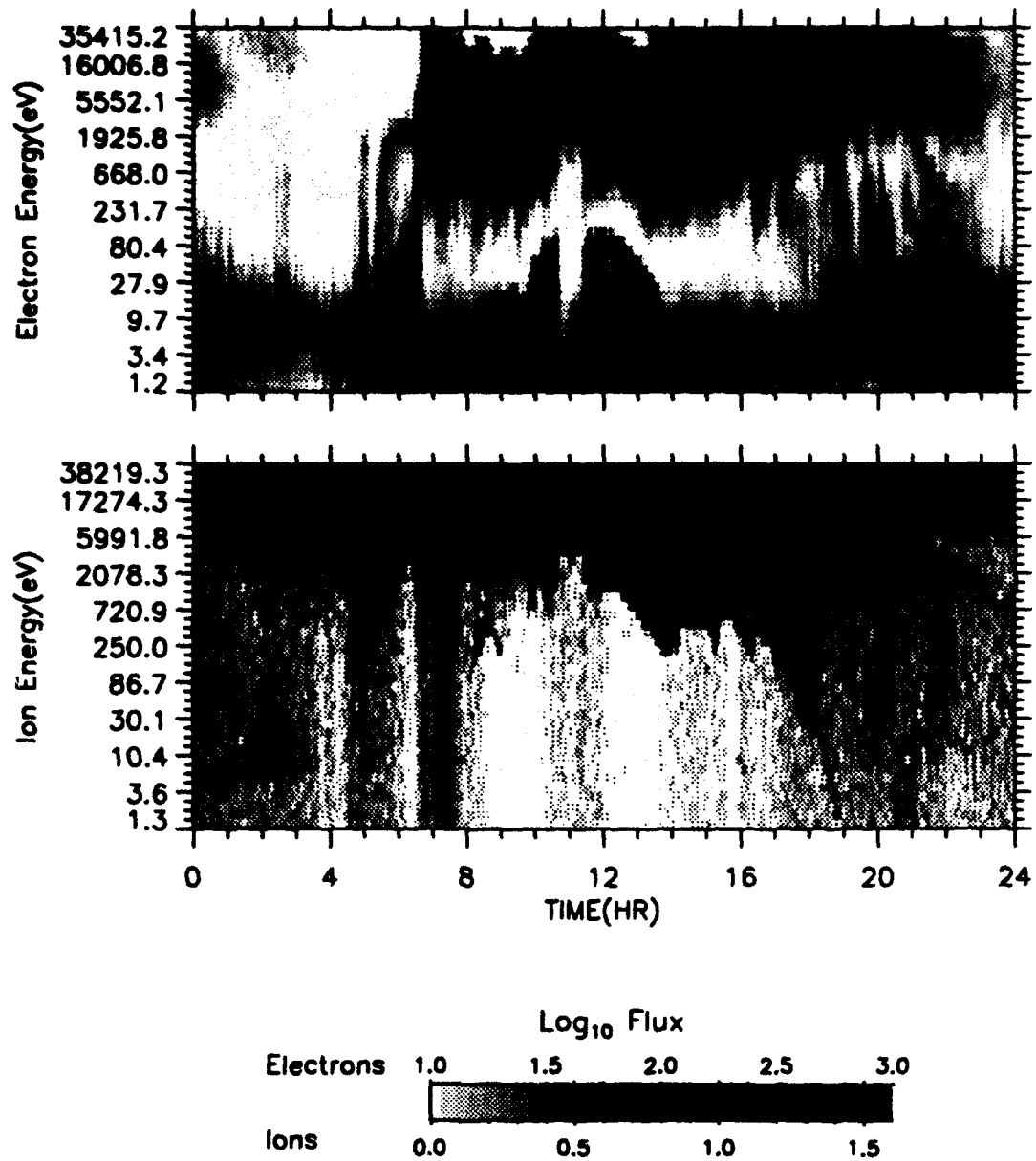
Plot run 28-May-1993 11:02:36.00   Naval Postgraduate School

Figure 9 Energy vs Time Spectrogram--Field Aligned

42

Los Alamos National Laboratory Magnetospheric Plasma Analyzer

1989-046   14-APR-1990

Perpendicular

Electron Energy(eV)
35415.2
16006.8
5552.1
1925.8
668.0
231.7
80.4
27.9
9.7
3.4
1.2

Ion Energy(eV)
38219.3
17274.3
5991.8
2078.3
720.9
250.0
86.7
30.1
10.4
3.6
1.3

TIME(HR)
0   4   8   12   16   20   24

Log₁₀ Flux

| Electrons | 1.0 | 1.5 | 2.0 | 2.5 | 3.0 |

| Ions | 0.0 | 0.5 | 1.0 | 1.5 |
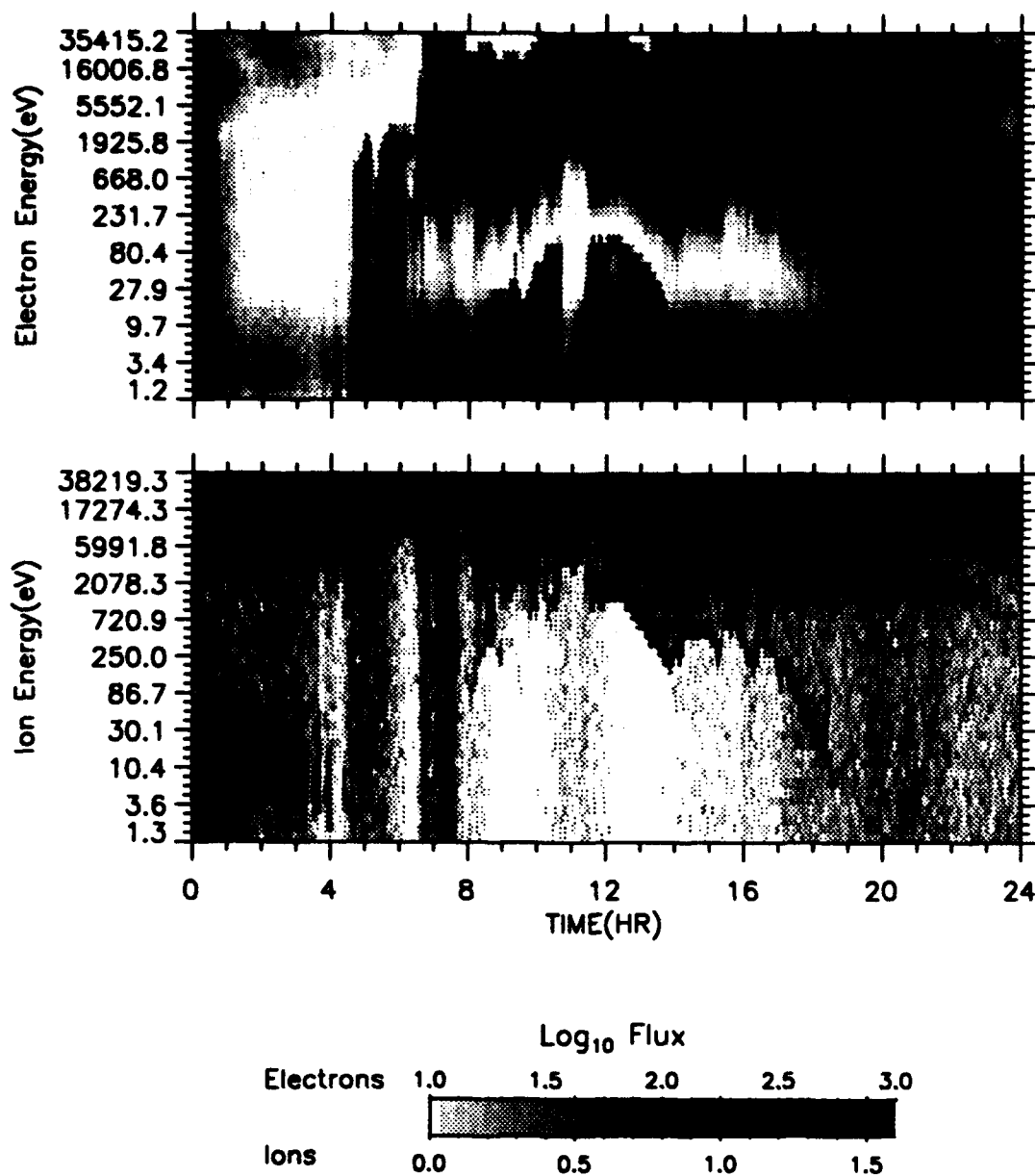
Plot run 28-May-1993 11:04:15.00   Naval Postgraduate School
Figure 10 Energy VS Time Spectrogram--Perpendicular

43

LANL MPA — 1989-046
Detector 3
14-APR-90   6:40:08

1 — 3270.09 eV

1 — 3270.09 eV

Log Diffl Energy Flux

Log Dist. Fcn
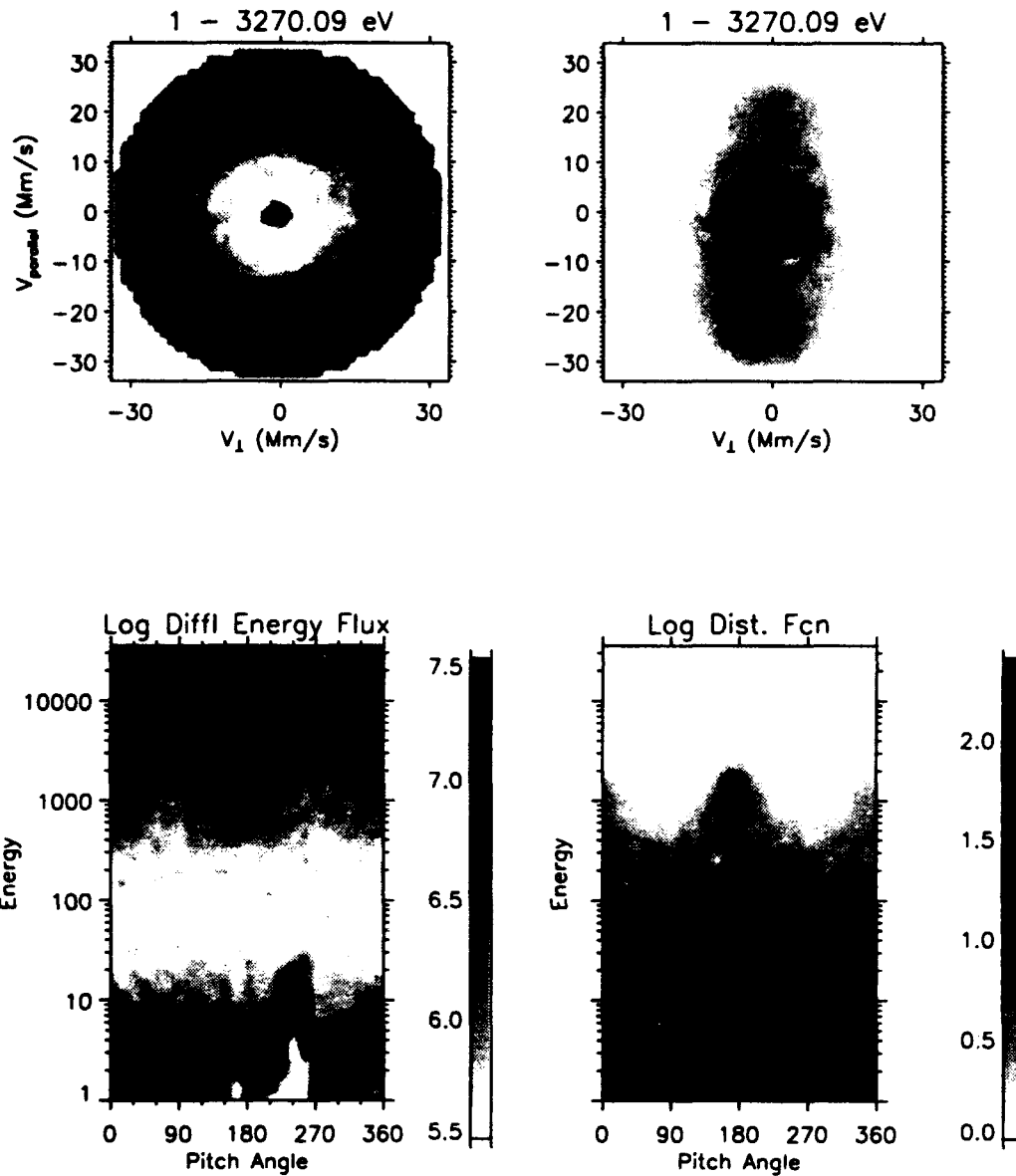
Figure 11   Energy versus Pitch Angle Spectrogram

44
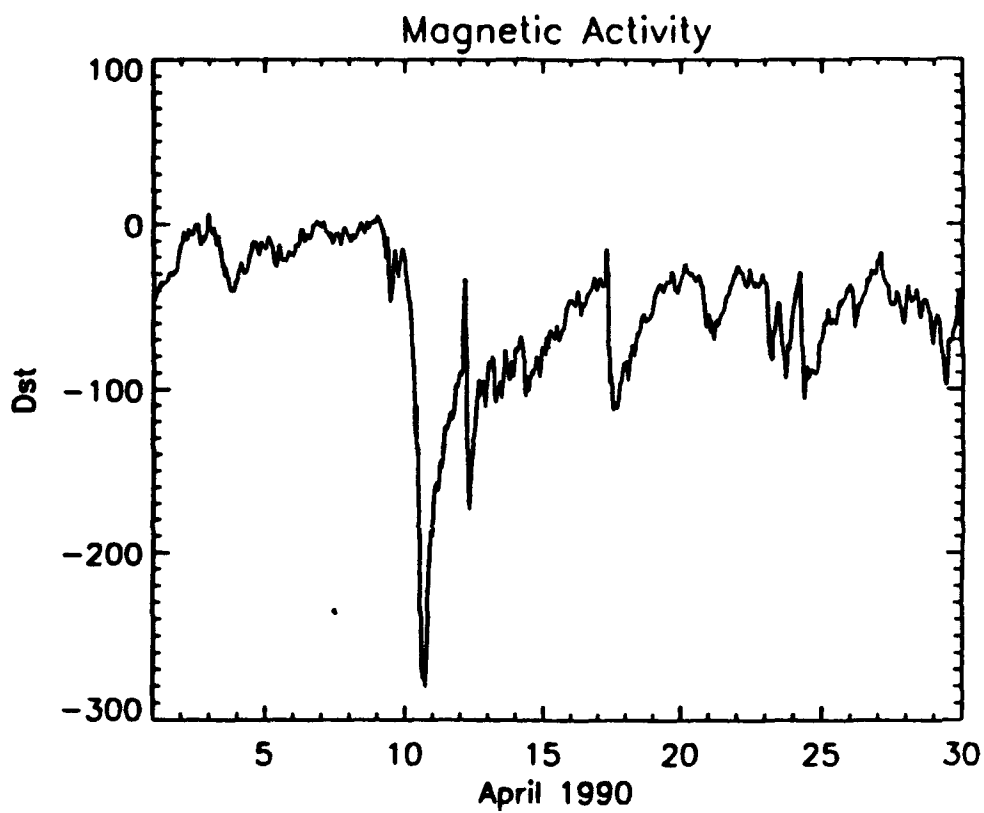
Figure 12 Magnetic Activity, April 12 through April 21,1990

45

1989−046   16−APR−1990

Field−Aligned

Log$_{10}$ Flux

Electrons   0.5   1.0   1.5   2.0   2.5

Ions   0.0   0.5   1.0   1.5
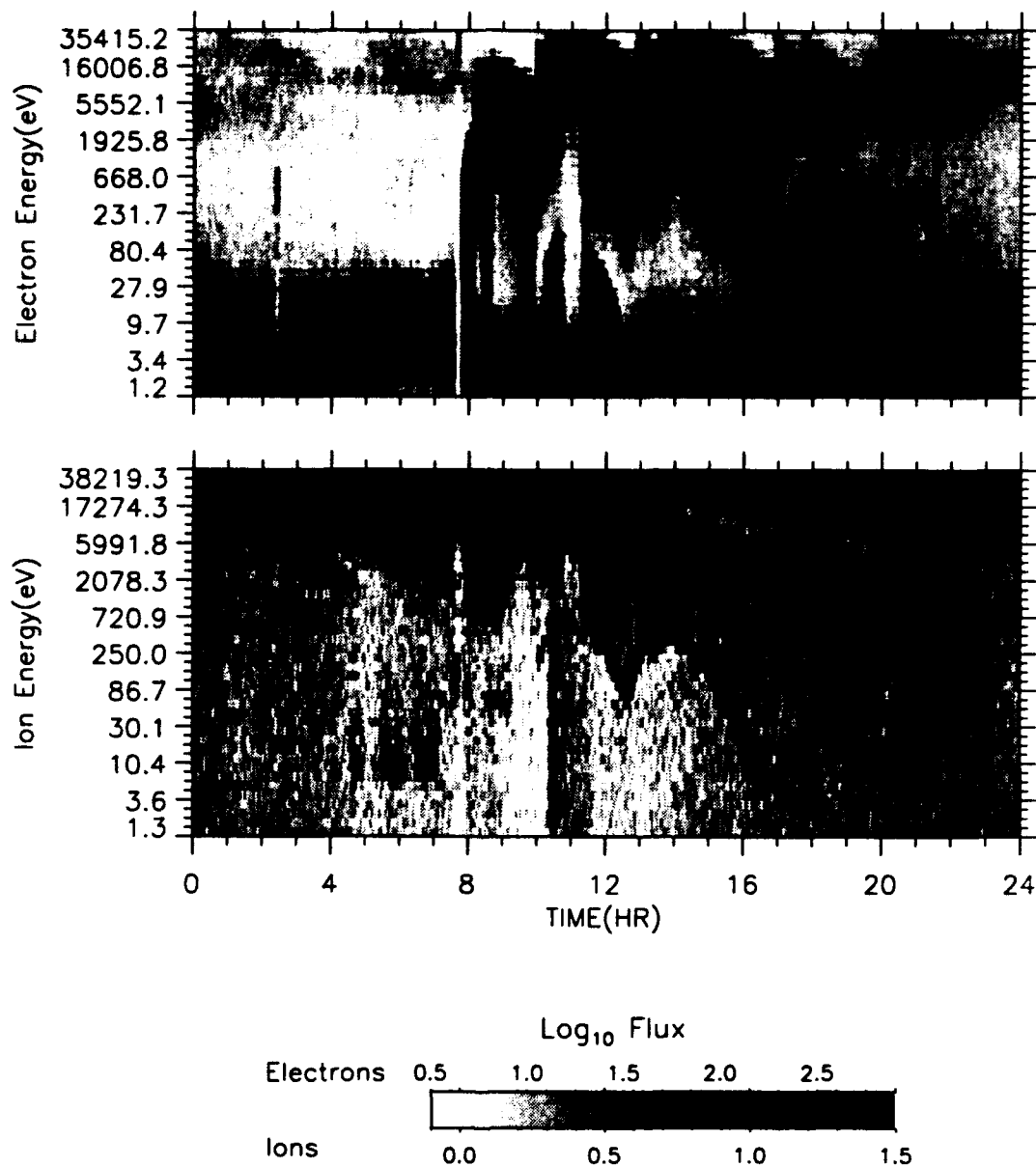
Plot run 27−Jul−1993 17:31:37.00   Naval Postgraduate School

Figure 13 Field Aligned Spectrogram for April 16, 1990

46

Los Alamos National Laboratory Magnetospheric Plasma Analyzer

1989-046   21-APR-1990

Field-Aligned

Log$_{10}$ Flux
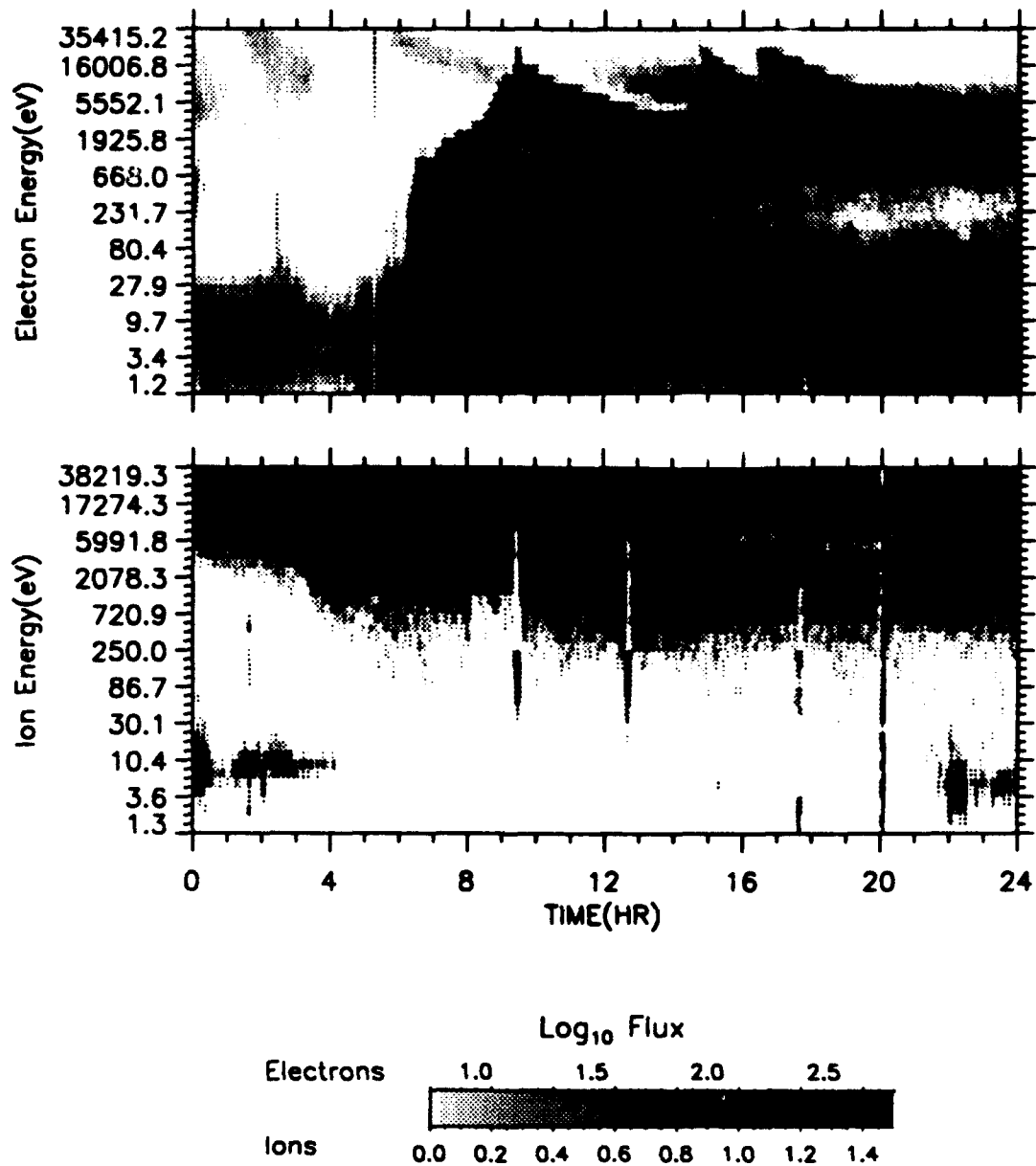
Figure 14   Field Aligned Spectrogram for April 21, 1990

1989−046   10−DEC−1989
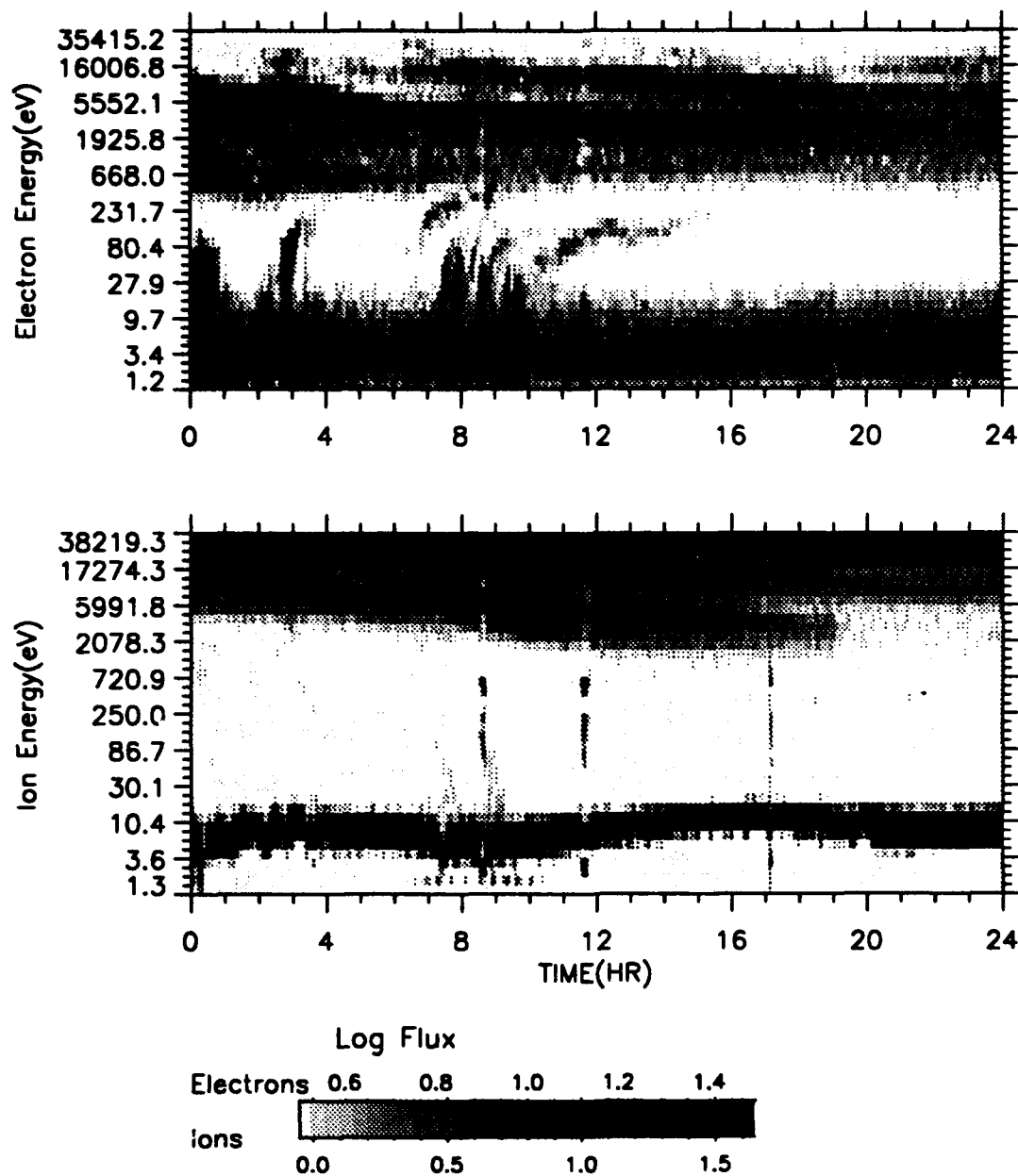
Plot run 27−May−1993 18:25:52.00   Naval Postgraduate School

Figure 15   Energy versus Time Spectrogram, December 10, 1990

48

Los Alamos National Laboratory Magnetospheric Plasma Analyzer

1989-046   15-APR-1990

Field-Aligned

Log₁₀ Flux

Log_{10} Flux

Electrons   0.5   1.0   1.5   2.0   2.5

Ions   0.0   0.5   1.0   1.5
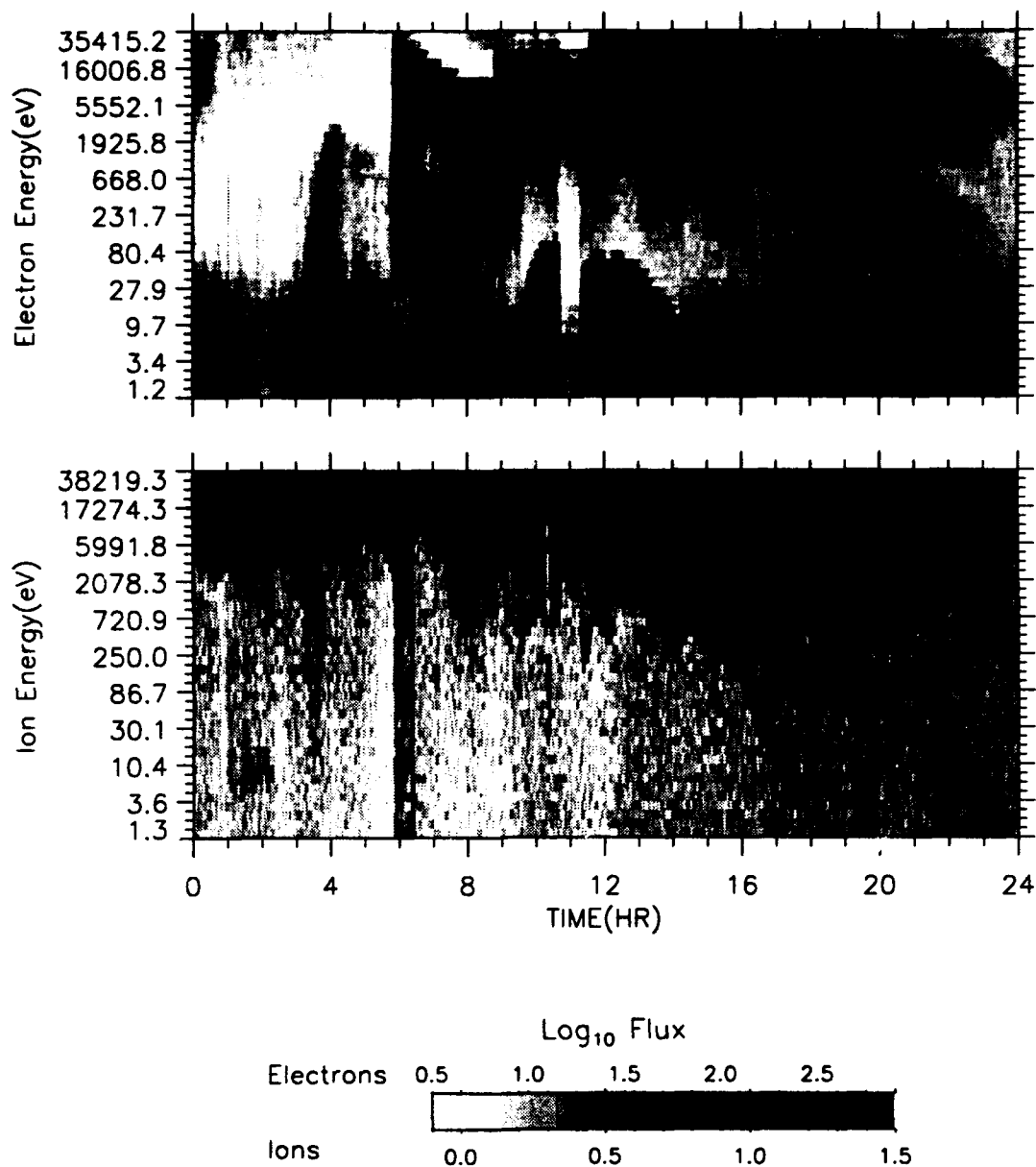
Plot run 16-Jul-1993 15:36:22.00   Naval Postgraduate School

Figure 16   Energy versus Time Spectrogram, April 15, 1990

49

Los Alamos National Laboratory Magnetospheric Plasma Analyzer

1990-095   05-APR-1993

Field-Aligned

Log₁₀ Flux

Electrons 0.5   1.0   1.5   2.0   2.5

Ions   0.0   0.5   1.0   1.5
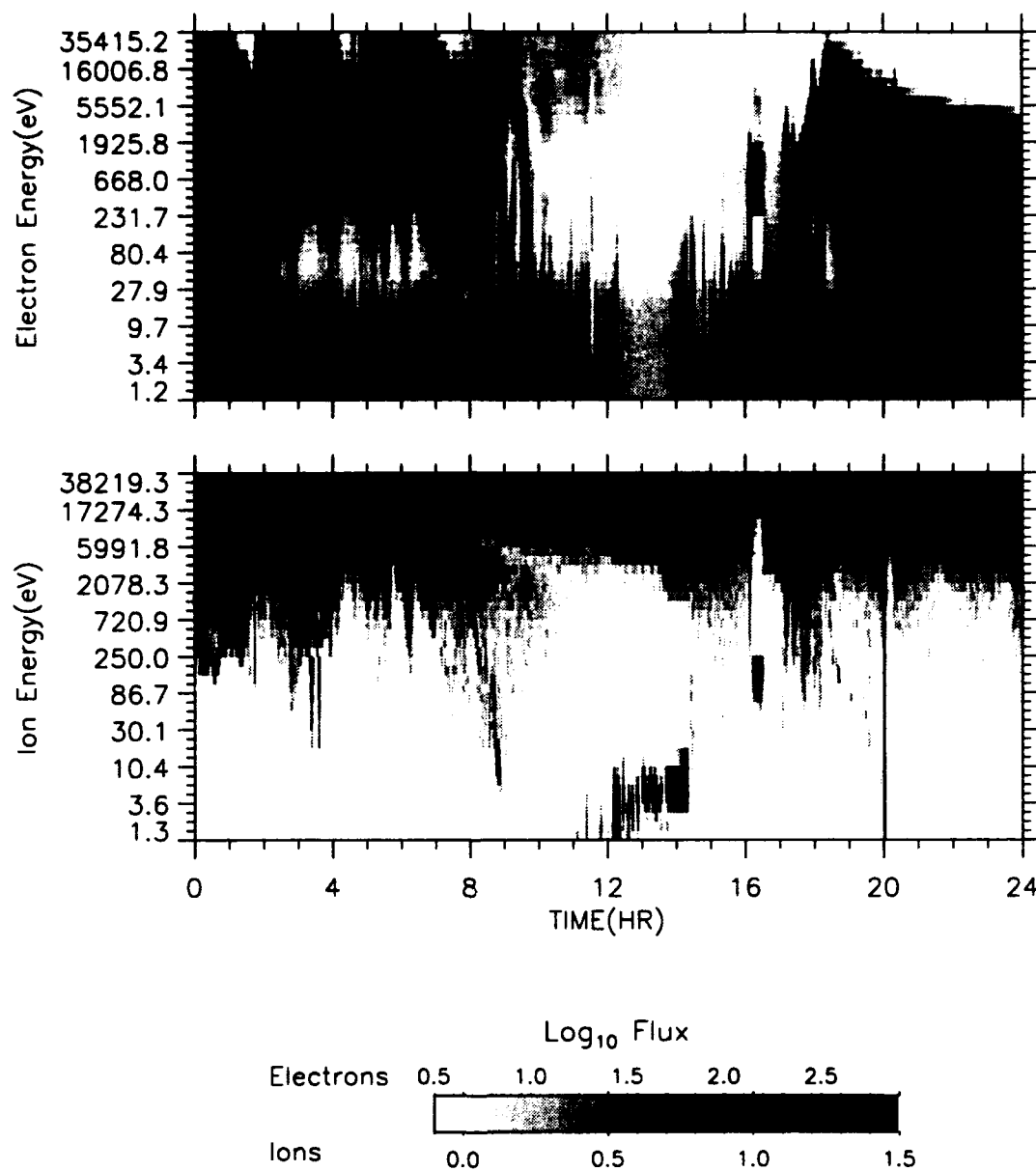
Plot run 27-Aug-1993 14:17:47.00   Naval Postgraduate School

Figure 17   Energy versus Time Spectrogram, April 5, 1990

50
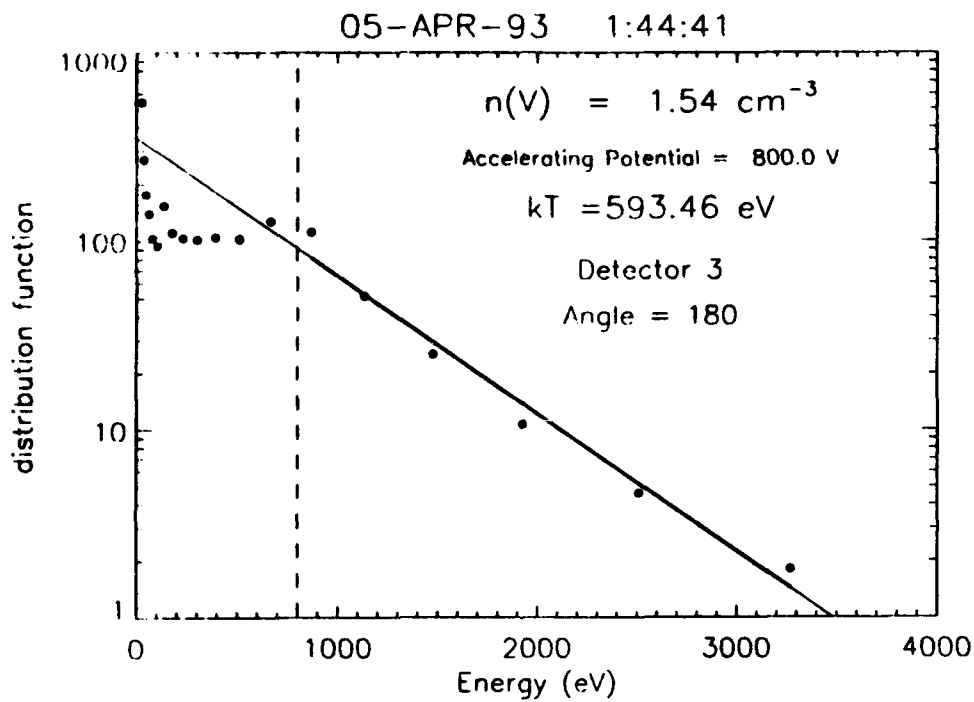
Figure 18 Distribution versus Energy, April 5, 1993

Los Alamos National Laboratory Magnetospheric Plasma Analyzer

1989-046   19-APR-1990

Field-Aligned

Log₁₀ Flux

$$\text{Log}_{10} \text{ Flux}$$

Electrons   0.5   1.0   1.5   2.0   2.5

Ions   0.0   0.5   1.0   1.5
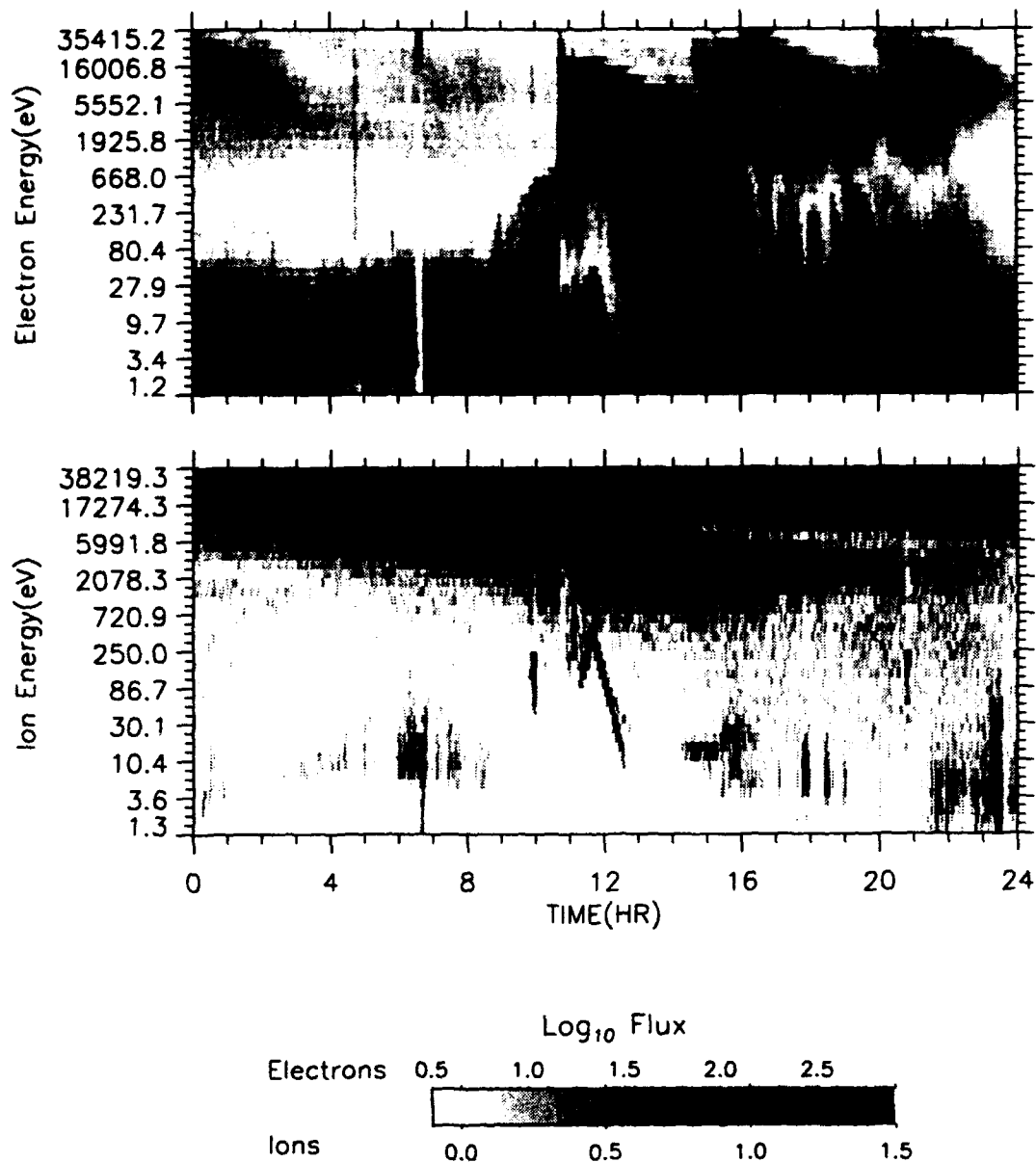
Plot run 19-Aug-1993 10:36:41.00   Naval Postgraduate School

Figure 19   Energy versus Time Spectrogram for April 19, 1990
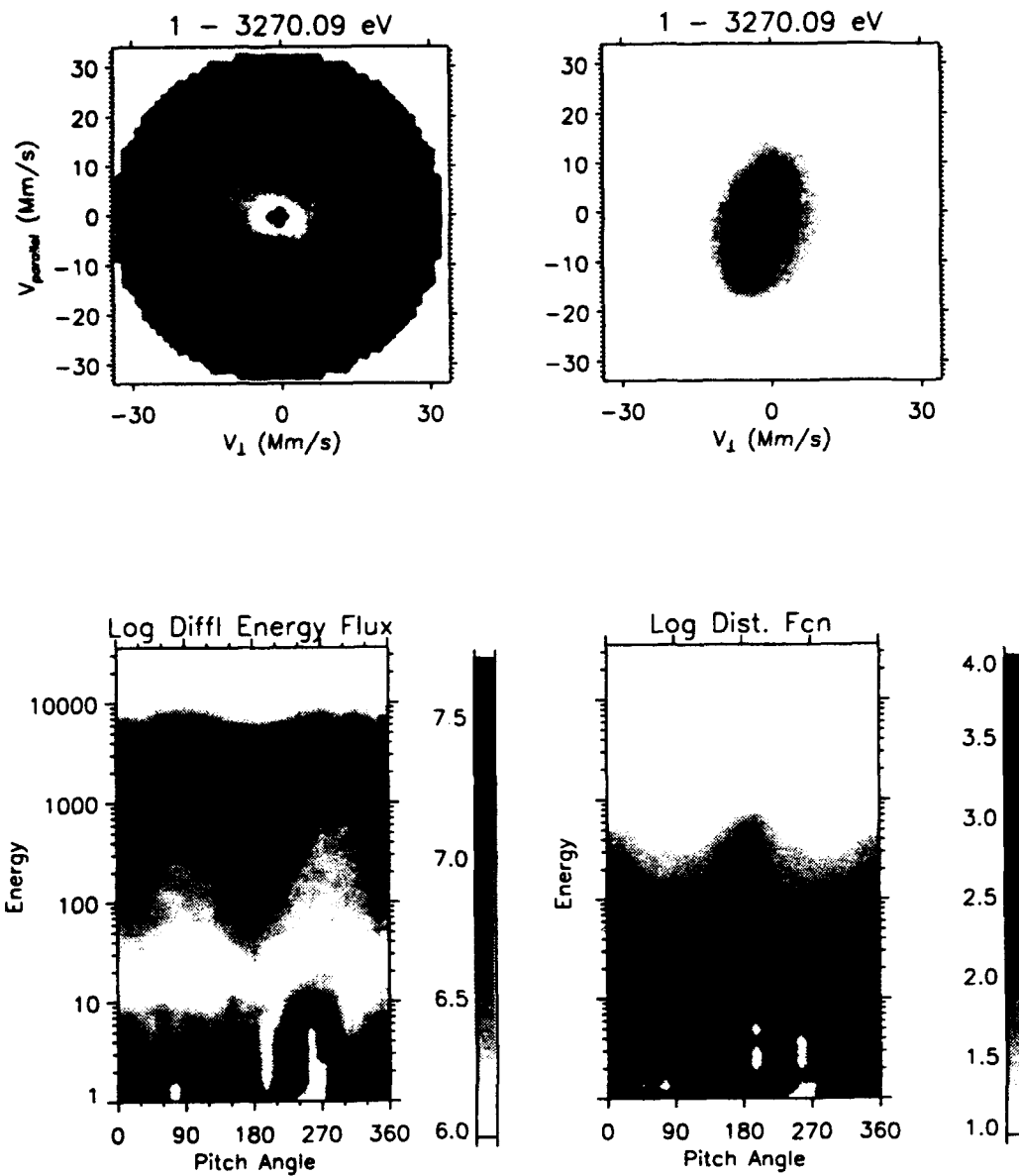
LANL MPA — 1989—046
Detector 3
19—APR—90   10:43:30

1 — 3270.09 eV

1 — 3270.09 eV

Log Diffl Energy Flux

Log Dist. Fcn
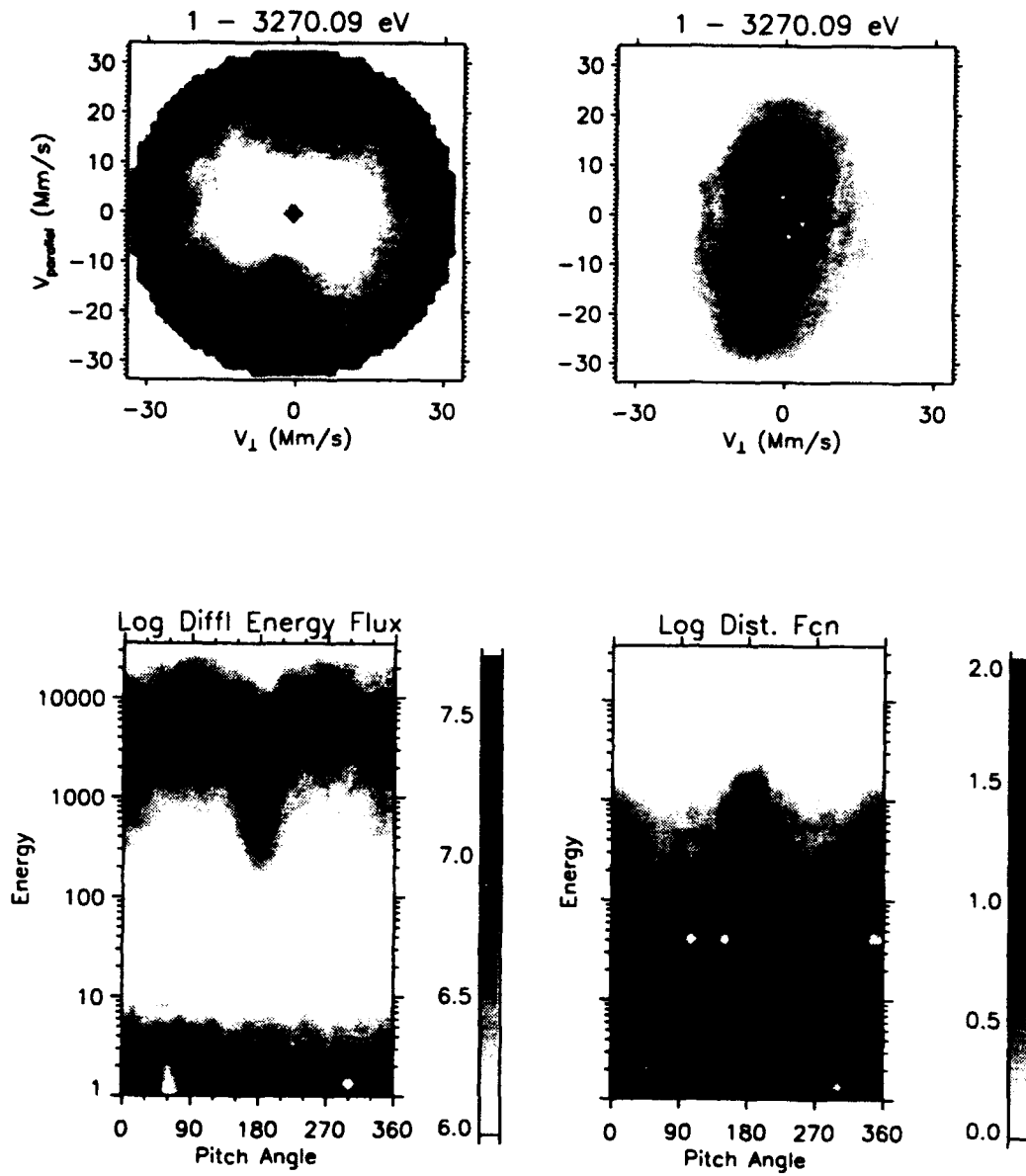
Figure 20   Energy versus Pitch Angle—Detector 3—April 19

53

LANL MPA — 1989—046
Detector 4
19—APR—90   10:43:30

1 — 3270.09 eV

1 — 3270.09 eV

Log Diffl Energy Flux

Log Dist. Fcn
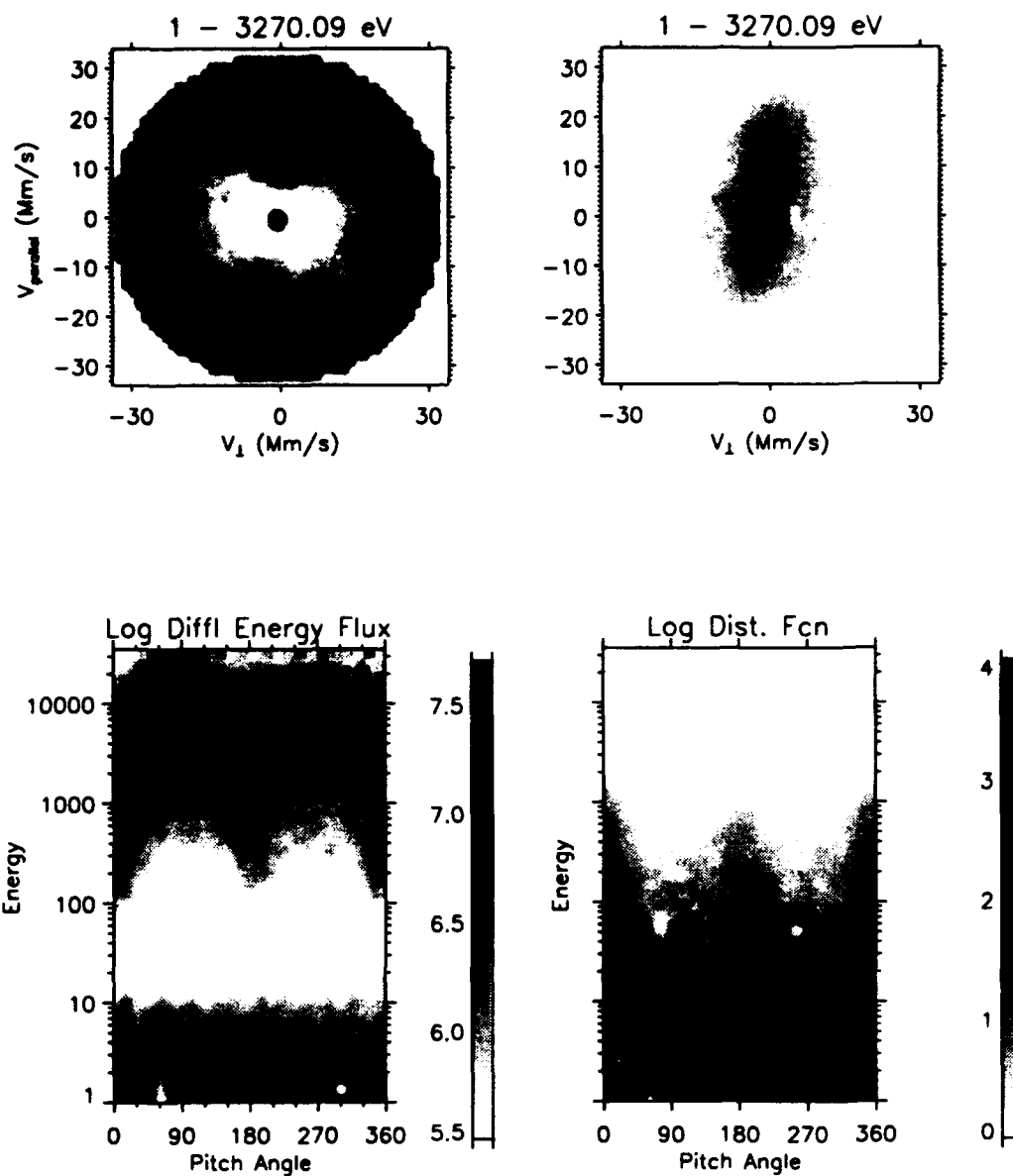
Figure 21 Energy versus Pitch Angle--Detector 4--April 19

54
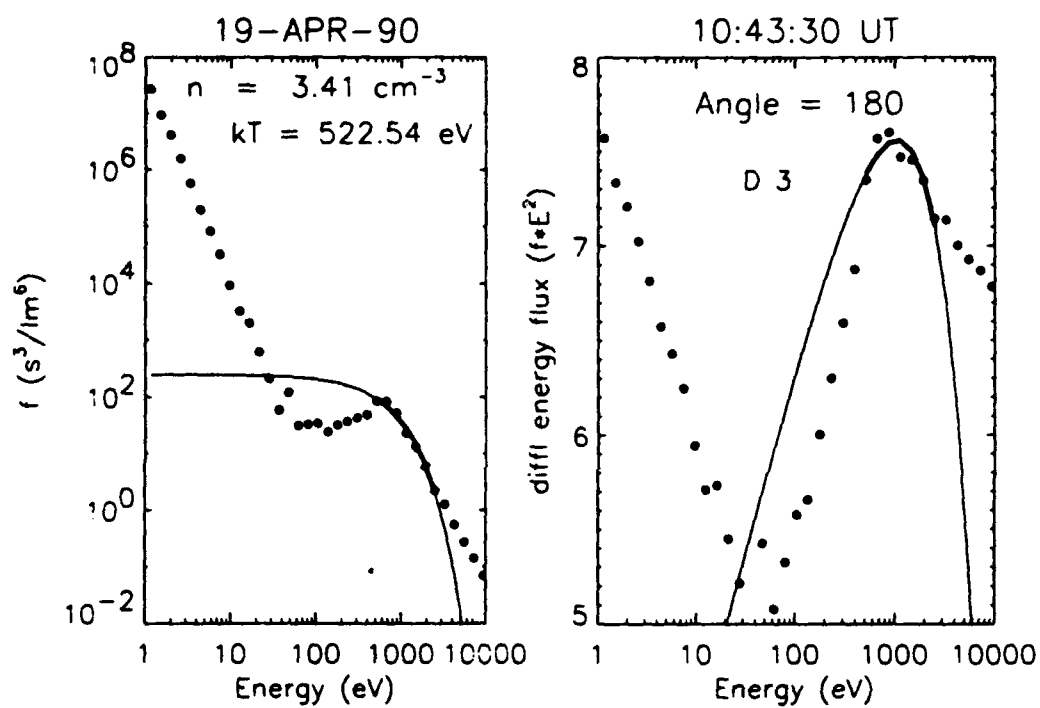
Figure 22   Distribution versus Energy--Detector 3--April 19

55
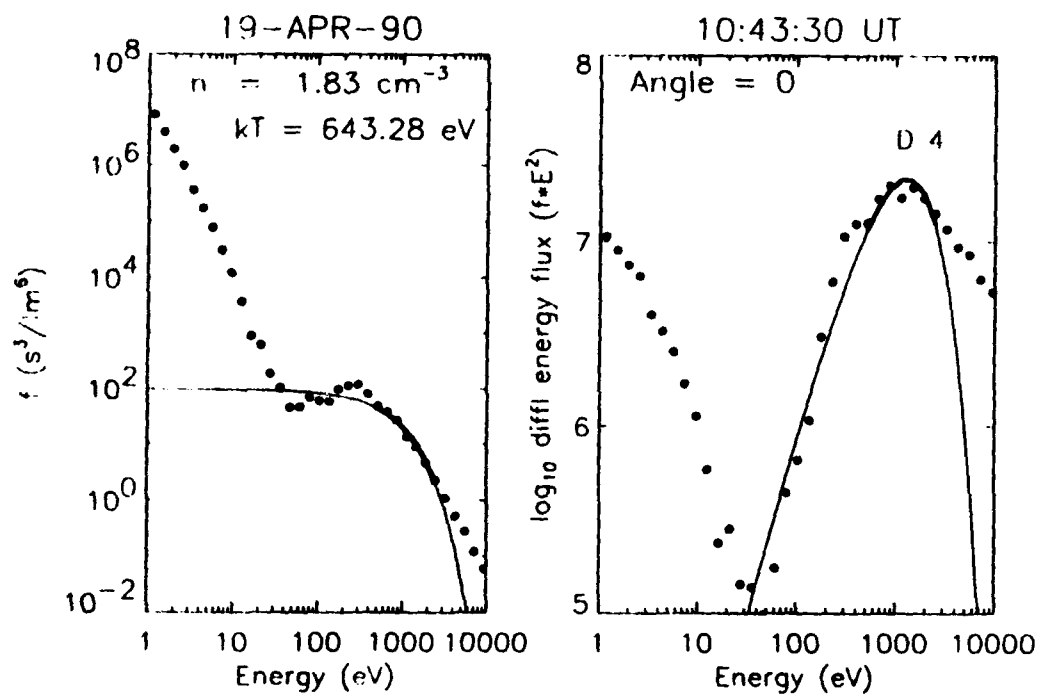
Figure 23   Distribution versus Energy--Detector 4--April 19
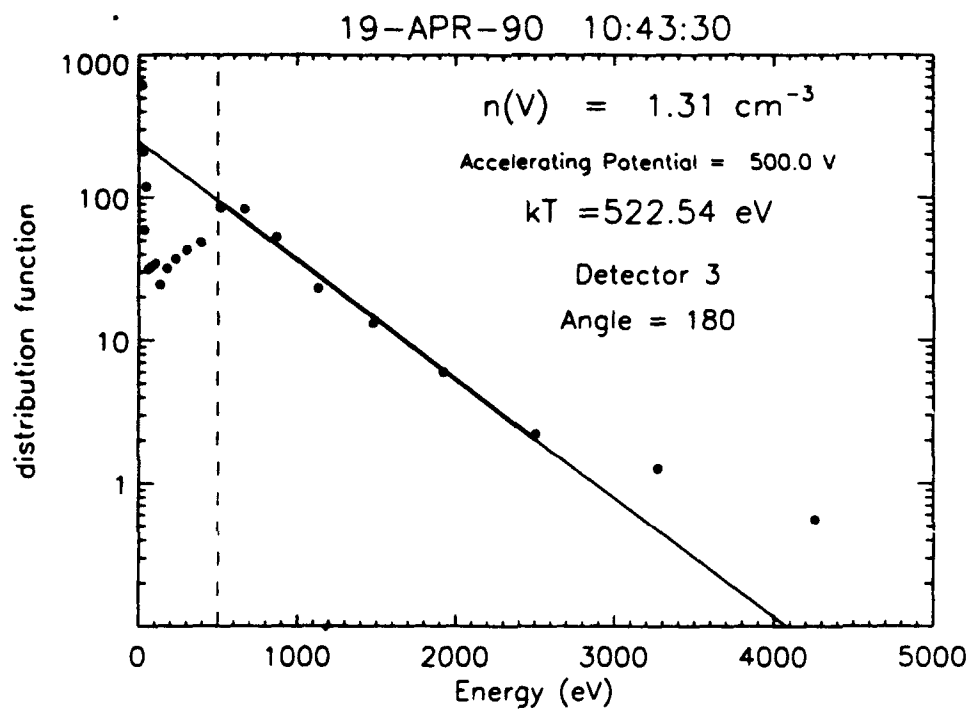
**Figure 24 Distribution versus Energy--Detector 3--April 19
Corrected Density Calculation**

57
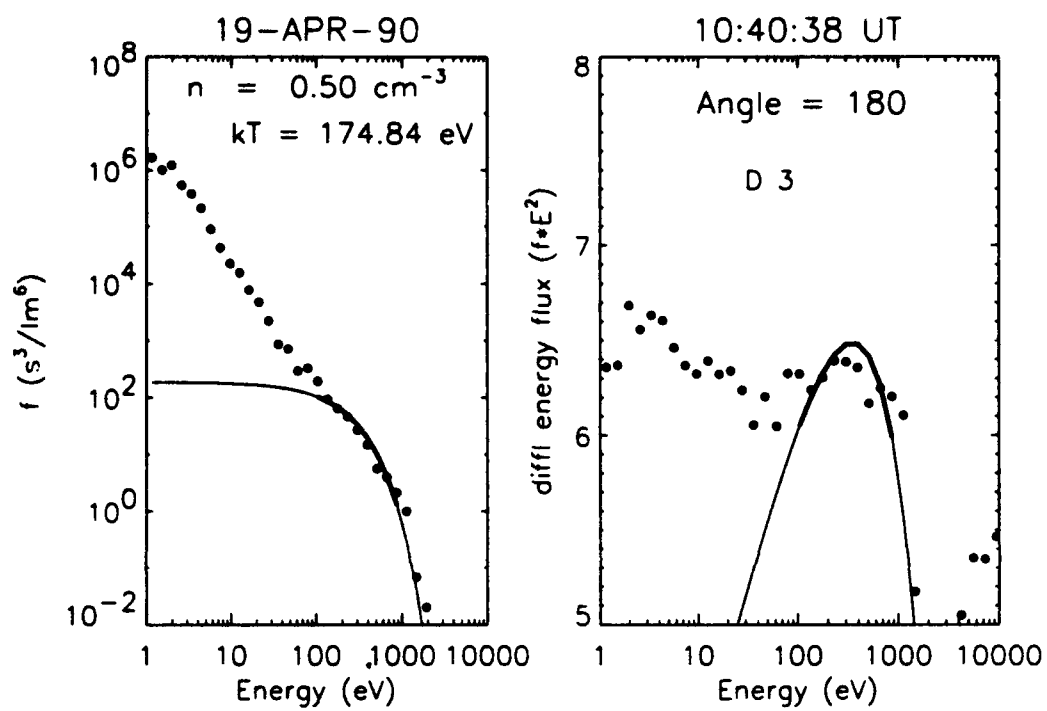
Figure 25 Distribution versus Energy--April 19--10:40:38 UT
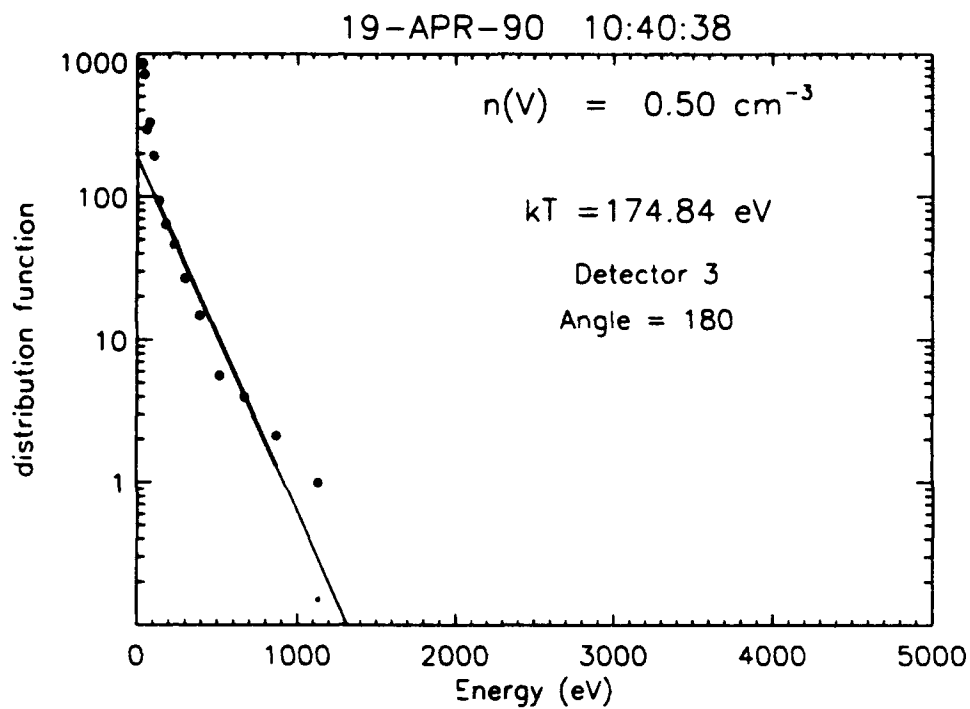
Figure 26   Distribution versus Energy--April 19--10:40:38 UT
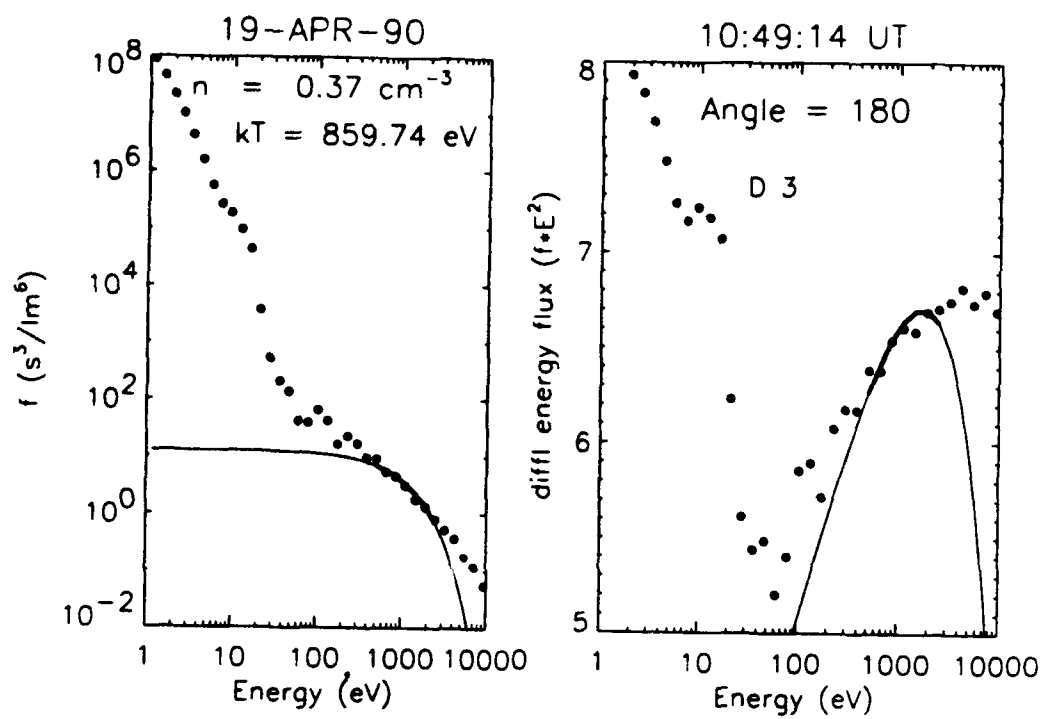
Figure 27 Distribution versus Energy--April 19--10:49:14 UT
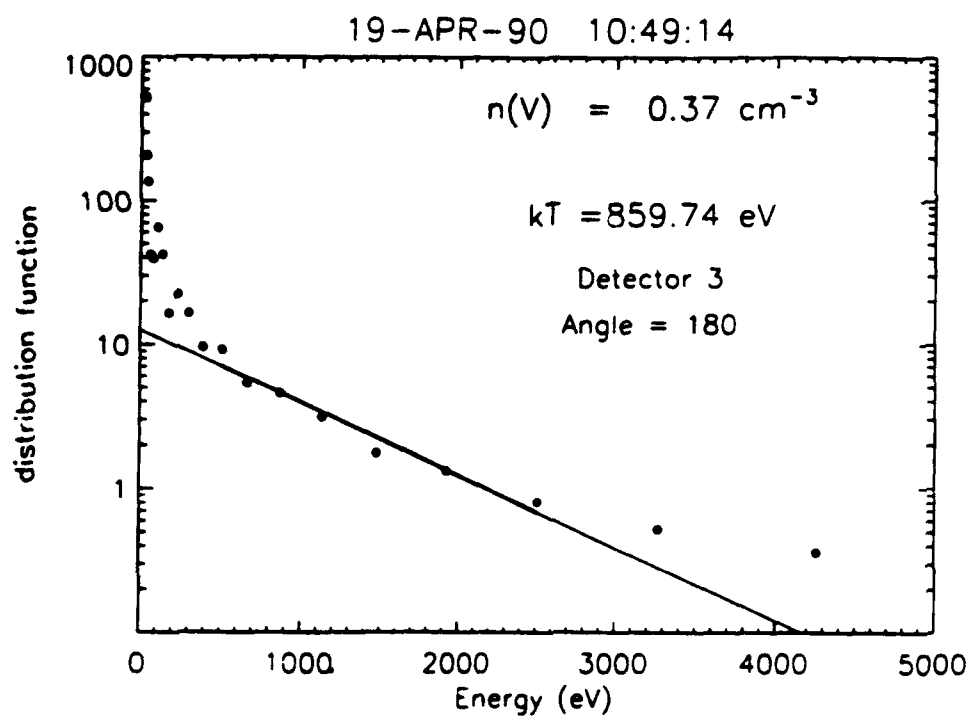
Figure 28 Distribution versus Energy--April 19--10:49:14 UT

61

Los Alamos National Laboratory Magnetospheric Plasma Analyzer

1989-046   18-APR-1990

Field-Aligned

Log₁₀ Flux

Electrons   0.5   1.0   1.5   2.0   2.5

Ions   0.0   0.5   1.0   1.5
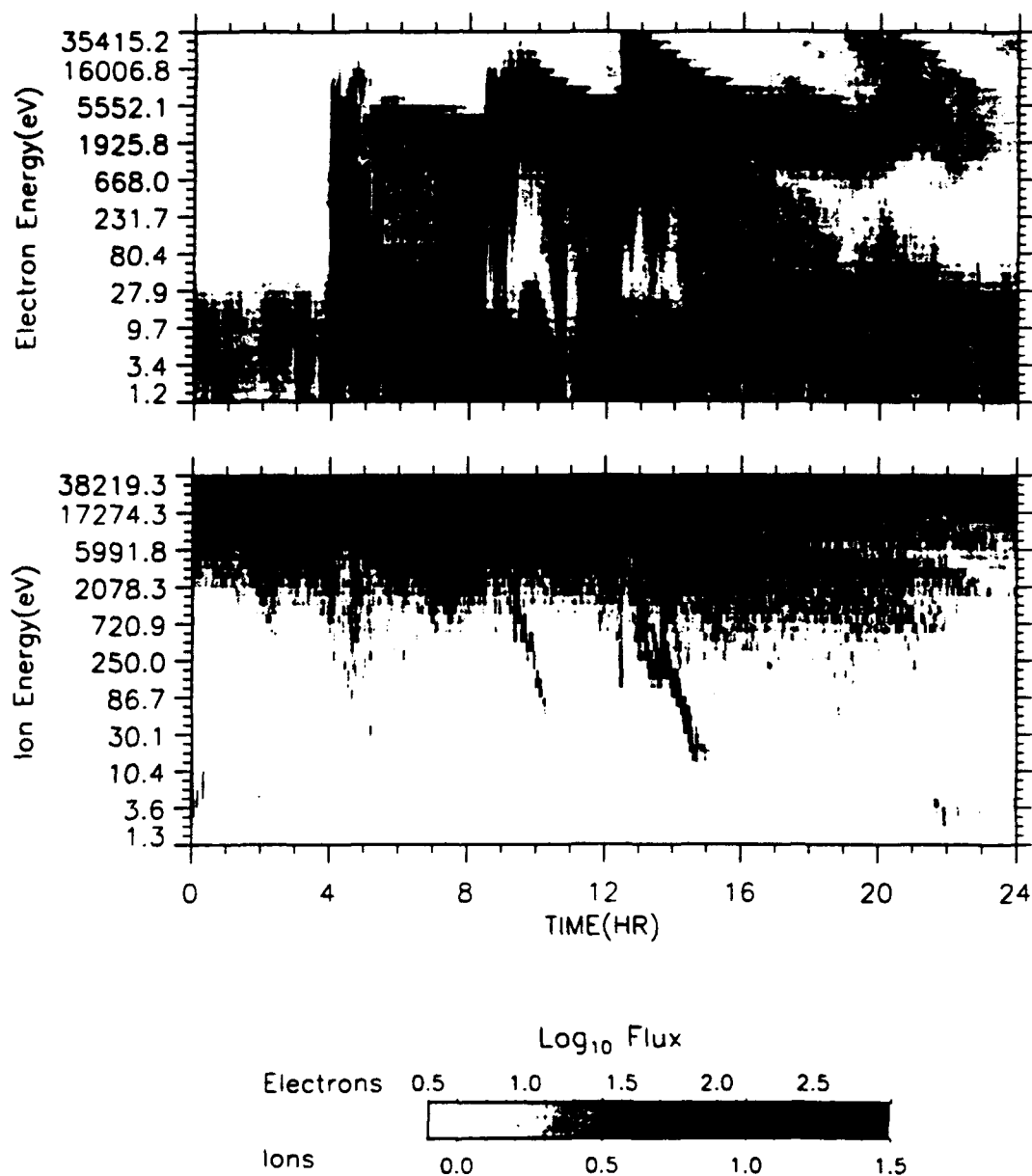
Plot run 19-Aug-1993 10:34:35.00   Naval Postgraduate School

Figure 29   Energy versus Time Spectrogram for April 18, 1990

62

LANL MPA – 1989–046
Detector 3
18–APR–90   8:43:43

1 – 3270.09 eV

1 – 3270.09 eV

Log Diffl Energy Flux

Log Dist. Fcn

Figure 30   Energy versus Pitch Angle--April 18--08:43:43
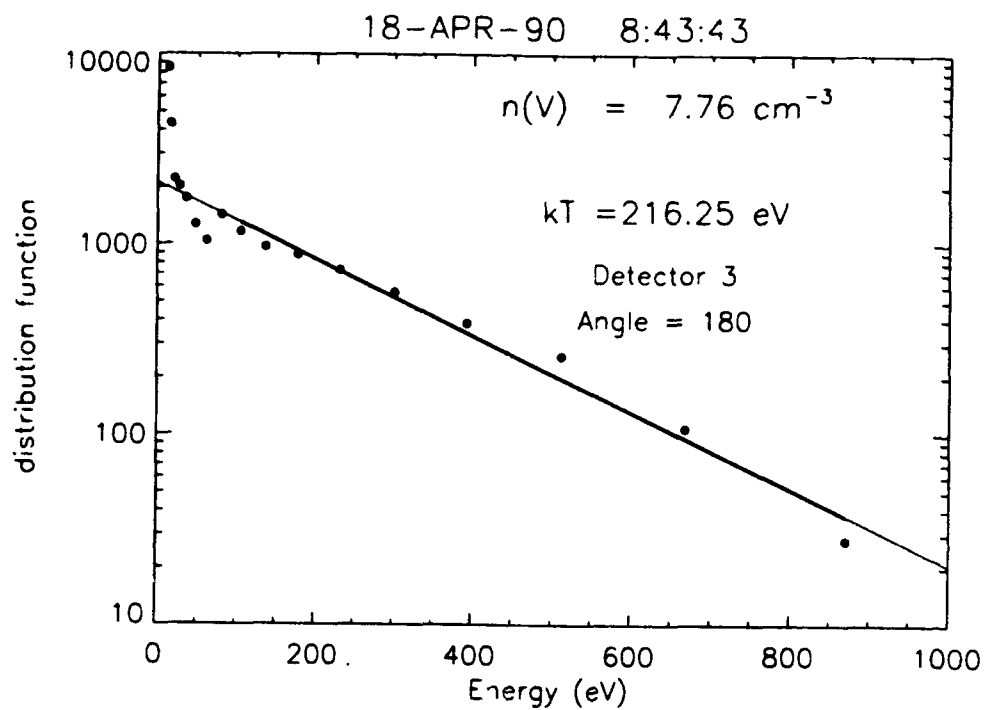
Figure 31   Distribution versus Energy--April 18--08:43:43

64

LANL MPA – 1989–046
Detector 3
18–APR–90   8:46:35
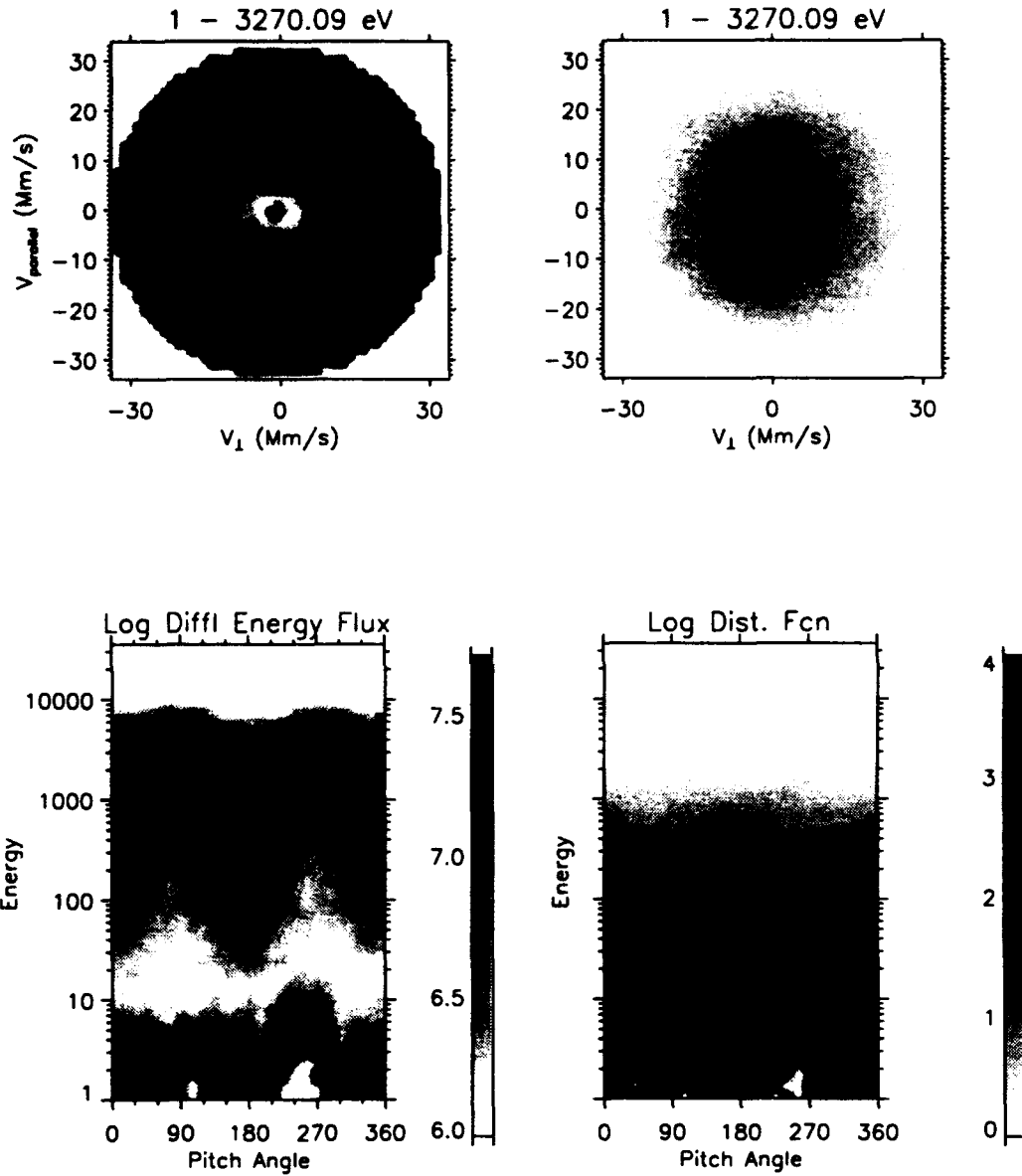
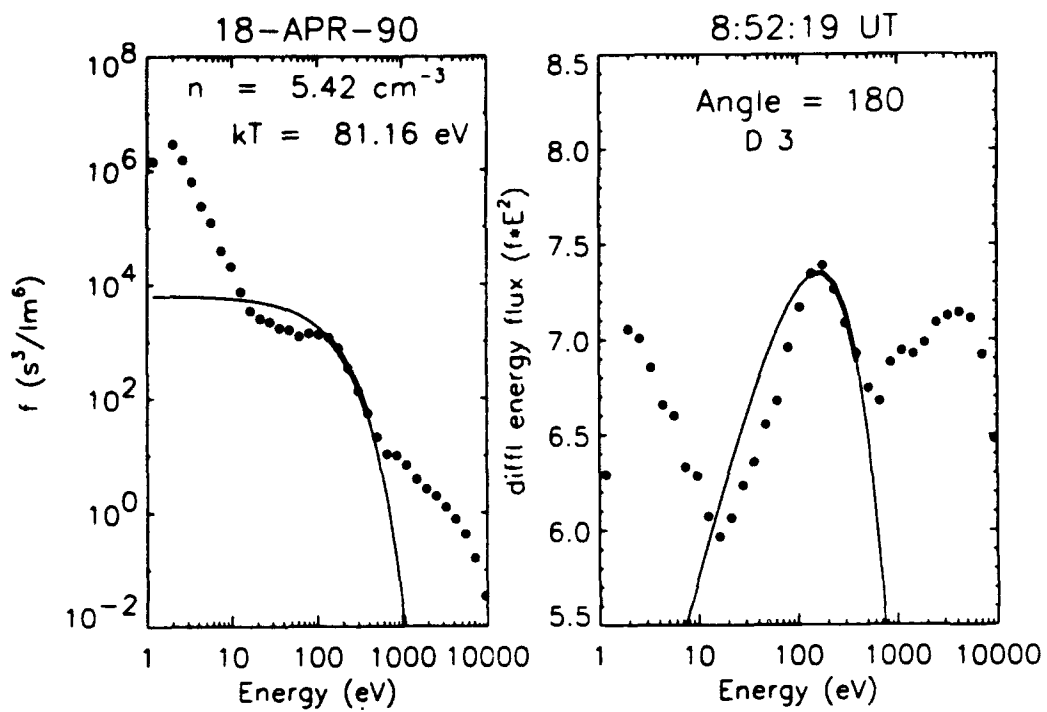Figure 32   Energy versus Pitch Angle--April 18--08:46:35

65
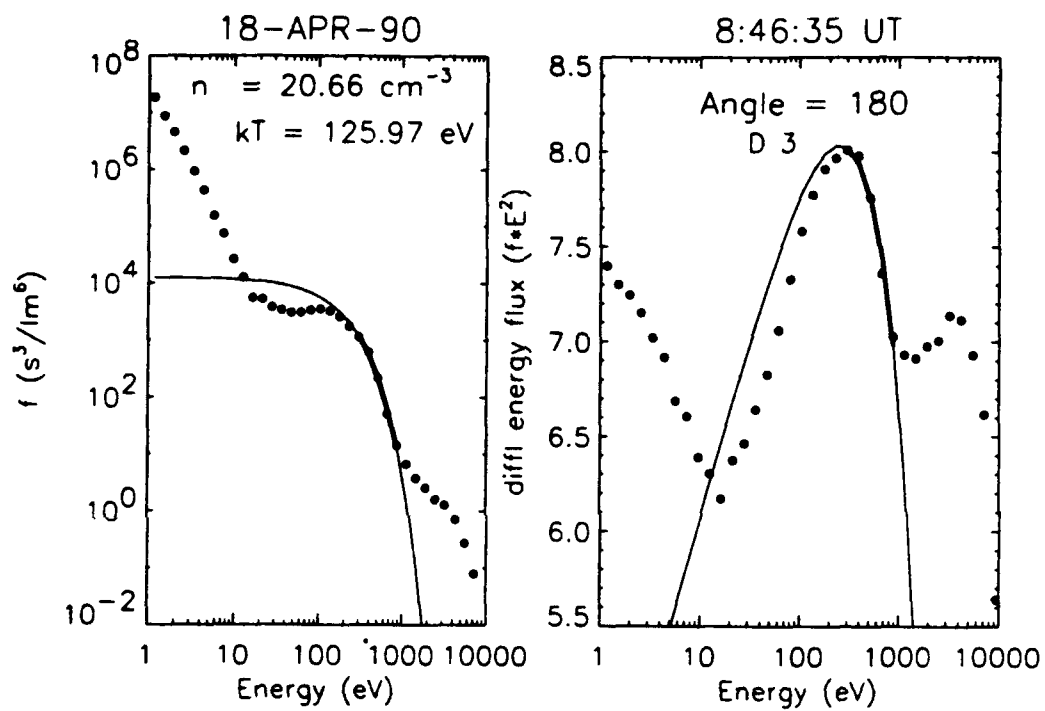
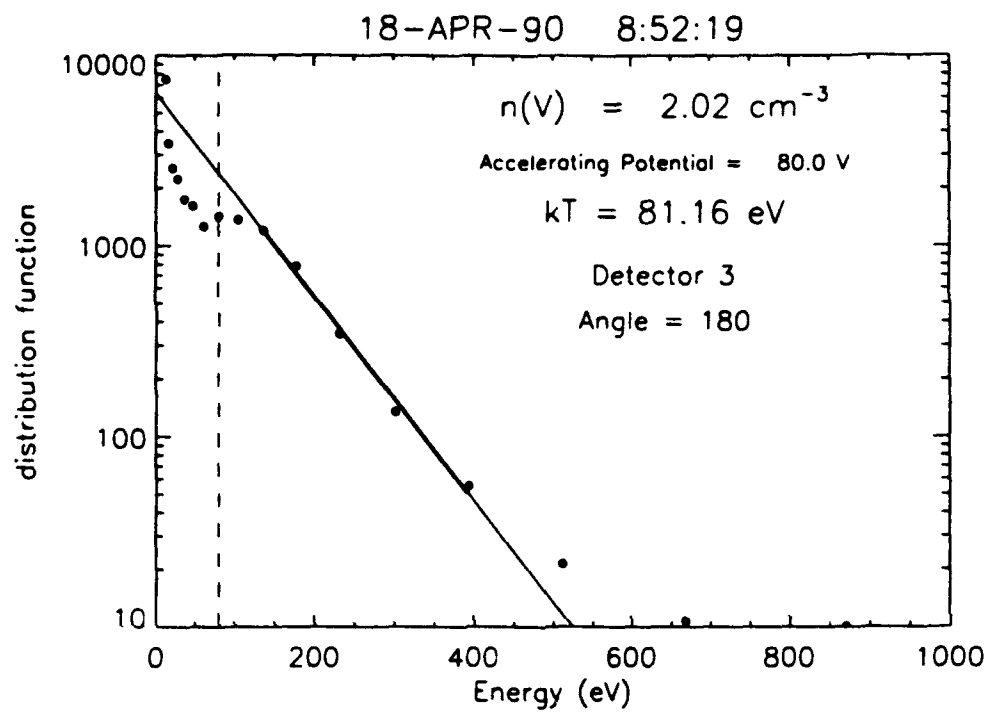**Figure 33 Distribution versus Energy--April 18--08:46:35**

18–APR–90   8:46:35

n(V) = 9.34 cm^{-3}

Accelerating Potential = 100.0 V

kT = 125.97 eV

Detector 3

Angle = 180

distribution function
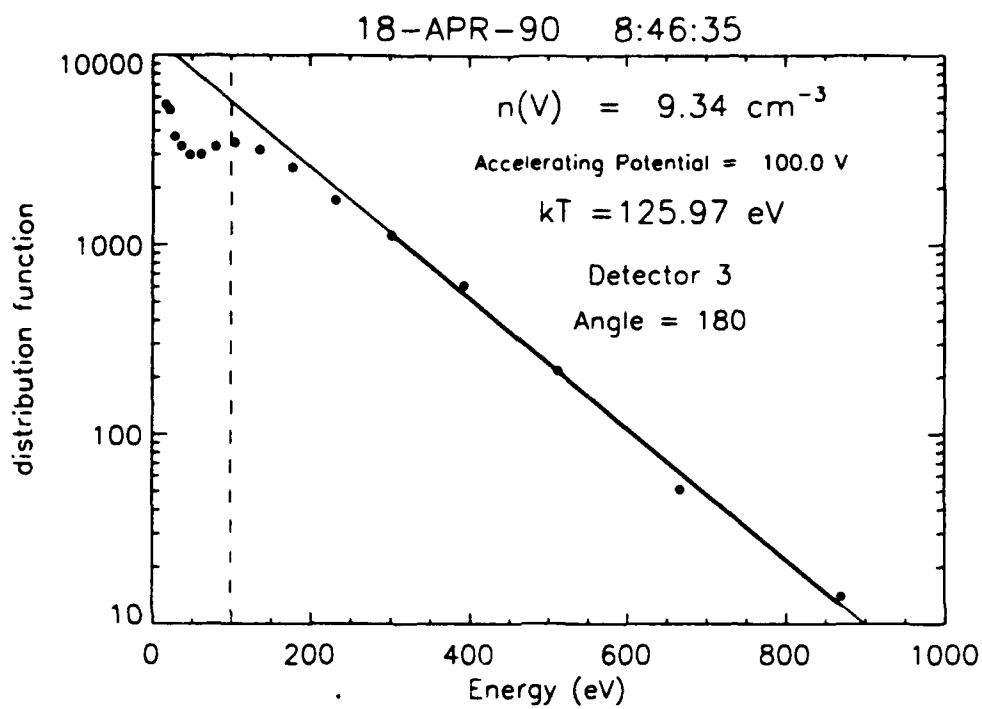
Energy (eV)

Figure 34   Distribution versus Energy--April 18--08:46:35

67

LANL MPA — 1989-046
Detector 3
18-APR-90   8:49:27

1 — 3270.09 eV

1 — 3270.09 eV

Log Diffl Energy Flux

Log Dist. Fcn
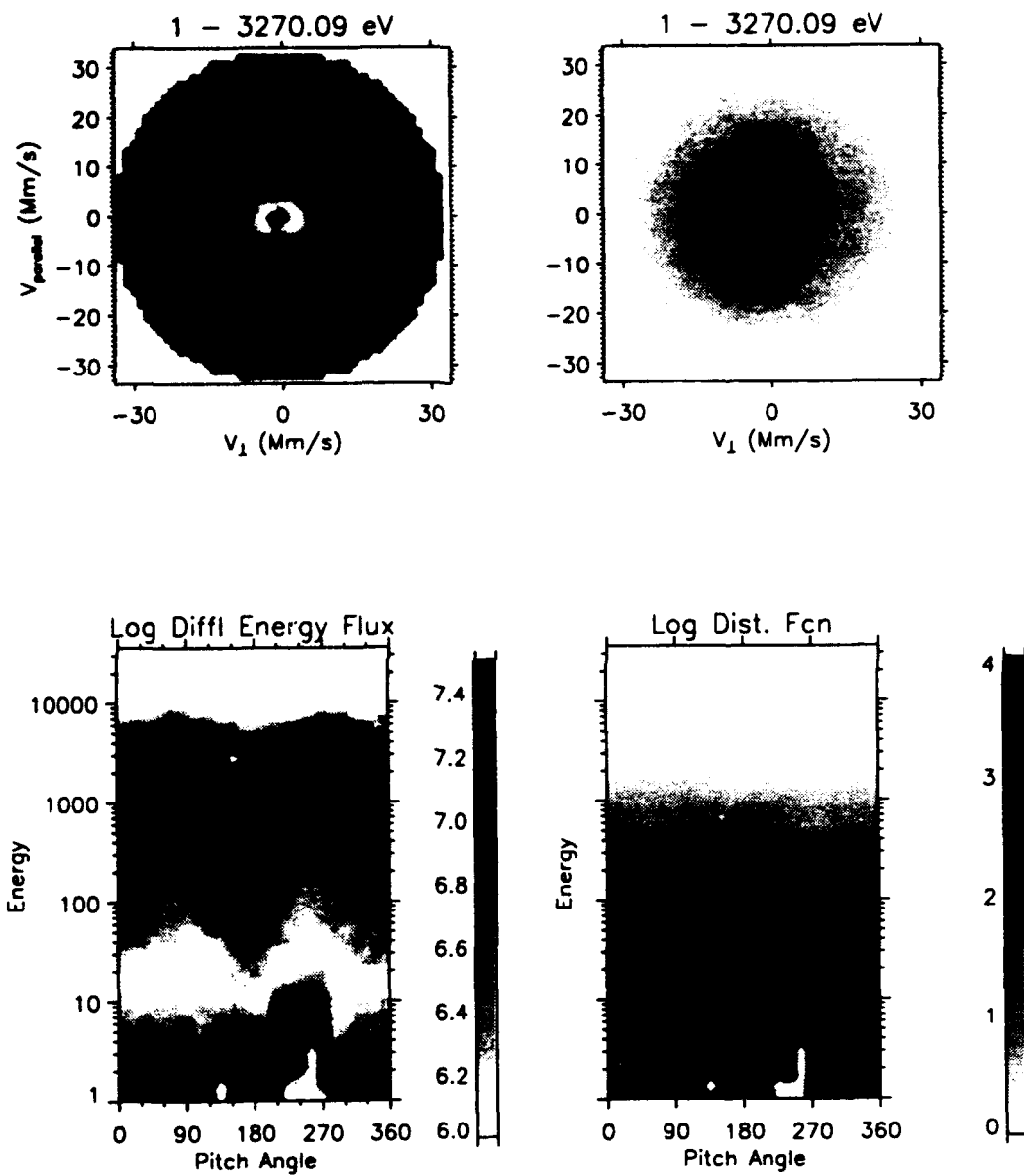
Figure 35   Energy versus Pitch Angle--April 18--08:49:27
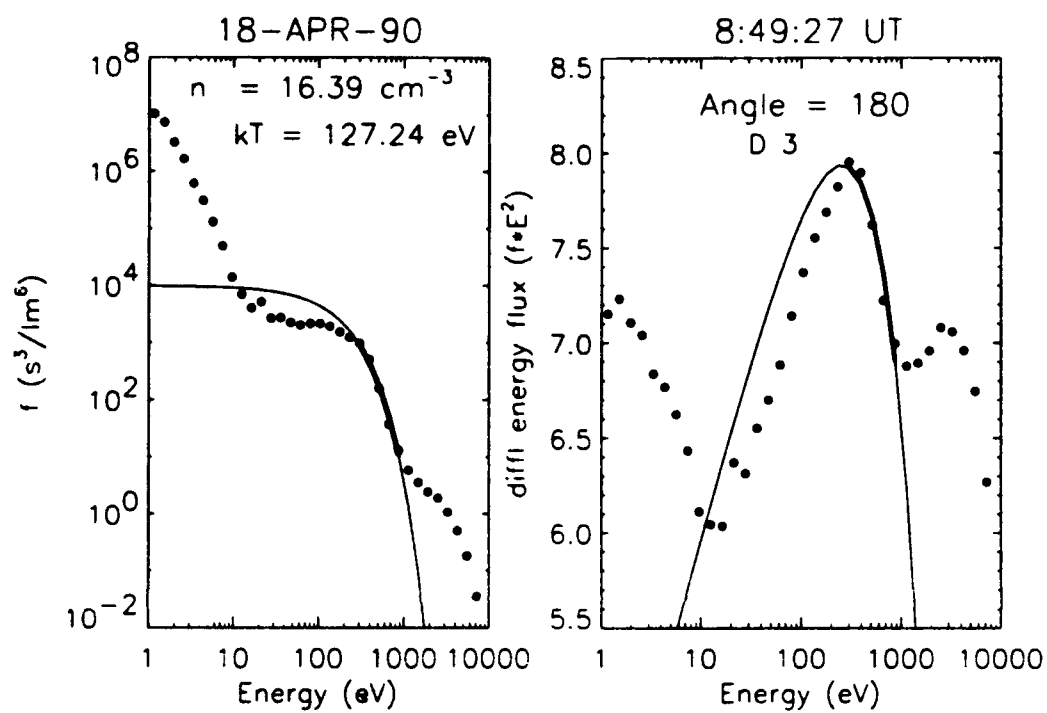
Figure 36   Distribution versus Energy--April 18--08:49:27
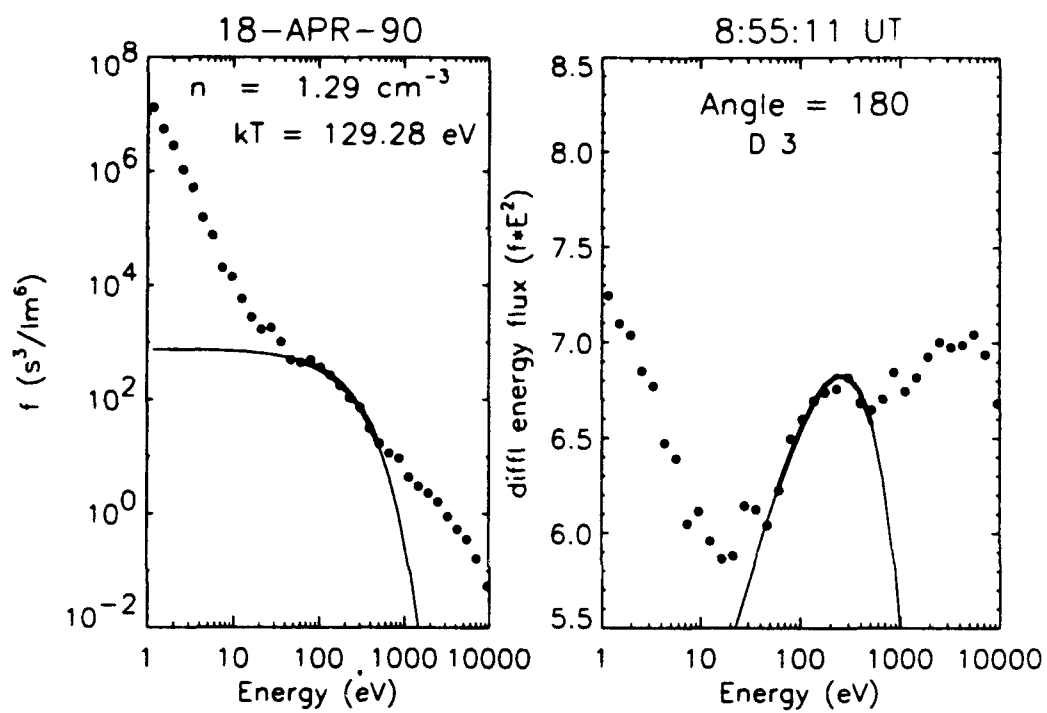
69
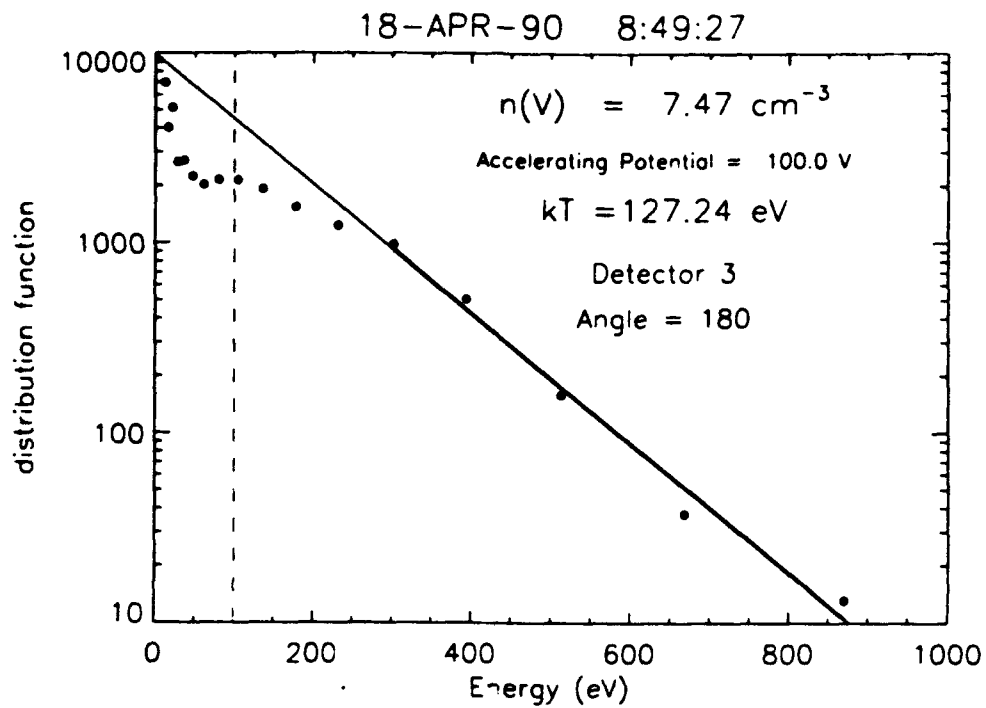
Figure 37 Distribution versus Energy--April 18--08:49:27

LANL MPA – 1989–046
Detector 3
18–APR–90   8:52:19
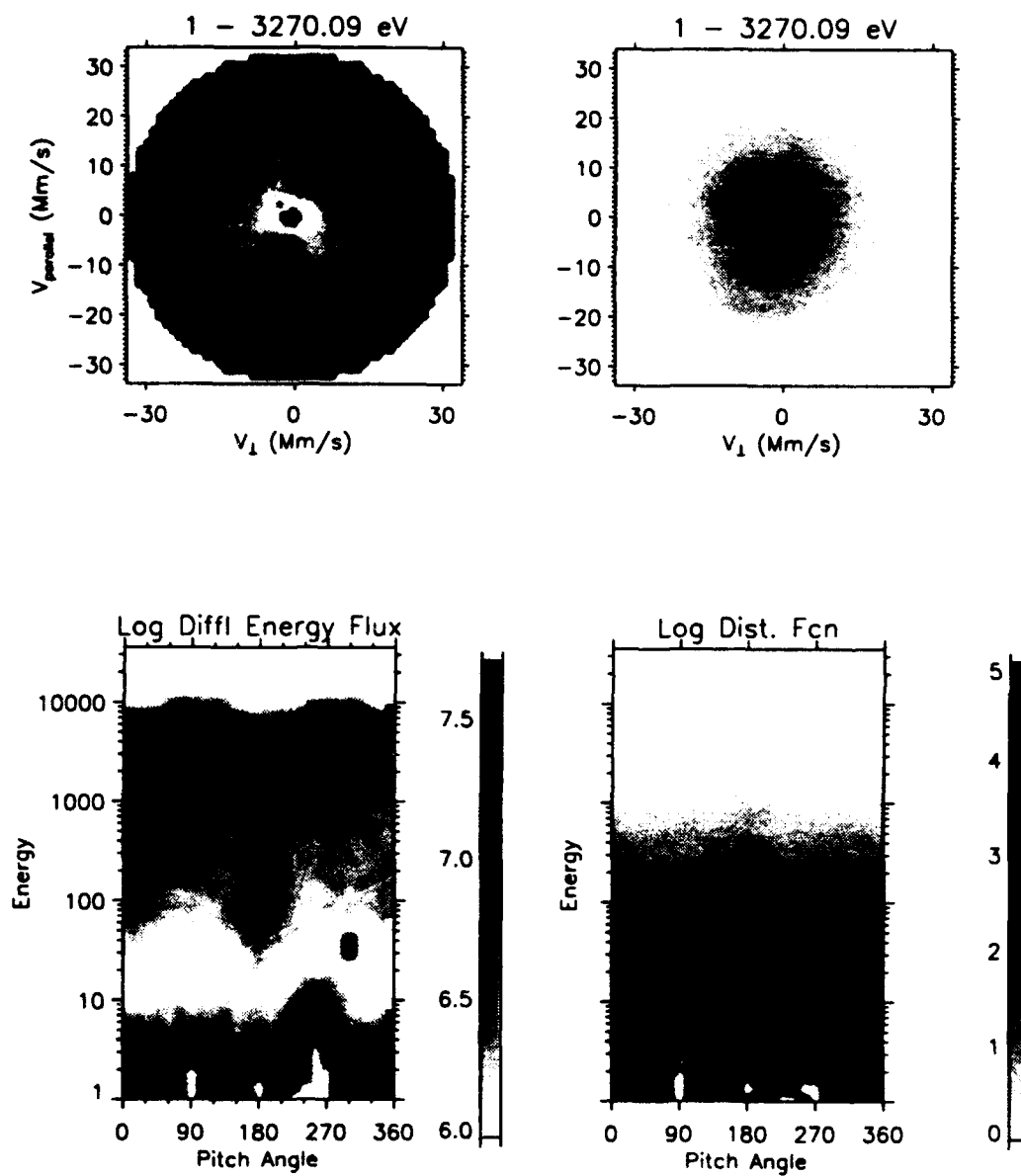
Figure 38 Energy versus Pitch Angle--April 18--08:52:19

71

Figure 39   Distribution versus Energy--April 18--08:52:19

18–APR–90   8:52:19

$n(V) = 2.02$ cm^{-3}

Accelerating Potential = 80.0 V

kT = 81.16 eV

Detector 3

Angle = 180

Figure 40   Distribution versus Energy--April 18--08:52:19

73

Figure 41   Distribution versus Energy--April 18--08:55:11
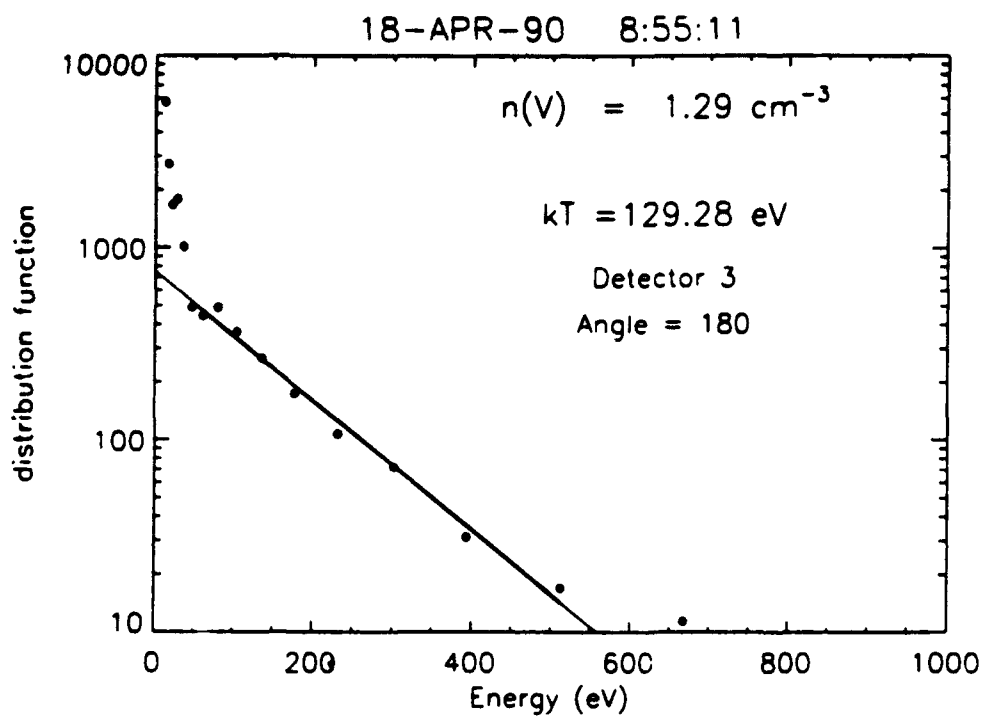
Figure 42 Distribution versus Energy--April 18--08:55:11

Los Alamos National Laboratory Magnetospheric Plasma Analyzer

1989−046   12−APR−1990

Field−Aligned

Log₁₀ Flux

Electrons   0.5   1.0   1.5   2.0   2.5

Ions   0.0   0.5   1.0   1.5
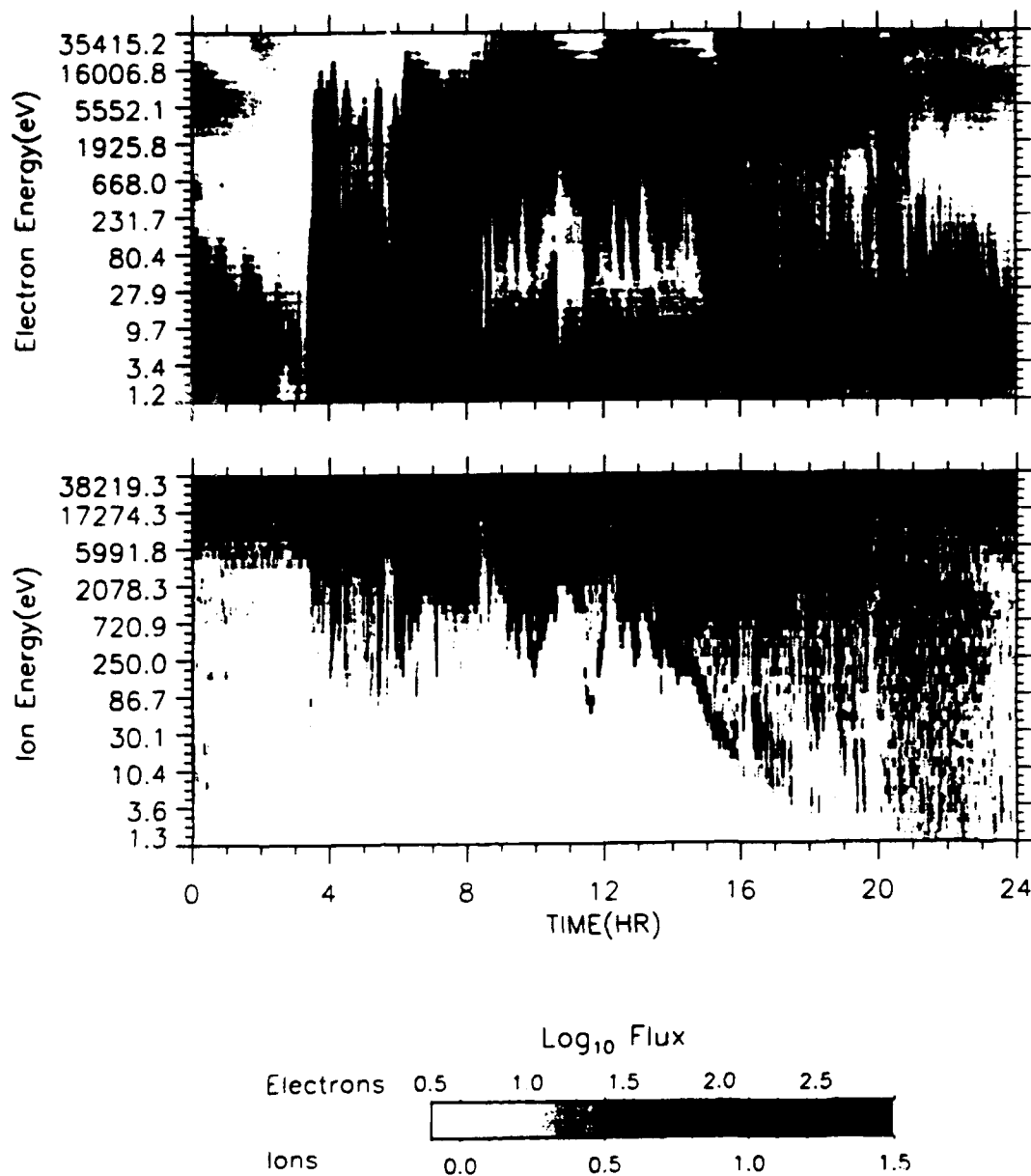
Plot run 22−Sep−1993 17:24:09.00   Naval Postgraduate School

Figure 43   Energy versus Time Spectrogram for April 12, 1990

76

LANL MPA – 1989–046
Detector 3
12–APR–90   5:21:08

1 – 3270.09 eV

1 – 3270.09 eV

Log Diffl Energy Flux

Log Dist. Fcn
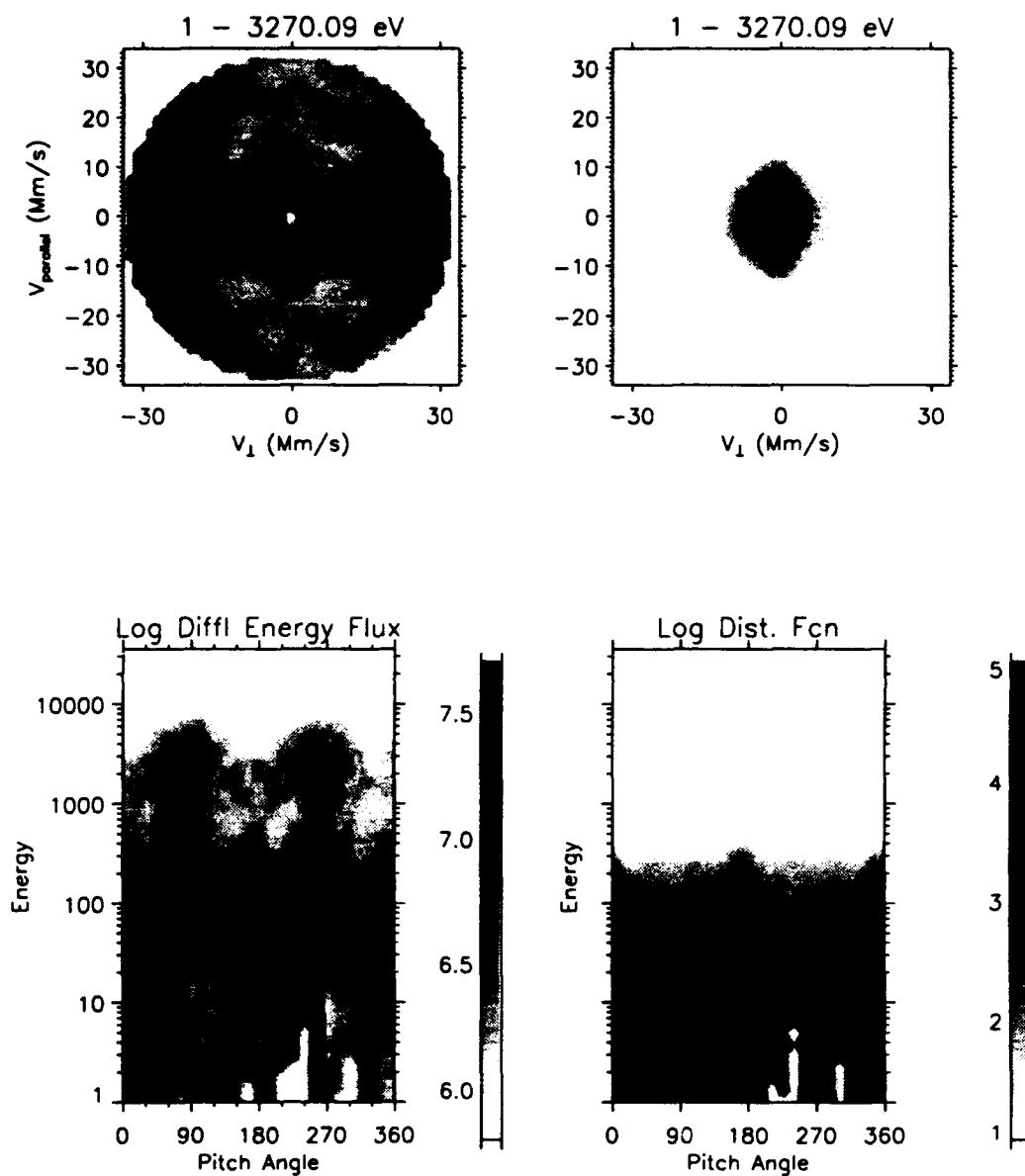
Figure 44   Energy versus Pitch Angle—April 12—05:21:08
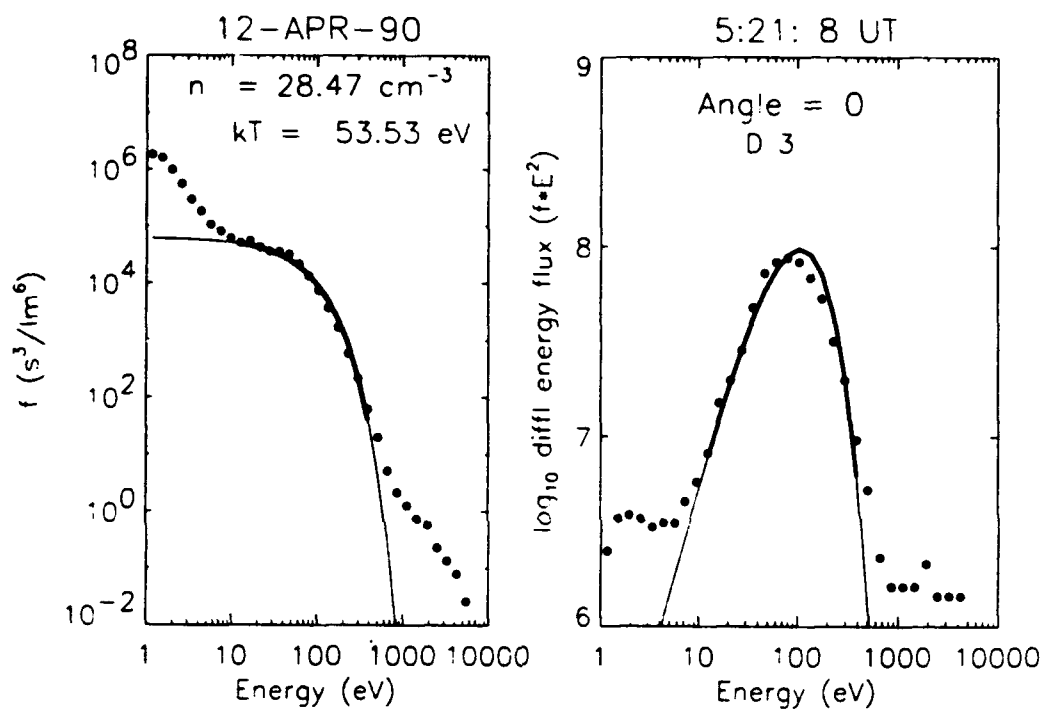
Figure 45   Distribution versus Energy--April 12--05:21:08
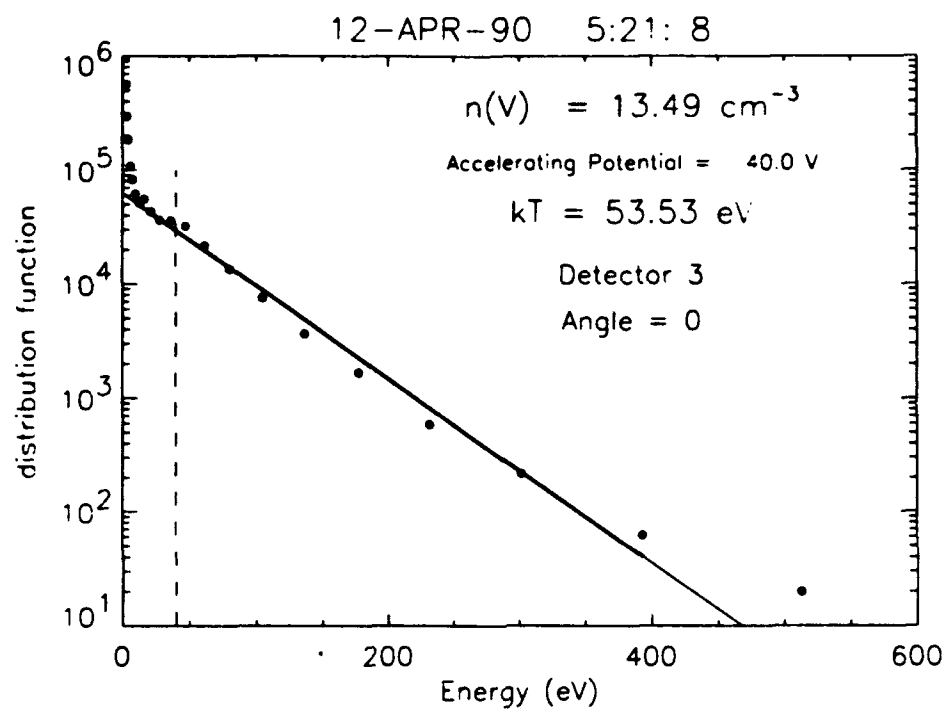
Figure 46   Distribution versus Energy--April 12--05:21:08

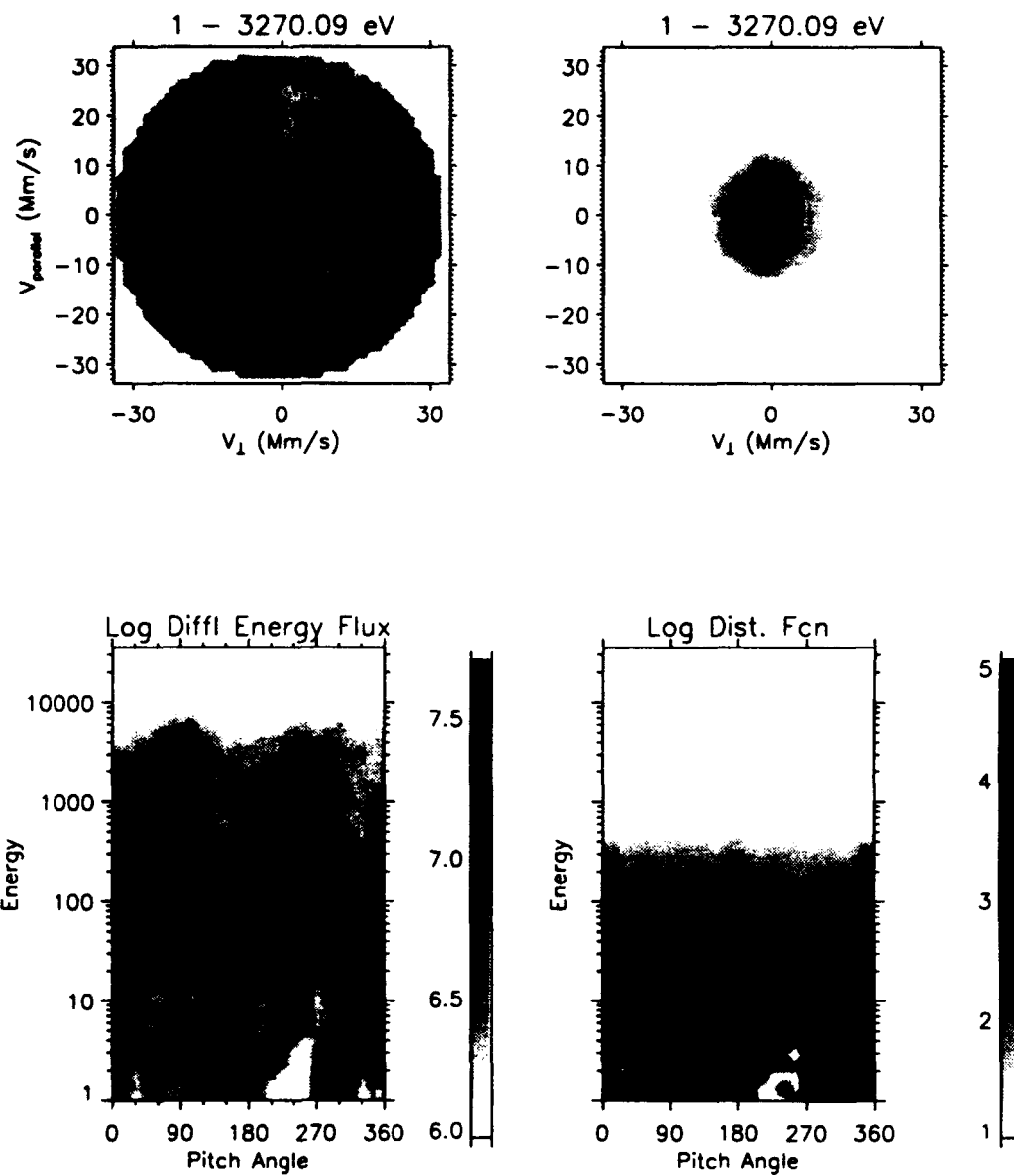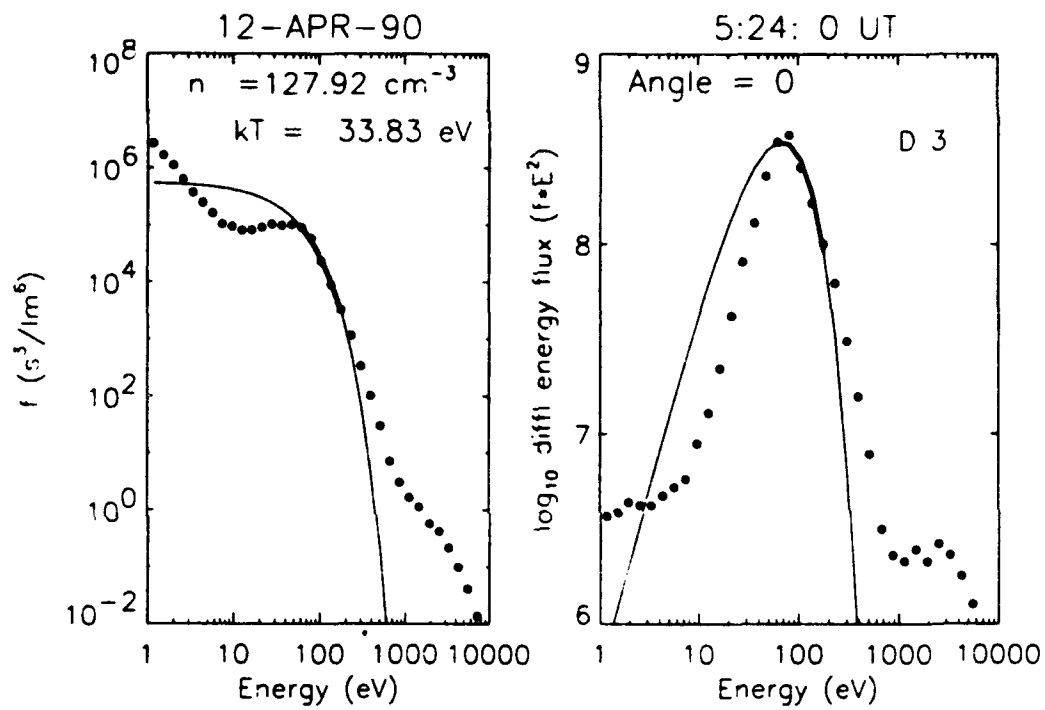LANL MPA — 1989–046
Detector 3
12–APR–90   5:24:00

1 — 3270.09 eV

1 — 3270.09 eV

Log Diffl Energy Flux

Log Dist. Fcn

Figure 47   Energy versus Pitch Angle--April 12--05:24:00

Figure 48 Distribution versus Energy--April 12--05:24:00

81
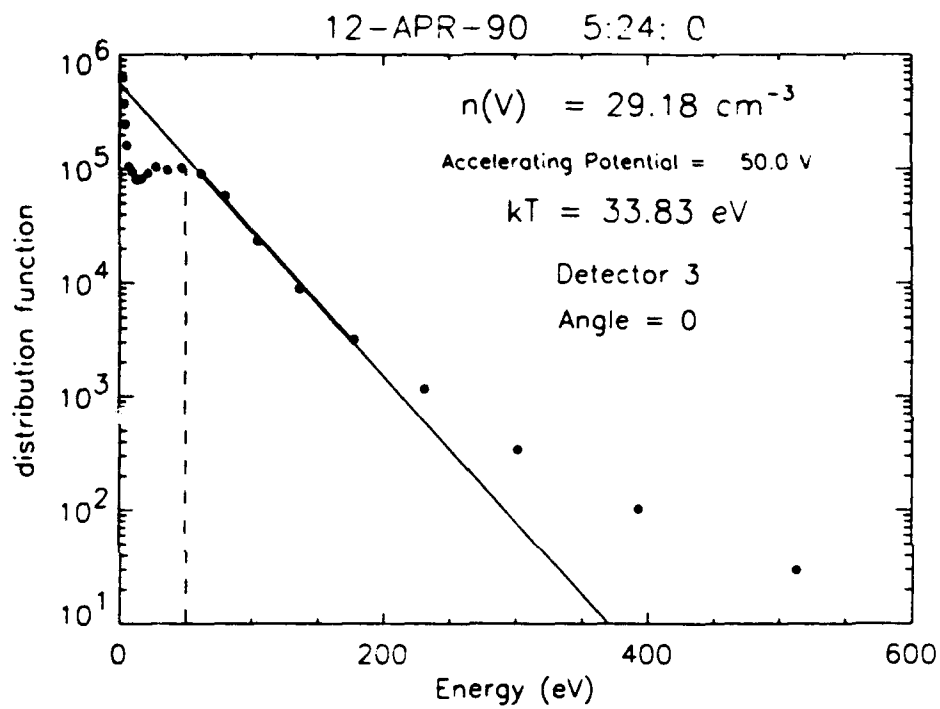
Figure 49 Distribution versus Energy--April 12--05:24:00

82

LANL MPA — 1989—046
Detector 3
12—APR—90   5:26:52

1 — 3270.09 eV

1 — 3270.09 eV
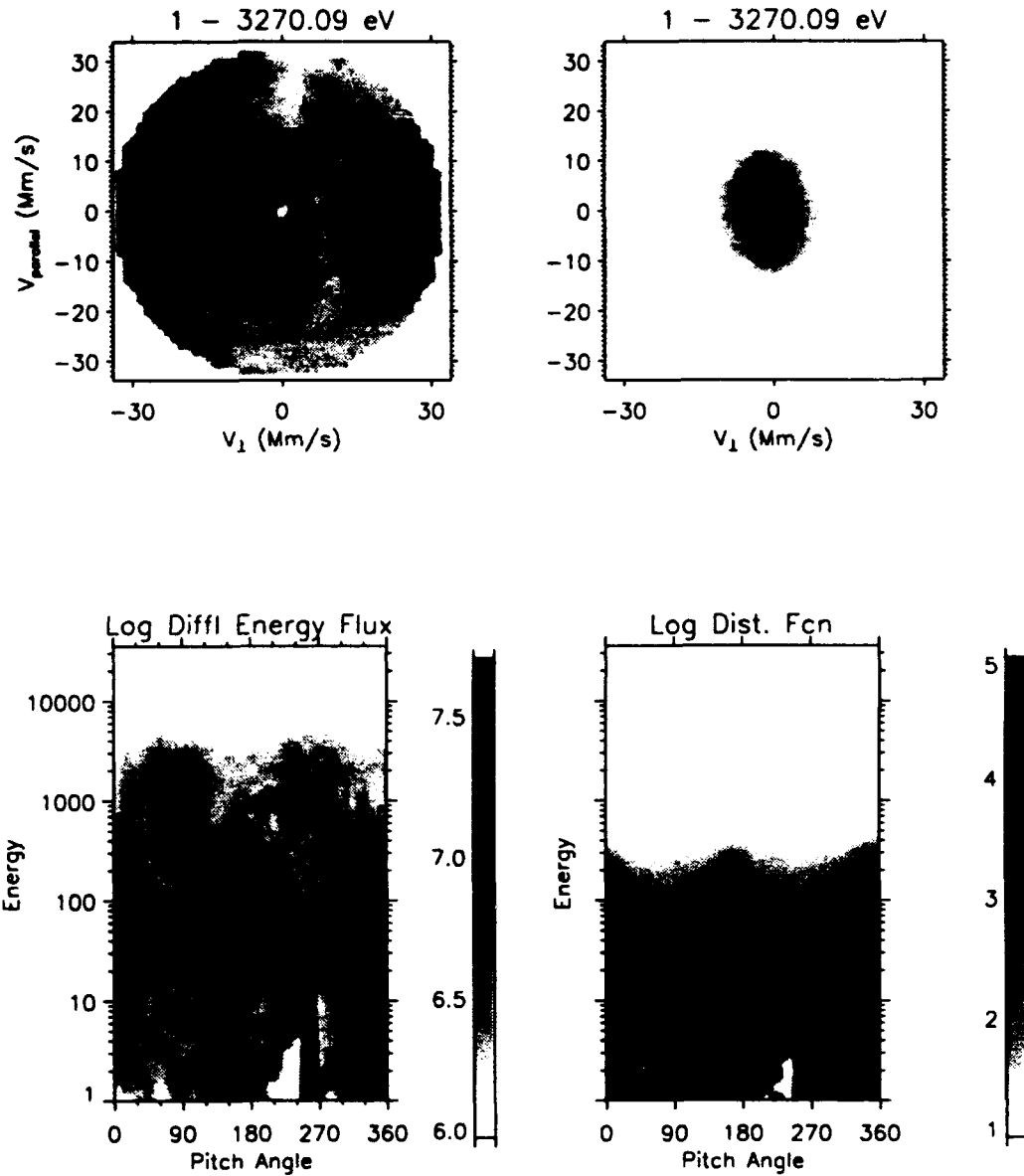
Log Diffl Energy Flux

Log Dist. Fcn

Figure 50   Energy versus Pitch Angle--April 12--05:26:52
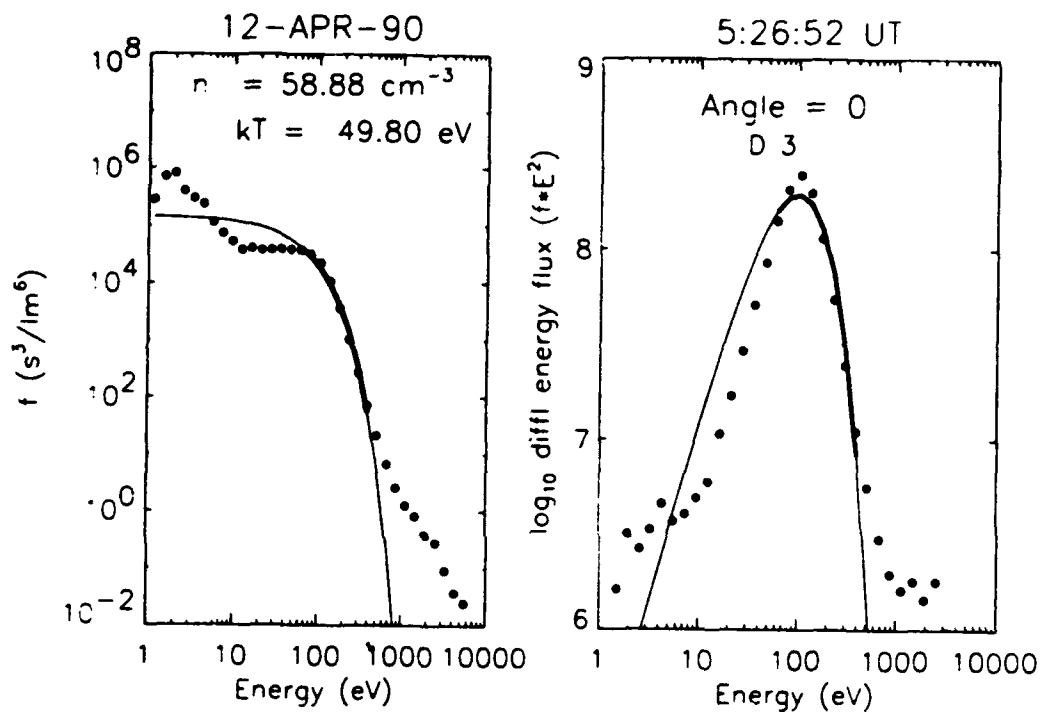
83

Figure 51 Distribution versus Energy--April 12--05:26:52
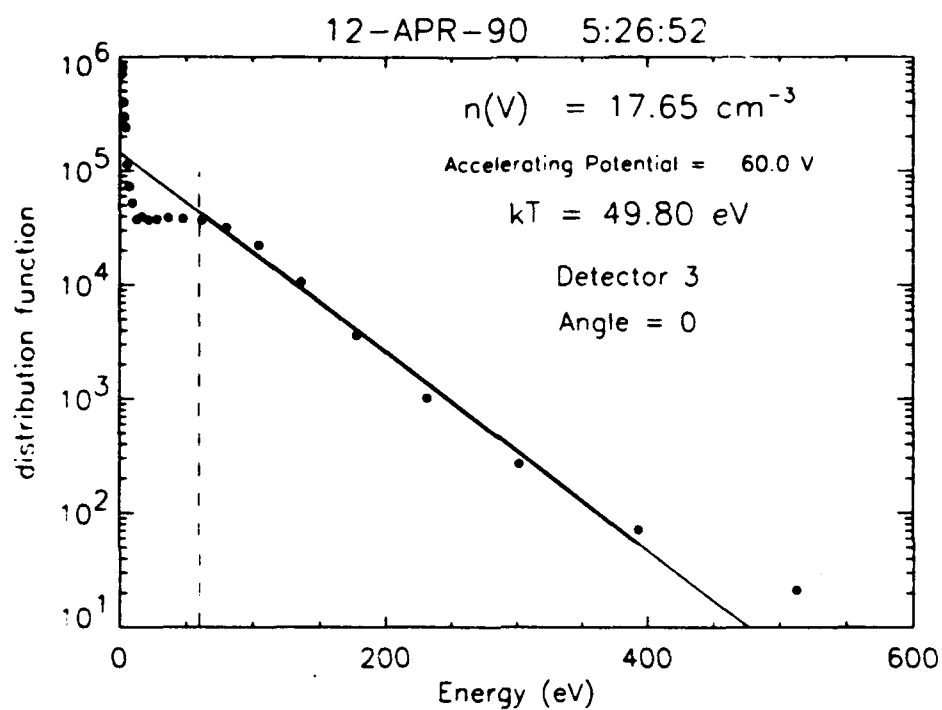
Figure 52   Distribution versus energy--April 12--05:26:52

LANL MPA – 1989–046
Detector 3
12–APR–90   5:29:44

1 – 3270.09 eV

1 – 3270.09 eV

Log Diffl Energy Flux
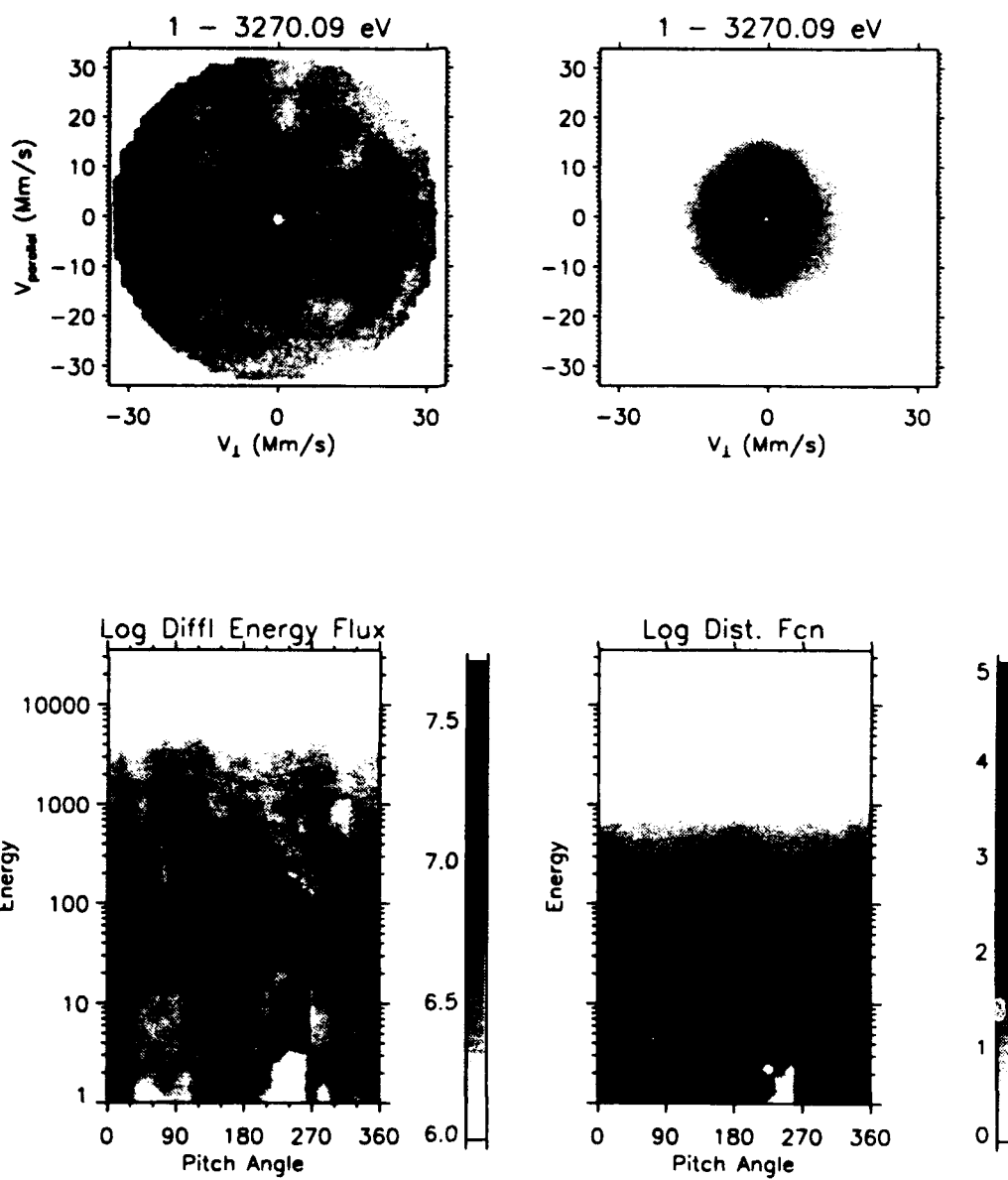
Log Dist. Fcn

Figure 53   Energy versus Pitch Angle--April 12--05:29:44
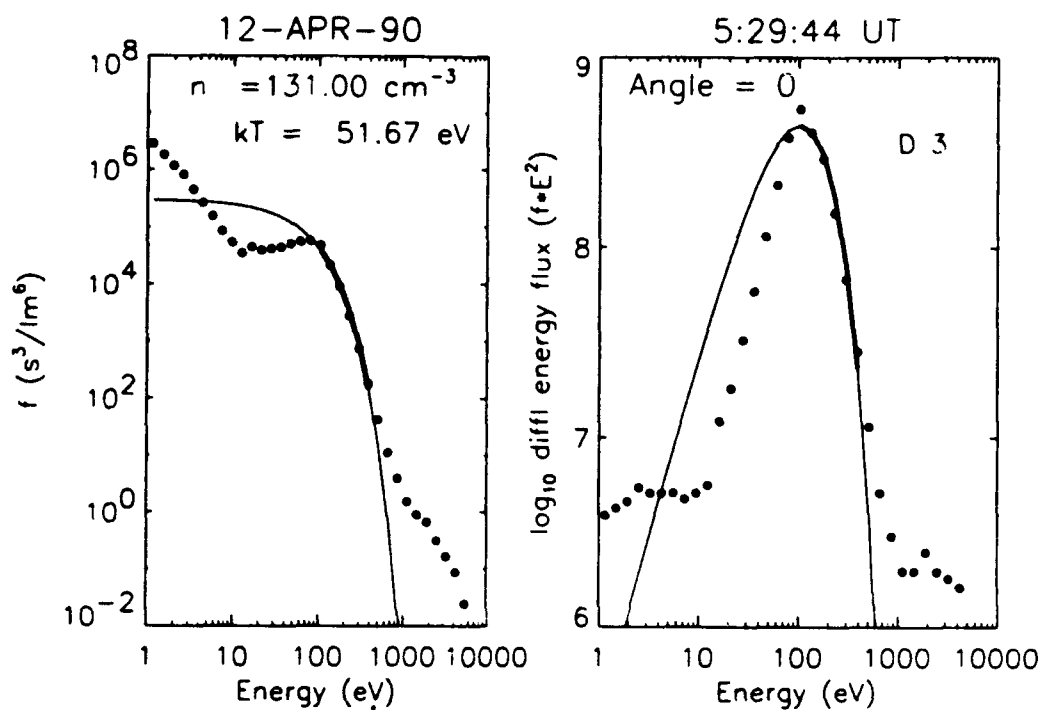
Figure 54   Distribution versus Energy--April 12--05:29:44

87
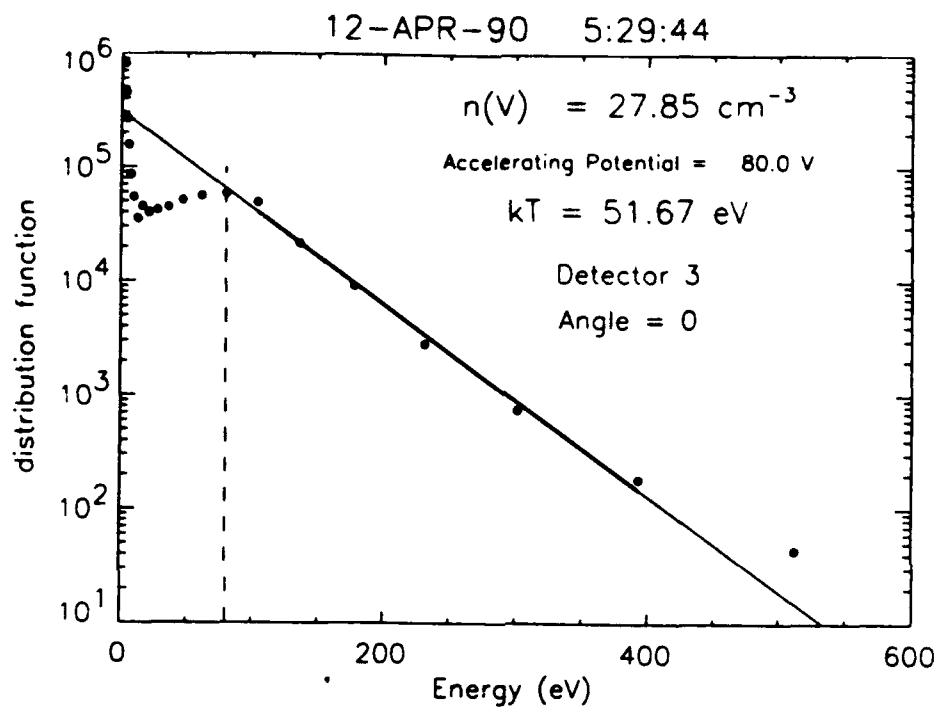
Figure 55 Distribution versus Energy--April 12--05:29:44
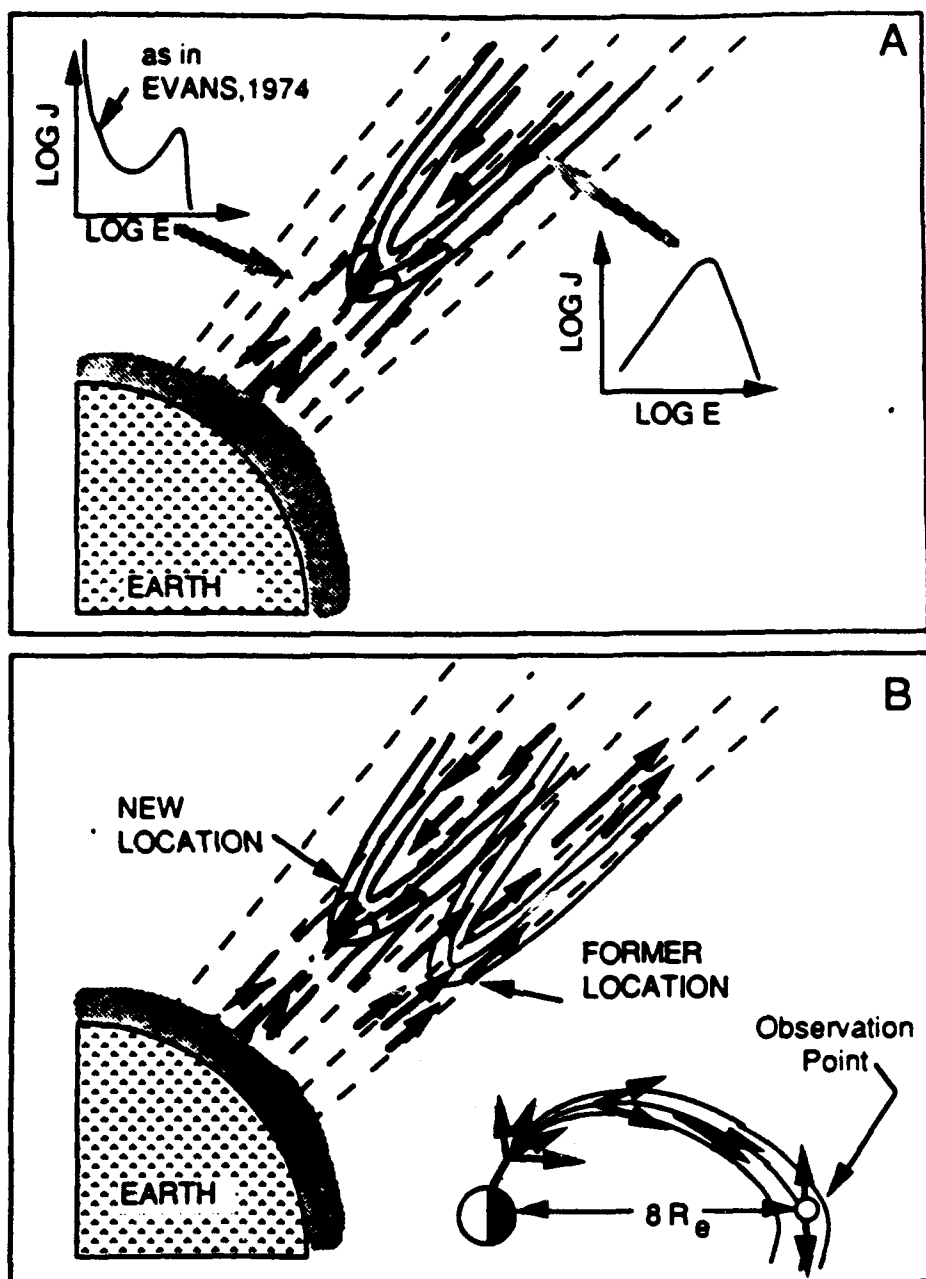
Figure 5. A representation of a discrete auroral structure (panel A) and how a displacement of the potential could allow auroral albedo electrons to be injected into the magnetosphere (panel B).

Figure 56   Acceleration Potential Structure, Klumpar (1989)

LANL MPA – 1989–046
Detector 3
17–APR–90   11:13:27

1 – 3270.09 eV

1 – 3270.09 eV

Log Diffl Energy Flux

Log Dist. Fcn
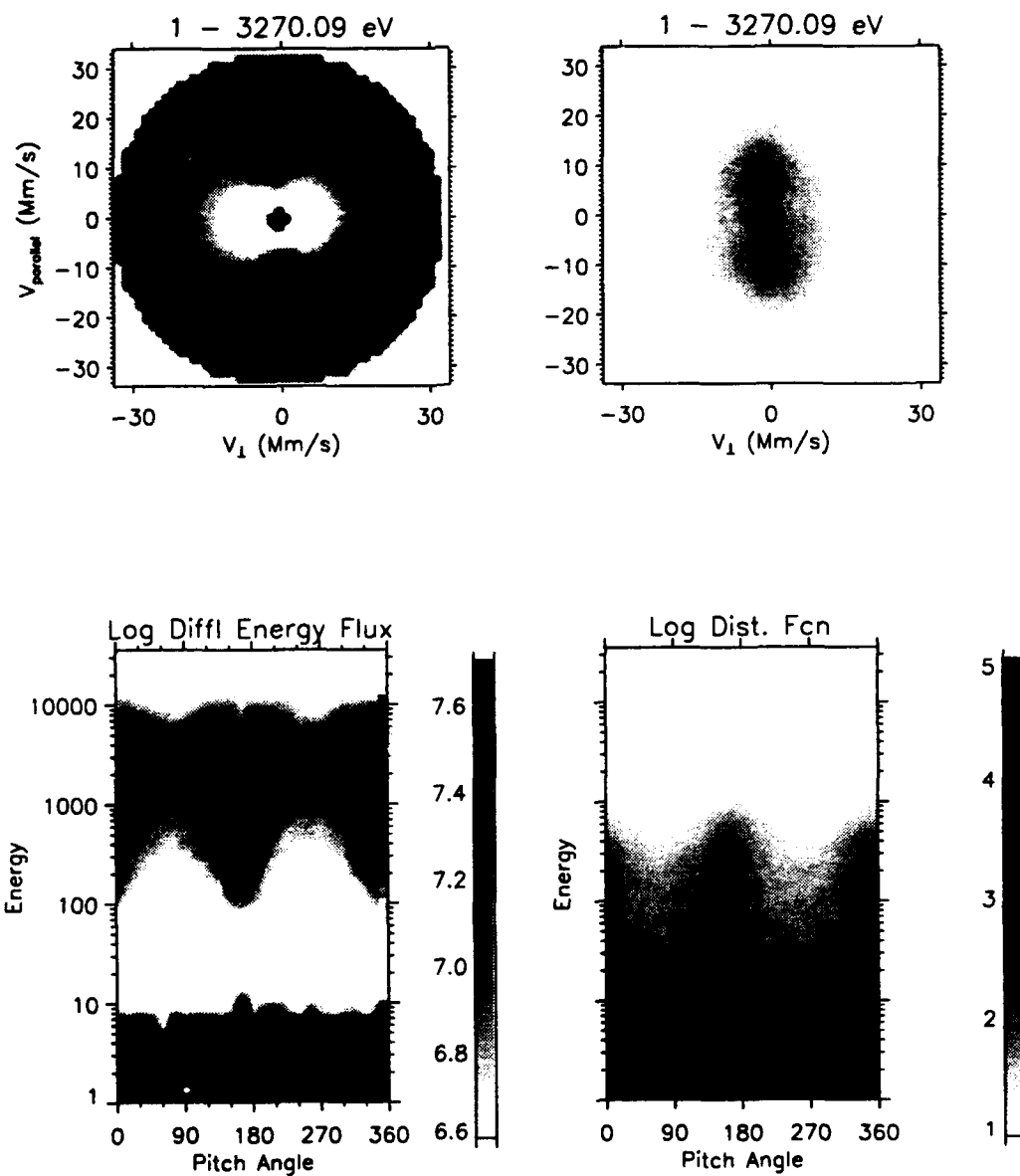
Figure 57   Energy versus Pitch Angle--April 17, 1990

90

LANL MPA — 1989-046
Detector 3
17-APR-90   12:30:52

1 — 3270.09 eV

1 — 3270.09 eV

Log Diffl Energy Flux

Log Dist. Fcn

Figure 58   Energy versus Pitch Angle--April 17, 1990

LIST OF REFERENCES

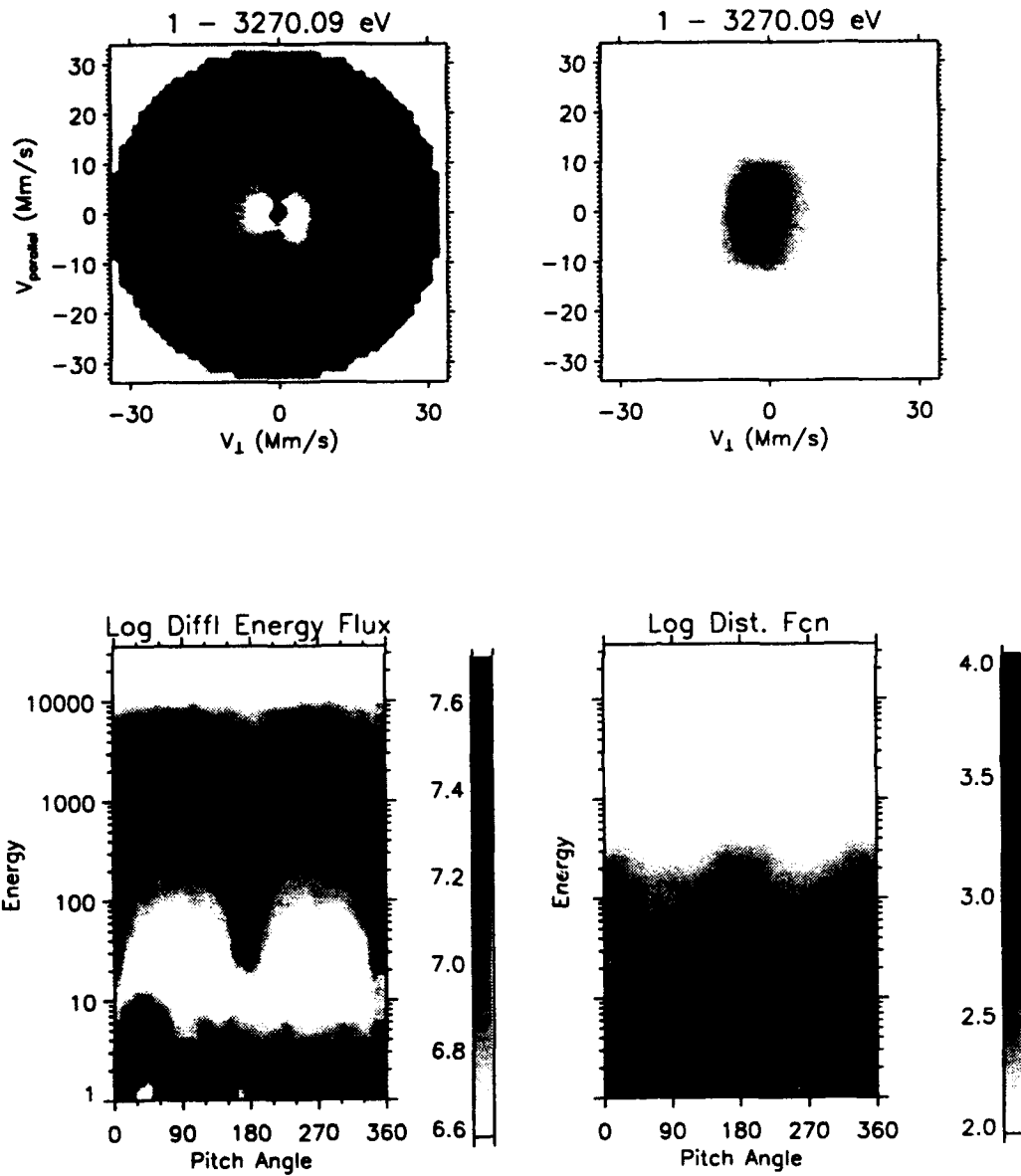Bame, S.J., *Magnetospheric Plasma Analyzer for Spacecraft with Constrained Resources*, Review of Science Instrumentation, Vol. 64, No. 4, p. 1026, April, 1993.

Eather, R.H., S.B. Mende, and R.J.R. Judge, *Plasma Injection at Synchronous Orbit and Spatial and Temporal Auroral Morphology*, Journal of Geophysical Research, Vol. 81, No. 16, p. 2805, June, 1976.

Hada, T., A. Nishida, and T. Terasawa, *Bi-directional Electron Pitch Angle Anisotropy in the Plasma Sheet*, Journal of Geophysical Research, Vol. 86, No. A13, p. 11,211, December, 1981.

Hones, E.W.Jr., J.R. Ashbridge, S. J. Bame, and S. Singer, *Energy spectra and angular distributions of particles in the plasma sheet and their comparison with rocket measurements over the auroral zone*, Journal of Geophysical Research, Vol. 76, No. 1, p. 63, January 1971.

Johnstone, A.D., D.M. Walton, and R. Liu, *Pitch Angle Diffusion of Low-Energy Electrons by Whistler Mode Waves*, Journal of Geophysical Research, Vol. 98, No. A4, p. 5959, April, 1993.

Klumpar, D.M., J.M. Quinn, and E.G. Shelley, *Counter-Streaming Electrons at the Geomagnetic Equator Near 9 R_E*, Geophysical Research Letters, Vol. 15, No. 11, P. 1295, October, 1988.

Klumpar, D.M., *Near Equatorial Signatures of Dynamic Auroral Processes*, in Physics of Space Plasmas, edited by T. Chang, G.B. Crew, and J.R. Jasperse, Scientific Publishers, 1990.

Lin, C.S., B. Mauk, G.K. Parks, S. DeForest, and C.E. McIlwain, *Temperature Characteristics of Electron Beams and Ambient Particles*, Journal of Geophysical Research, Vol. 84, No. A6, p. 2651, June, 1979.

Lin, C.S., J.L. Burch, J.D. Winningham, and J.D. Menietti, *DE-1 Observations of Counterstreaming Electrons at High Altitudes*, Geophysical Research Letters, Vol. 9, No. 9, p. 925, September, 1982.

92

Mauk, B., and C.E. McIlwain, *ATS-6 UCSD Auroral Particles Experiment*, IEEE Trans. Aerosp. Electron. Syst., AES-11, p. 1125, 1975.

McComas, D.J., *Magnetospheric Plasma Analyzer (MPA): Initial Three-Spacecraft Observations from Geosynchronous Orbit*, Submitted to Journal of Geophysical Research, November, 1992.

McIlwain, Carl E., *Auroral Electron Beams Near the Magnetic Equator*, in Physics of the Hot Plasma in the Magnetosphere, edited by B. Hultqvist and L. Stenflo, p. 91, Plenum, New York, 1975.

Mende, S.B., and E.G. Shelley, *Coordinated Electron Flux and Simultaneous Auroral Observations*, Journal of Geophysical Research, Vol. 81, p. 97, 1976.

Mizera, Paul F., and Joseph F. Fennell, *Signatures of Electric Fields from High and Low Altitude Particles Distributions*, Geophysical Research Letters, Vol. 4, No. 8, p. 311, August, 1977.

Moore, T.E., and R.L. Arnoldy, *Plasma Pitch Angle Distributions Near the Substorm Injection Front*, Journal of Geophysical Research, Vol. 87, No. A1, p. 265, January, 1982.

Parks, G.K.,C.S. Lin,B. Mauk,S. DeForest,and C.E. McIlwain, *Characteristics of Magnetospheric Particle Injection Deduced From Events Observed on August 18, 1974*, Journal of Geophysical Research, Vol. 82, No. 32, p. 5 2 0 8 , November, 1977.

Parks, G.K., B. Mauk, C. Gurgiolo, and C.S. Lin, *Observations of Plasma Injection*, in Dynamics of the Magnetosphere, edited by S.I. Akasofu, p. 371, D. Reidel, 1979.

Tascione, Thomas F., *Introduction to the Space Environment*, p.45-100, Orbit Book Company, 1988.

Tetreault, David, *Theory of Electric Fields in the Auroral Acceleration Region*, Journal of Geophysical Research, Vol. 9 No. A3, p. 3549, March, 1991.

INITIAL DISTRIBUTION LIST

		No. Copies
1.	Defense Technical Information Center Cameron Station Alexandria VA 22304-6145	2
2.	Library, Code 052 Naval Postgraduate School Monterey CA 93943-5002	2
3.	Director, Navy Space Systems Division (N63) Space and Electronics Warfare Directorate Chief of Naval Operations Washington DC 20350-2000	1
4.	Commander Navy Space Command Dahlgren, Virginia 22448-5170	1
5.	Dr. R.C. Olsen, Code Ph/Os Department of Physics Naval Postgraduate School Monterey, CA 93943-5000	1
6.	Dr. M. Thomsen Mail Stop D438, SST-8 LANL Los Alamos, New Mexico 87545	1
7.	Dr. D.J. McComas Mail Stop D438, SST-8 LANL Los Alamos, New Mexico 87545	1
8.	Dr. Tom Moore ES53 NASA/MSFC Huntsville, AL 35812	1
9.	Dr. Roger Arnoldy Sci. and Eng. Res. Bldg. University of N.H. Durham, N.H. 03824	1

10. Dr. David Klumpar   1
    Lockheed Space Science Lab (91-20)
    3251 Hanover St., Bldg. 255
    Palo Alto, CA 94304

11. Dr. T. Hada   1
    Kyushu University
    Coll. Gen. Education
    4-2-1 Ropponmatsu Chusku
    Fukuoka 810
    Japan

12. Dr. Carl McIlwain   1
    University of California, San Diego
    CASS-011
    9500 Gilman Drive
    La Jolla, CA 92093

13. Lt. Raymond Gaw   1
    29 Underwood Lane
    Middletown, RI 02840